

# UC Berkeley

## SEMM Reports Series

### Title

Laboratory tests of column-foundation moment transfer connections with headed anchors

### Permalink

<https://escholarship.org/uc/item/7q48p6s2>

### Authors

Worsfold, Benjamin

Moehle, Jack

### Publication Date

2019-08-01

Report No.  
UCB/SEMM-2019/01

Structural Engineering  
Mechanics and Materials

Laboratory Tests of Column-Foundation Moment Transfer  
Connections with Headed Anchors

By

Benjamin L. Worsfold and Jack P. Moehle

August 2019

Department of Civil and Environmental Engineering  
University of California, Berkeley



## ABSTRACT

Steel and precast columns are commonly designed to transfer moment to concrete foundations through cast-in-place headed anchors. Three different design methods have been used to design the connections: 1) Anchoring-to-concrete provisions considering concrete breakout (e.g., ACI 318-14 Chapter 17), 2) the strut-and-tie method (e.g., ACI 318-14 Chapter 23), and 3) joint shear design methods (e.g., ACI 352R-02). The results obtained from these methods can differ by up to an order of magnitude. A full-scale interior column-foundation connection with headed anchors located away from the foundation edges was designed, built, and tested in a laboratory. Practicing engineers were consulted so the specimen geometry and materials would closely resemble current construction practice on the West Coast of the United States. The test specimen was loaded under cyclic quasi-static loading with no axial load until failure so as to isolate the effect of moment. The experimental results suggest that, of the three design methods, the concrete breakout equations of ACI 318-14 provide the most appropriate method for designing the connections. The results of the breakout equations could be further improved by including an additional factor that accounts for the presence of the nearby compressive force due to flexural compression in the connected steel column. Strut-and-tie models underestimated the experimental failure load by about 90% of the measured load while the joint shear equations overestimated the measured strength by 59%.



## **ACKNOWLEDGMENTS**

The authors would like to thank the following individuals for their invaluable insight and for graciously investing their time and energy into this project. Their involvement made this test possible and greatly improved the quality of the research results.

Rafael Sabelli, director of seismic design at Walter P Moore

James Malley, senior principal of Degenkolb Engineers

John Silva, senior director of codes and standards at HILTI

Roberto Piccinin, group manager code development and research at HILTI

The authors would also like to thank the managers and staff of the Structural Engineering Laboratory UC Berkeley for their support and problem-solving abilities during the design, construction, and testing phases of the project.

The authors would also like to thank the sponsors of this project:

HILTI

ACI Foundation, Concrete Research Council

Ron Klemencic chairman and C.E.O. of Magnusson Klemencic Associates



# CONTENTS

ABSTRACT.....	III
ACKNOWLEDGMENTS.....	V
CONTENTS.....	VII
LIST OF TABLES.....	IX
LIST OF FIGURES.....	XI
<b>1 INTRODUCTION.....</b>	<b>1</b>
<b>2 LITERATURE AND DESIGN METHOD REVIEW.....</b>	<b>2</b>
2.1 CONCRETE BREAKOUT FAILURE FOR ANCHORS EMBEDDED ON CONCRETE.....	2
2.2 STRUT-AND-TIE METHOD.....	9
2.2.1 Strength of Struts.....	10
2.2.2 Strength of Ties.....	11
2.2.3 Strength of Nodal Zones.....	12
2.3 BEAM-COLUMN JOINT DESIGN.....	13
<b>3 SPECIMEN DESIGN.....</b>	<b>18</b>
3.1 SPECIMEN REQUIREMENTS.....	18
3.2 SPECIMEN GEOMETRY AND DESIGN.....	19
3.3 CALCULATIONS OF CONNECTION STRENGTH.....	27
3.3.1 Concrete Breakout Equations (ACI 318-14 Ch.17 Anchoring to Concrete).....	27
3.3.2 Strut-and-Tie Model (ACI 318-14 Ch. 23 Strut-and-Tie Models).....	31
3.3.3 Horizontal Joint Shear Equations (ACI 352R-02 Design of Beam-Colum Connections).....	36
3.3.4 Summary of Connection Capacities.....	42
<b>4 TEST SET-UP.....</b>	<b>43</b>
4.1 INSTRUMENTATION.....	44
4.2 LOADING PROTOCOL.....	49
<b>5 RESULTS.....</b>	<b>51</b>
5.1 CRACK PATTERNS.....	51
5.2 INSTRUMENTATION READINGS.....	56
5.3 SPECIMEN SLIDING, ELONGATION AND SUPPORT UPLIFT.....	79
<b>6 DISCUSSION.....</b>	<b>82</b>
<b>7 CONCLUSIONS.....</b>	<b>85</b>
<b>8 REFERENCES.....</b>	<b>86</b>
<b>APPENDIX A. MATERIAL PROPERTIES.....</b>	<b>89</b>
<b>APPENDIX B. CONCRETE MIXTURE DESIGN.....</b>	<b>102</b>
<b>APPENDIX C. AS-BUILT SPECIMEN DRAWINGS.....</b>	<b>103</b>
<b>APPENDIX D. ADDITIONAL SPECIMEN DESIGN CALCULATIONS.....</b>	<b>112</b>
<b>APPENDIX E. CHANNEL LIST.....</b>	<b>138</b>
<b>APPENDIX F. INSTRUMENTATION LOCATION.....</b>	<b>141</b>
<b>APPENDIX G. PHOTOGRAPHS.....</b>	<b>143</b>





## LIST OF TABLES

Table 2-1. Strut coefficient $\beta_s$ (ACI Committee 318, 2014).....	11
Table 2-2. Node coefficient $\beta_n$ (ACI Committee 318, 2014).....	12
Table 3-1. Summary of mean ultimate load in anchor group using different failure criteria with no safety factor .....	42
Table 4-1. Amplitude of displacement-controlled loading protocol .....	49
Table 5-1. Maximum displacement and force applied to column free end per cycle.....	57
Table 5-2. Approximate ductility capacity calculation per loaded anchor group .....	57
Table 5-3. Maximum load and load at breakout for east and west anchor groups (kips).....	62
Table 6-1. Summary of mean anchor group loads at failure for various design methods and the experimental results with no safety factors.....	82
Table A- 1. Concrete compressive strength results .....	90
Table A- 2. Concrete modulus of elasticity test results .....	91
Table A- 3. Concrete splitting tensile strength results on test day (21 days from casting).....	92
Table A- 4. Fracture energy specimen geometry and properties.....	94
Table A- 5. Geometric considerations and material properties.....	94
Table A- 6. Fracture energy weight and failure load.....	96
Table A- 7. Fracture energy and statistical values.....	97
Table A- 8. Reinforcing bar properties for hoop reinforcing bar #4G60 based on ASTM-A706 .....	100
Table A- 9. Properties of mat reinforcing bars #6G100 based on ASTM-A706 .....	101
Table D- 1. Summary of considered limit states and the factor of safety versus column yielding .....	112



## LIST OF FIGURES

Figure 2-1. Tensile stress distribution perpendicular.....	3
Figure 2-2. Assumed geometry for concrete breakout cone (ACI Committee 318, 2014).....	4
Figure 2-3. ACI 318 Models for basic concrete breakout strength of a single anchor in tension in cracked concrete $Nb$ .....	4
Figure 2-4. Histogram of measured to calculated concrete cone failure loads for headed anchors subjected to concentric tension (Eligehausen, et al., 1992) .....	5
Figure 2-5. Ratio of measured to calculated concrete cone failure loads for headed anchors subjected to tension as a function of concrete compressive strength (Eligehausen, et al., 1992)...	5
Figure 2-6. Influence of compression force on concrete cone breakout capacity after Zhao (1993) (Eligehausen, et al., 2006).....	7
Figure 2-7. Influence of compression force on concrete cone breakout capacity as a function of ratio internal lever arm to embedment depth. Modified from (Eligehausen, et al., 2006).....	8
Figure 2-8. Strut-and-tie model example for a deep beam (ACI Committee 318, 2014).....	9
Figure 2-9. Type 2 connections $\gamma$ -values (Joint ACI-ASCE Committee 352, 2002).....	14
Figure 2-10. Joint forces at critical sections. T = tensile force; C = compressive force; V = shear force; subscript b for beam, subscript c for column; and subscript s for slab (Joint ACI-ASCE Committee 352, 2002).....	15
Figure 2-11. Location of hooks and headed bars (Joint ACI-ASCE Committee 352, 2002) .....	15
Figure 2-12. Effective joint area (ACI 318-14 R18.8.4).....	16
Figure 2-13. Breakout failure precluded in joint by keeping anchorage length greater than or equal to $d/1.5$ (ACI 318-14 R25.4.4.2c).....	17
Figure 3-1. Isometric view of specimen and loading frame.....	19
Figure 3-2. Elevation view of longitudinal cross section of specimen.....	21
Figure 3-3. Elevation view of transverse cross section of specimen.....	22
Figure 3-4. Plan view of specimen .....	23
Figure 3-5. Details of specimen base plate and shear lug.....	24
Figure 3-6. Detail of specimen anchor.....	25
Figure 3-7. Detail of specimen hoops.....	26
Figure 3-8. Strut-and-tie Model 1 .....	31
Figure 3-9. Pseudo concrete column dimensions .....	36
Figure 3-10. Free body diagram complete specimen.....	39
Figure 3-11. Free body diagram internal forces acting on node.....	39
Figure 3-12. Free body diagrams for horizontal (left) and vertical joint shear (right) .....	40
Figure 4-1. Specimen set-up and instrumentation .....	43
Figure 4-2. Cross section A-A of specimen showing instrumentation .....	45
Figure 4-3. Cross section B-B of specimen showing instrumentation .....	46
Figure 4-4. Sketch of strain gages on second-from-top and second-from-bottom hoops.....	47
Figure 4-5. Plan view of base plate showing numbering of anchors and load cells.....	47
Figure 4-6. Plan view sketch of instrumentation.....	48
Figure 4-7. Loading protocol imposed to column free end modified from FEMA-461 (2007) ...	50
Figure 4-8. Column free end displacement versus time triangulated with wire pots attached to the column free end, pauses in loading appear as horizontal lines .....	50

Figure 5-1. Specimen crack pattern after failure, 12 in. x 12 in. grid, top view and two lateral views .....	51
Figure 5-2. Specimen crack pattern after failure, 12 in. x 12 in. grid, east and west breakout cones identified.....	52
Figure 5-3. Location of specimen saw cut .....	53
Figure 5-4. Slab cross section of east section showing two horizontal cracks.....	53
Figure 5-5. Exposed bottom surface of east breakout cone inside joint .....	54
Figure 5-6. Minimal damage observed on specimen bottom surface as seen from the east.....	55
Figure 5-7. Longitudinal force – displacement relationship of the column free end as measured by actuator load cells and the triangulation of wire pot attached to column free end (positive displacement east movement).....	56
Figure 5-8. Plan view of the displacement of the column free end triangulated with measurements from wire pots 1 and 3 attached to the column free end (positive displacement is north and east) .....	58
Figure 5-9. Transverse force – displacement relationship of the column free end as measured by actuator load cells and the triangulation of wire pot attached to column free end (positive displacement east movement).....	59
Figure 5-10. Plot of the load in each north anchor versus the load in the corresponding symmetric south anchor for the east and west anchor groups separately.....	60
Figure 5-11. Plot of the load in the two inner anchors against the load in the two outer anchors for the east and west anchor groups.....	61
Figure 5-12. Load in each anchor group as measured by load cells on each anchor (negative load represents a compressive force).....	62
Figure 5-13. Anchor group load against base plate uplift as measured by load cells on each anchor and linear potentiometers on base plate and slab .....	63
Figure 5-14. Strains in four legs of hoops plotted versus time; second-from-top and second-from-bottom hoops are plotted.....	64
Figure 5-15. Absolute rotation of slab and base plate versus time.....	65
Figure 5-16. Column free end displacement divided into contributions from the slab rotation, the relative base plate rotation, the elastic column deflection, the column shear deflection and experimental error versus time .....	66
Figure 5-17. At the instant of breakout of the east cone, the rotation of the slab and the base plate versus time (top) and the column free end displacement divided into contributions from the slab rotation, the relative base plate rotation, the elastic column deflection, and experimental error versus time (bottom) .....	67
Figure 5-18. At the instant of breakout of the west cone, the rotation of the slab and the base plate versus time (top) and the column free end displacement divided into contributions from the slab rotation, the relative base plate rotation, the elastic column deflection, and experimental error versus time (bottom).....	68
Figure 5-19. Base plate with large moment (AISC, 2006) .....	69
Figure 5-20. Comparison between the theoretical and the measured load in both anchor groups; assuming uniform bearing pressure distribution under base plate for theoretical; taking experimental loads from load cells on anchors .....	70
Figure 5-21. Vertical displacements of the top surface of the slab measured with two rows of linear potentiometers at maximum positive and negative displacement for cycle seven (before breakout).....	71

Figure 5-22. Vertical displacements of the top surface of the slab measured with two rows of linear potentiometers 5 s before and 5 s after breakout failure for both loading directions .....	72
Figure 5-23. Strains of the inner and outer top reinforcing bars measured with strain gages spaced 21 in. on center at maximum positive and negative displacements for cycle seven (Note: the second from the right gage of the outer bar malfunctioned, the average of the adjacent gages is plotted instead).....	73
Figure 5-24. Strains of the inner and outer bottom reinforcing bars measured with strain gages spaced 21 in. on center at maximum positive and negative displacements for cycle seven (Note: the fourth from the left gage of the inner bar and the first and third from the left gage of the outer row malfunctioned, the average of the adjacent gages is plotted instead).....	74
Figure 5-25. Strains of top reinforcing bars measured with strain gages spaced 21 in. on center 5 s before and 5 s after breakout failure for both loading directions (Note: two strain gages failed when the west anchor group failed).....	75
Figure 5-26. Strains of bottom reinforcing bars measured with strain gages spaced 21 in. on center 5 s before and 5 s after breakout failure for both loading directions (Note: the fourth from the left gage of the inner bar and the first and third from the left gage of the outer row malfunctioned, the average of the adjacent gages is plotted instead).....	76
Figure 5-27. Strains in the reinforcing bar perpendicular to the longitudinal bars measured with strain gages spaced 14 in. on center at maximum positive and negative displacements for cycle seven (Note: the second from the left gage malfunctioned, the average of the adjacent gages is plotted instead) .....	77
Figure 5-28. Strains in the bar perpendicular to the longitudinal bars measured with strain gages spaced 14 in. on center 5 s before and 5 s after breakout failure for both loading directions (Note: the second from the left gage malfunctioned, the average of the adjacent gages is plotted instead) .....	78
Figure 5-29. Specimen sliding measured along the slab centerline in the direction of loading relative to the laboratory floor, positive sliding is movement towards the east.....	79
Figure 5-30. Slab longitudinal elongation during testing, .....	80
Figure 5-31. Specimen uplift at west and east supports.....	81
Figure A- 1. Concrete compressive strength .....	90
Figure A- 2. Concrete stress - strain results on testing day (21 days from casting) .....	91
Figure A- 3. Concrete Fracture Energy test set-up .....	93
Figure A- 4. Fracture energy specimen geometry .....	93
Figure A- 5. Load – Time graph small fracture energy beams .....	94
Figure A- 6. Load – Time graph medium fracture energy beams .....	95
Figure A- 7. Load – Time graph large fracture energy beams .....	95
Figure A- 8. Normalized load versus depth relationship .....	96
Figure A- 9. Coarse ¾” aggregate LA abrasion test ASTM-C131 .....	98
Figure A- 10 Coarse ¾” aggregate ASTM-C136 gradation.....	99
Figure A- 11. Stress - strain graph for hoop reinforcing bar #4G60 ASTM-A706.....	100
Figure A- 12. Stress - strain graph for mat reinforcing bar #6G100 .....	101
Figure B- 1. Concrete mixture design 347EG9E1 by Central Concrete.....	102
Figure B- 2. Concrete mixture batch ticket with actual weights .....	102

Figure G- 1. Support type 1 form .....	143
Figure G- 2. Support type 2 form with through holes .....	143
Figure G- 3. Support type 1 form with reinforcement ready to cast #1.....	144
Figure G- 4. Support type 1 form with reinforcement ready to cast #2.....	144
Figure G- 5. Casting support type 1 October 25, 2017 #1 .....	145
Figure G- 6. Casting support type 1 October 25, 2017 #2.....	145
Figure G- 7. Support type 1 hours after casting bottom section.....	146
Figure G- 8. Support type 1 casting top section October 25, 2017 #1.....	146
Figure G- 9. Support type 1 casting top section October 25, 2017 #2.....	147
Figure G- 10. Support type 2 casting October 25, 2017 .....	147
Figure G- 11. Specimen form and support type 2 form in the background .....	148
Figure G- 12. Anchors delivery .....	148
Figure G- 13. Installation of strain gages #1 .....	149
Figure G- 14. Installation of strain gages #2.....	149
Figure G- 15. Specimen form with reinforcement ready to cast #1 .....	150
Figure G- 16. Specimen form with reinforcement ready to cast #2 .....	150
Figure G- 17. Specimen form with reinforcement ready to cast #3 .....	151
Figure G- 18. Specimen anchors ready to cast.....	152
Figure G- 19. Specimen form with reinforcement ready to cast #3 .....	152
Figure G- 20. Specimen casting November 21, 2017.....	153
Figure G- 21. Specimen hours after casting November 21, 2017 #1 .....	153
Figure G- 22. Specimen hours after casting November 21, 2017 #2 .....	154
Figure G- 23. Removal of foam from specimen to reveal hole for shear lug #1.....	155
Figure G- 24. Removal of foam from specimen to reveal hole for shear lug #2.....	156
Figure G- 25. Column delivery .....	156
Figure G- 26. Support type 1 demolding .....	157
Figure G- 27. Demolding specimen.....	158
Figure G- 28. Specimen on temporary supports.....	158
Figure G- 29. Moving supports into final position .....	159
Figure G- 30. Specimen moved onto supports with overhead crane.....	159
Figure G- 31. Specimen in final position on supports #1 .....	160
Figure G- 32. Specimen in final position on supports #2 .....	160
Figure G- 33. Specimen in final position with column #1.....	161
Figure G- 34. Specimen in final position with column #2.....	161
Figure G- 35. Instrumentation cable management .....	162
Figure G- 36. Crack marking during a pause while testing December 12, 2017 .....	163
Figure G- 37. Specimen top surface after test as seen from the west December 12, 2017.....	164
Figure G- 38. Specimen top surface after test as seen from the east December 12, 2017.....	164
Figure G- 39. Specimen bottom surface after test as seen from the west December 12, 2017...	165
Figure G- 40. Specimen bottom surface after test as seen from the east December 12, 2017....	165
Figure G- 41. Construction of fracture energy molds for large beams.....	166
Figure G- 42. Medium fracture energy beams hours after casting November 21, 2017 .....	167
Figure G- 43. Large fracture energy beams hours after casting November 21, 2017 .....	167
Figure G- 44. Fracture energy beams with top plate attached with hydrostone .....	168
Figure G- 45. Fracture energy beams after removing from lime bath.....	168
Figure G- 46. Medium fracture energy beams held together and saw cut.....	169

Figure G- 47. All fracture energy beams removed from lime bath and saw cut..... 169  
Figure G- 48. Cylinders hours after casting November 21, 2017..... 170  
Figure G- 49. Cylinder compression testing ..... 170  
Figure G- 50. Reinforcing bar testing ..... 171





# 1 INTRODUCTION

Steel and precast columns are commonly designed to transfer moment to concrete foundations through cast-in-place headed anchors. Three different design methods have been used to design the connections:

1. Anchoring-to-concrete provisions considering concrete breakout (e.g., ACI 318-14 Chapter 17);
2. The strut-and-tie method (e.g., ACI 318-14 Chapter 23); and
3. Joint shear design methods (e.g., ACI 352R-02).

The strengths calculated by these three methods can differ by up to an order of magnitude (see section 3.3.4 and Table 3-1). Some practicing engineers gravitate towards the latter two methods as designs based on concrete breakout equations can be more conservative and costly. Some proponents of strut-and-tie modeling contend that a properly designed footing will have internal force-resisting mechanisms that can be arranged naturally to resist the internal forces associated with anchoring the anchor bolts, thereby avoiding breakout failure. A common counter argument is that if breakout capacities are reached, breakout failure will occur regardless.

A laboratory test was done to provide benchmark physical data by which to test the applicability of these three aforementioned design methods. This report describes the details of the test. The specimen comprised a full-scale interior column-foundation connection with headed anchors located well away from the edge of the footing. The specimen was tested until failure under cyclic quasi-static loading following procedures of FEMA-461 (2007) with no column axial load. Practicing engineers were consulted so the specimen geometry and materials would closely resemble elements of current construction practice on the West Coast of the United States.

## **2 LITERATURE AND DESIGN METHOD REVIEW**

### **2.1 CONCRETE BREAKOUT FAILURE FOR ANCHORS EMBEDDED IN CONCRETE**

A common method for anchoring attachments to concrete is through steel rods with an enlarged bearing surface or head embedded in the concrete. To anchor structural members to concrete foundations, it is common to use threaded bolts with a nut acting as the head, with or without washers. ACI 318-14 Chapter 17 provides building code requirements for the design of such anchors. For single headed bars or groups of headed bars subjected to tensile loads, four failure modes are to be checked:

1. Steel failure
2. Concrete breakout
3. Pull out
4. Concrete side-face blowout

The present research focuses primarily on the concrete breakout failure mode.

When a tensile force is applied to a headed anchor, the load is transferred to the concrete through the bearing surface of the head as normal pressure. This produces tensile stresses locally around the head. When the tensile stresses exceed the tensile capacity of the concrete, cracks initiate around the anchor head. It has been observed experimentally (Eligehausen and Sawade, 1989) that at loads as low as 30% of the ultimate breakout load, discrete cracks have already initiated at the anchor head. As the load increases, the cracks propagate towards the surface in a radially symmetric pattern forming a cone-like segment of concrete. At 90% of the ultimate load, the cracks have traveled only about 30% of the distance from the anchor head to the surface. Figure 2-1 shows the strains along the failure plane at 30% and 90% of the maximum load. If a load is steadily increased until failure, the cracks will travel all the way to the surface and detach the concrete cone. A breakout-type failure is easily identifiable due to the cone-shaped segment of detached concrete.

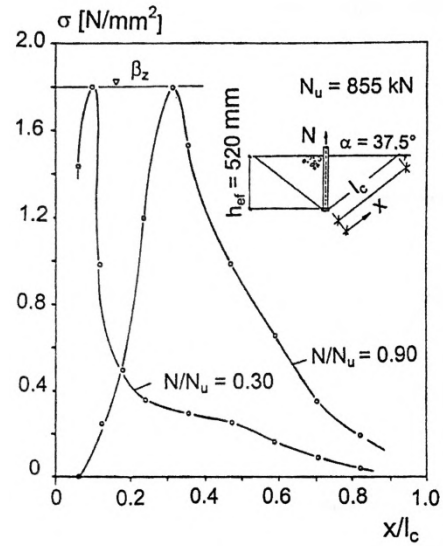


**Figure 2-1. Tensile stress distribution perpendicular to the failure cone surface (Eligehausen and Sawade, 1989)**

ACI 318-14 breakout equations are based on the so-called CCD-method (Concrete Capacity Design) (Fuchs, et al., 1995). This method assumes a 35° slope for the cone as shown in Figure 2-2 and a uniform stress along the failure surface, which results in the following equation for basic concrete breakout strength of a single anchor in tension in cracked concrete:

$$N_b = k_c \sqrt{f'_c} h_{ef}^\alpha \quad (1)$$

Where:

$N_b$ : Basic concrete breakout strength of a single anchor in tension in cracked concrete in lb

$k_c$ : Coefficient  $k_c = 24$  for anchors with  $h_{ef} < 11$  in. and  $k_c = 16$  for anchors with  $11 \text{ in.} \leq h_{ef} \leq 25$  in.

$f'_c$ : Concrete compressive strength in units of psi

$h_{ef}$ : Effective embedment depth in units of in. (See Figure 2-2)

$\alpha$ : Exponent  $\alpha = 1.5$  for anchors with  $h_{ef} < 11$  in. and  $\alpha = 5/3$  for anchors with  $11 \text{ in.} \leq h_{ef} \leq 25$  in.

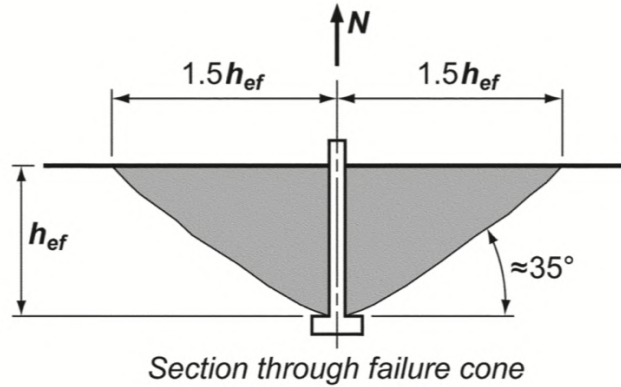


**Figure 2-2. Assumed geometry for concrete breakout cone (ACI Committee 318, 2014)**

The values of  $k_c$  and  $\alpha$  in equation (1) were determined from a large database of test results in uncracked concrete at the 5<sup>th</sup> percent fractile (Fuchs, et al., 1995), which were then adjusted for cracked concrete (Eligehausen, et al., 1995). For anchors with large embedments (11 in.  $\leq h_{ef} \leq$  25 in.), it has been shown that the values of  $k_c$  and  $\alpha$  developed for small embedment lengths can be overly conservative. Alternate values of  $k_c$  and  $\alpha$  have been adopted for these larger embedment lengths. To visualize the effect of these new factors, Figure 2-3 plots both models for two values of  $f'_c$ . The transition from one model to the next at  $h_{ef} = 11$  in. is clear.

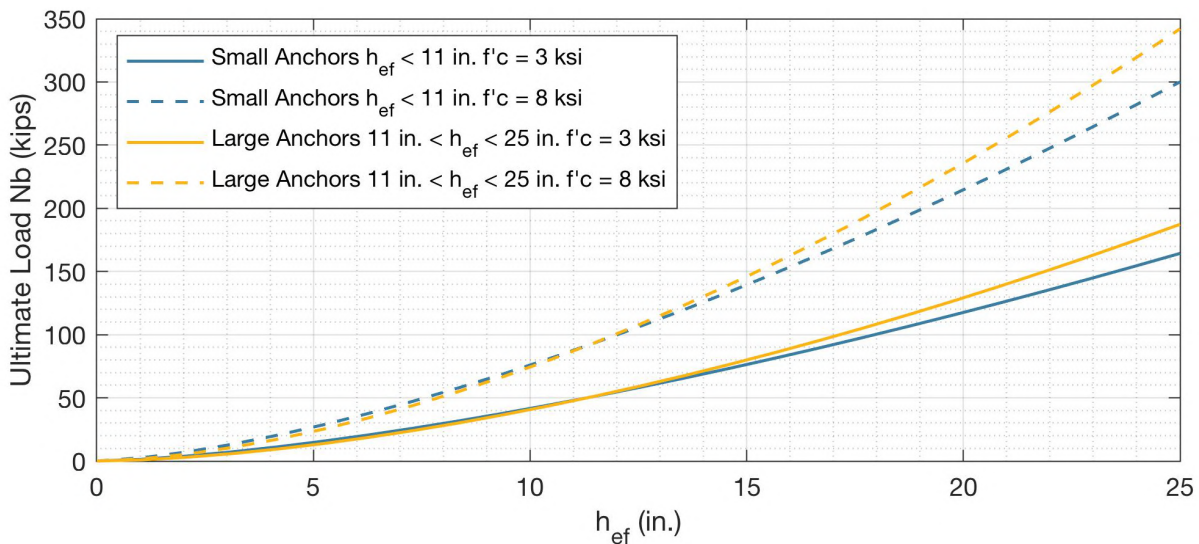


**Figure 2-3. ACI 318 Models for basic concrete breakout strength of a single anchor in tension in cracked concrete  $N_b$**

Equation (1) uses the concrete compressive strength as a proxy for tensile strength, elastic modulus, and other concrete properties. This simplification contributes to scatter in experimental results. Figure 2-4 shows a histogram of the ratio of measured to calculated anchor failure loads for 318 single headed anchor tests. The average value is 0.99 and there is significant scatter.

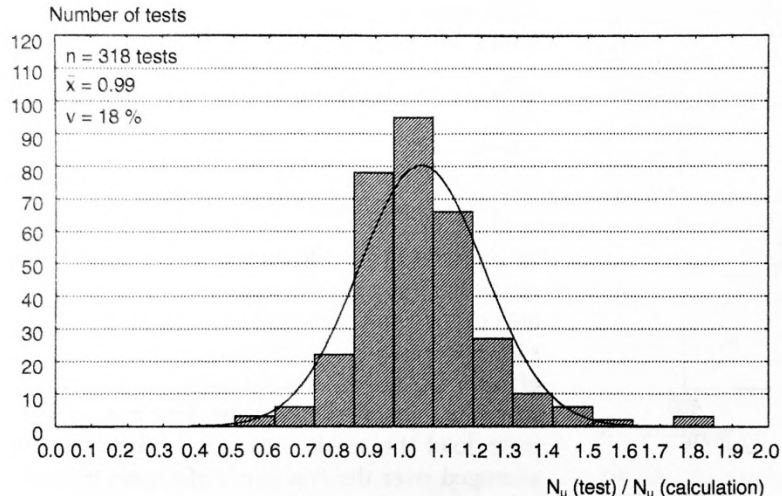


**Figure 2-4. Histogram of measured to calculated concrete cone failure loads for headed anchors subjected to concentric tension (Eligehausen, et al., 1992)**

Similarly, Figure 2-5 shows the ratio of measured to calculated anchor failure loads for varying concrete compressive strength. Significant scatter is observed. The lower 5% percentile of these results is used in ACI 318. A factor of 1.33 is commonly used to convert from a 5% to the 50% value.

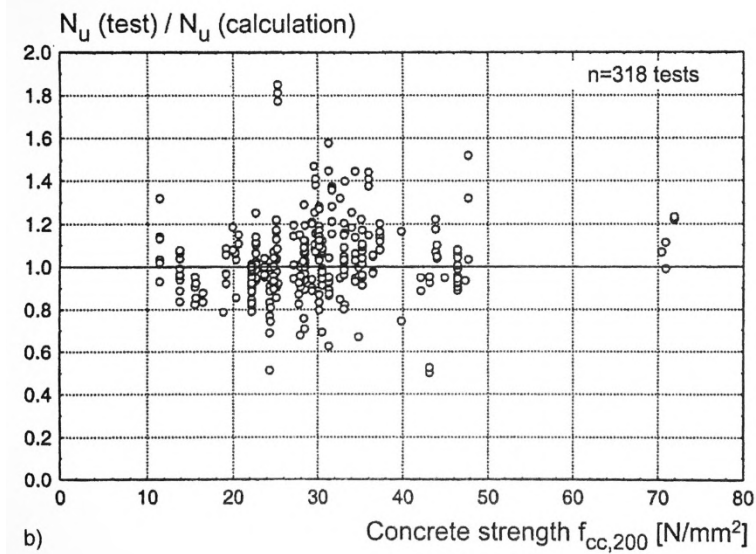


**Figure 2-5. Ratio of measured to calculated concrete cone failure loads for headed anchors subjected to tension as a function of concrete compressive strength (Eligehausen, et al., 1992)**

Once the basic concrete breakout strength of a single anchor in tension in uncracked concrete is determined ( $N_b$ ), ACI 318-14 requires that this value be modified to consider group effects, load eccentricity, edge distance, and concrete cracking as follows:

For a single anchor:

$$N_{cb} = \frac{A_{Nc}}{A_{Nco}} \Psi_{ed,N} \Psi_{c,N} \Psi_{cp,N} N_b \quad (2)$$

For a group of anchors:

$$N_{cbg} = \frac{A_{Nc}}{A_{Nco}} \Psi_{ec,N} \Psi_{ed,N} \Psi_{c,N} \Psi_{cp,N} N_b \quad (3)$$

Where:

$N_{cb}$ : Nominal concrete breakout strength in tension of a single anchor

$N_{cbg}$ : Nominal concrete breakout strength in tension of a group of anchors

$A_{Nc}$  : Projected failure area of a single anchor or group in question

$A_{Nco} = 9h_{ef}^2$  : Projected concrete failure area of a single anchor if not affected by edges

The term  $A_{Nc}/A_{Nco}$  is known commonly as the “group factor” and models the capacity drop due to the presence of multiple anchors with overlapping potential cone failure surfaces. The “group factor” also considers a drop in capacity due to limited edge distance where the potential cone failure surface might intersect a lateral face before reaching the top surface.

The  $\Psi$  factors in equations (2) and (3) consider additional modifications. The modification factor for anchor groups loaded eccentrically in tension,  $\Psi_{ec,N}$ , is calculated as:

$$\Psi_{ec,N} = \frac{1}{\left(1 + \frac{2e'_N}{3h_{ef}}\right)} \quad (4)$$

Where:

$\Psi_{ec,N}$ : Modification factor for anchor groups loaded eccentrically in tension

$e'_N$ : Load eccentricity

The modification factor for edge effects of anchor groups in tension,  $\Psi_{ed,N}$ , is calculated as:

$$\begin{aligned} &\text{If } c_{a,min} \geq 1.5h_{ef}, \text{ then } \Psi_{ed,N} = 1.0 \\ &\text{If } c_{a,min} < 1.5h_{ef}, \text{ then } \Psi_{ed,N} = 0.7 + 0.3 \frac{c_{a,min}}{1.5h_{ef}} \end{aligned} \quad (5)$$

Where:

$\Psi_{ed,N}$ : Modification factor for edge effects of anchors in tension

$c_{a,min}$ : Shortest edge distance of any anchor in the group

The modification factor for cracked concrete,  $\Psi_{c,N}$ , is taken as:

$$\begin{aligned}\Psi_{c,N} &= 1.25 \text{ for uncracked concrete under service loads} \\ \Psi_{c,N} &= 1.00 \text{ for cracked concrete under service loads}\end{aligned}\quad (6)$$

For cast-in-place anchors, the splitting modification factor is taken as  $\Psi_{cp,N} = 1.0$ .

Numerical simulations and experimental testing have shown that for the case of a base plate resisting moment and anchored to concrete with multiple anchor groups, equation (3) can be overly conservative. The bearing of the base plate on the surface of the potential concrete breakout cone (see Figure 2-6) apparently increases the anchor group capacity. Figure 2-7 shows multiple proposed modification factors to describe this effect as a function of the joint aspect ratio. The joint aspect ratio serves as a proxy to determine if the compressive bearing force from the column is acting on the potential cone surface or if it is too far away to have a significant effect. Trends in laboratory test data (Mahrenholtz, et al., 2014) are consistent with the modification factor proposed by Herzog (2015).

$$\Psi_M = 2.5 - \frac{z}{h_{ef}} \geq 1.0 \quad (7)$$

Where:

$\Psi_M$ : Modification factor for compressive bearing force

$z$ : Lever arm. Distance between tension in anchor group and resultants of compressive bearing pressure

$h_{ef}$ : Anchor group effective depth

This factor is not included in ACI 318-14. Similar factors are permitted in some European codes like CEN/TS 1992-4-1:2009.

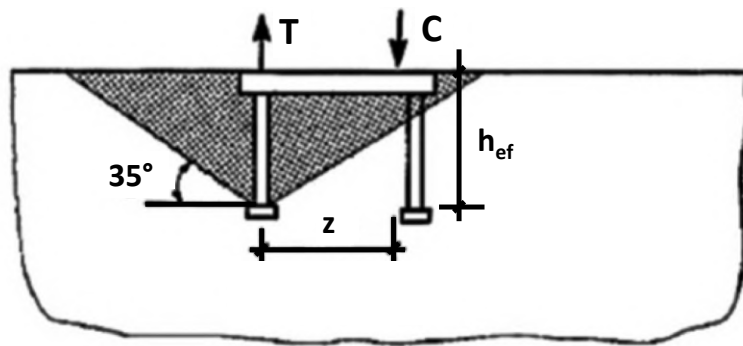


Figure 2-6. Influence of compressive force on concrete cone breakout capacity after Zhao (1993) (Eligehausen, et al., 2006)



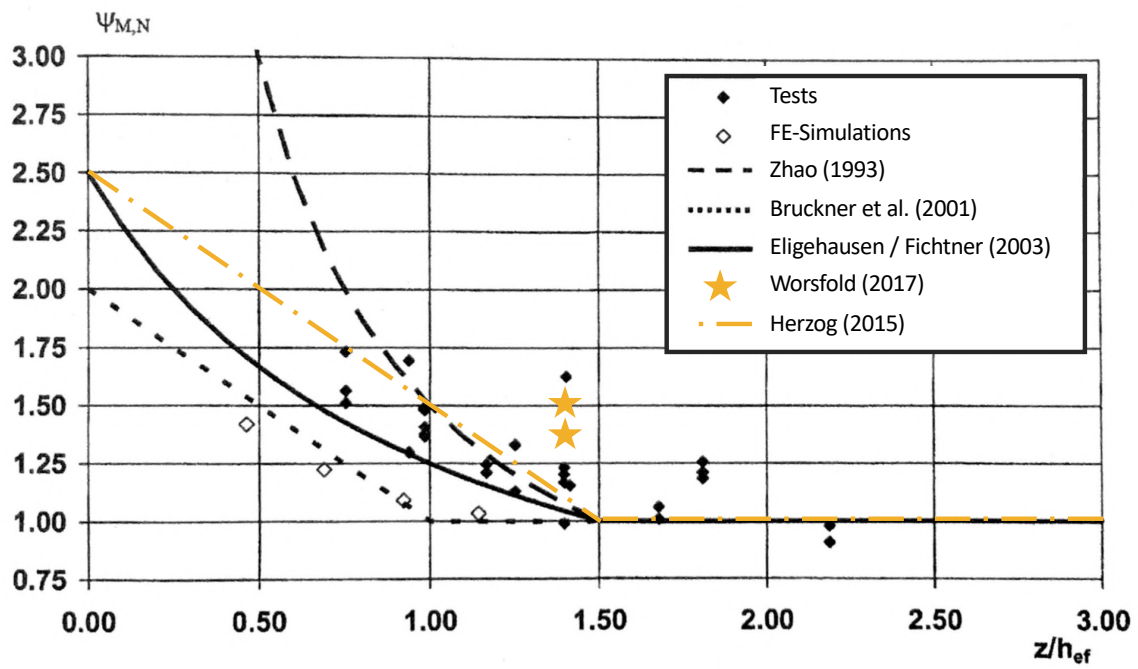


Figure 2-7. Influence of compression force on concrete cone breakout capacity as a function of ratio internal lever arm to embedment depth. Modified from (Eligehausen, et al., 2006)

## 2.2 STRUT-AND-TIE METHOD

Strength design of reinforced concrete members traditionally has been based on strengths of member cross sections. Such methods are especially effective for design of slender members at cross sections located away from geometric discontinuities or points of load application. They are less effective near geometric discontinuities and points of load application because of irregular stress flow near such discontinuities. The strut-and-tie method was developed to address the design of such discontinuity or D-regions.

Before a reinforced concrete member cracks, elastic analysis can adequately describe the force flow through a D-region. Once cracking has occurred, strut-and-tie models become a useful tool to describe the force flow through the member. A strut-and-tie model is created by devising a truss-type structure inside the reinforced concrete member that carries the loads from the point of application to the supports through elements that carry compression (struts), elements that carry tension (ties), and nodal zones at the intersection of struts and ties. Figure 2-8 illustrates a basic strut-and-tie model for a deep beam supporting a concentrated load. In a strut-and-tie model, all elements must be in equilibrium. Failure is defined when 1) a strut fails by crushing or by splitting longitudinally, 2) a tie yields in tension, or 3) a node fails to transfer the loads among the struts and ties that frame into it. Yielding of ties produces a ductile response and is, in principle, a preferred failure mode (Wight and MacGregor, 2009).

ACI 318-14 presents the strut-and-tie method as a set of requirements that can be used to design buildings using strut-and-tie models. The basic requirements are summarized in the following text.

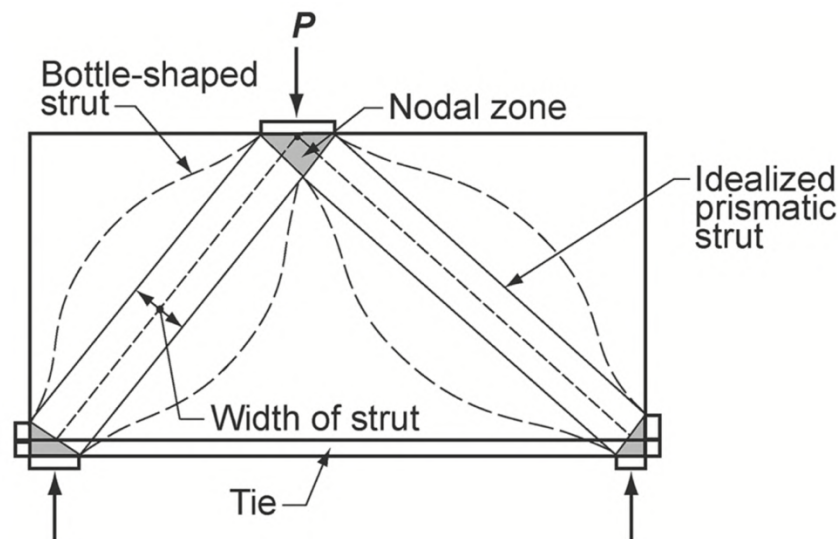


Figure 2-8. Strut-and-tie model example for a deep beam (ACI Committee 318, 2014)

### 2.2.1 Strength of Struts

According to ACI 318-14, each compression strut must satisfy:

$$\phi F_{ns} \geq F_{us} \quad (8)$$

Where:

$F_{us}$ : Compressive force carried by strut

$F_{ns}$ : Strut compressive strength

The strut compressive strength is calculated by:

$$F_{ns} = f_{ce} A_{cs} + A'_s f'_s \quad (9)$$

Where:

$f_{ce}$ : Effective compressive strength of concrete in a strut

$A_{cs}$ : Cross-sectional area at the end of the strut under consideration

$A'_s$ : Area of compression reinforcement along the length of the strut

$f'_s$ : Stress in the compression reinforcement at the nominal axial strength of the strut

The effective compressive strength depends on the strut coefficient and the concrete compressive strength:

$$f_{ce} = 0.85 \beta_s f'_c \quad (10)$$

The strut coefficient  $\beta_s$  is defined in Table 2-1 and depends on the strut geometry, the strut location, and the amount of reinforcement crossing the strut.

**Table 2-1. Strut coefficient  $\beta_s$  (ACI Committee 318, 2014)**

<b>Strut geometry and location</b>	<b>Reinforcement crossing a strut</b>	<b><math>\beta_s</math></b>
Struts with uniform cross-sectional area along length	NA	1.00
Struts located in a region of a member where the width of the compressed concrete at mid-length of the strut can spread laterally (bottle- shaped struts)	Satisfying 23.5	0.75
	Not Satisfying 23.5	$0.60\lambda$
Struts located in tension members or the tension zones of members	NA	0.40
All other cases	NA	$0.60\lambda$

### 2.2.2 Strength of Ties

According to ACI 318-14, each tension tie must satisfy:

$$\phi F_{nt} \geq F_{ut} \quad (11)$$

Where:

$F_{ut}$ : Tensile force carried by tie

$F_{nt}$ : Tie tensile strength

The tie tensile strength is calculated by:

$$F_{nt} = A_{ts} f_y \quad (12)$$

Where:

$f_y$ : Yield stress of longitudinal reinforcement in the tie

$A_{ts}$ : Area of longitudinal reinforcement in the tie

### 2.2.3 Strength of Nodal Zones

According to ACI 318-14, each nodal zone must satisfy:

$$\phi F_{nn} \geq F_{us} \quad (13)$$

Where:

$F_{us}$ : Compressive force carried by strut

$F_{nn}$ : Nominal compressive strength of nodal zone

The nodal zone compressive strength shall be calculated by:

$$F_{nn} = f_{ce} A_{nz} \quad (14)$$

Where:

$f_{ce}$ : Effective compressive strength of concrete at a face of a nodal zone

$A_{nz}$ : Area of node perpendicular to strut axis

The effective compressive strength of concrete at the outer face of a nodal zone shall be calculated as:

$$f_{ce} = 0.85 \beta_n f_c' \quad (15)$$

The node coefficient  $\beta_n$  is defined in Table 2-2.

**Table 2-2. Node coefficient  $\beta_n$  (ACI Committee 318, 2014)**

Configuration of nodal zone	$\beta_n$
Nodal zone bounded by struts, bearing areas, or both	1.00
Nodal zone anchoring one tie	0.80
Nodal zone anchoring two or more ties	0.60

## 2.3 BEAM-COLUMN JOINT DESIGN

Joint committee ACI-ASCE 352 has reported design recommendations for beam-column joints. Recommendations are given for proportioning, design, and reinforcement detailing of joints. In that report, a joint is defined as “that portion of the column within the depth of the deepest beam that frames into the column”. Joints are subdivided into type 1 (limited inelastic behavior required) and type 2 (inelastic behavior and large displacements expected).

Minimum confining requirements are given for type 2 connections. When using spiral reinforcement, the volumetric ratio should not be less than the larger of:

$$\begin{aligned}\rho_s &= 0.12 \frac{f'_c}{f_{yh}} \\ \rho_s &= 0.45 \left( \frac{A_g}{A_c} - 1 \right) \frac{f'_c}{f_{yh}}\end{aligned}\tag{16}$$

Where:

$f_{yh}$ : Yield strength of confining reinforcement not larger than 60 ksi

$A_g$ : Gross area of column section

$A_c$ : area of column core measured from outside edge to outside edge of either spiral or hoop reinforcement

Where rectangular hoops are used, the total cross-sectional area of hoops and ties in each direction should be at least equal to the larger of:

$$\begin{aligned}A_{sh} &= 0.3 \frac{s_h b_c'' f'_c}{f_{yh}} \left( \frac{A_g}{A_c} - 1 \right) \\ A_{sh} &= 0.09 \frac{s_h b_c'' f'_c}{f_{yh}}\end{aligned}\tag{17}$$

Where:

$s_h$ : Center-to-center spacing of hoops or hoops plus crossies

$b_c''$ : Core dimension of tied column, outside to outside edge of transverse reinforcement bars, perpendicular to the transverse reinforcement area  $A_{sh}$  being designed

The horizontal joint shear in both directions must satisfy:

$$\phi V_n \geq V_u\tag{18}$$

Where:

$$\phi = 0.85$$

$V_u$ : Horizontal joint shear demand

$V_n$ : Horizontal joint shear strength

The horizontal joint shear strength is calculated as:

$$V_n = \gamma \sqrt{f'_c} b_j h_c \quad (19)$$

Where:

$\gamma$ : Factor that depends on the joint geometry

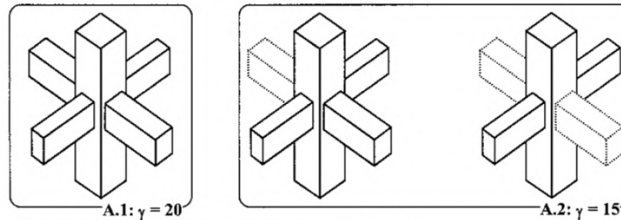
$b_j$ : Effective joint width

$h_c$ : Depth of the column in the direction of joint shear being considered

The  $\gamma$ -factor depends on the number and orientation of members framing into the joint as shown in Figure 2-9.

#### TYPE 2 CONNECTIONS

*CASE A: Two columns framing into the joint*



Note:  
Dashed lines represent either a frame member that does not exist or a member whose width is less than three-quarters of the width of the column or its total depth is less than three-quarters of the total depth of the deepest member framing into the joint

*CASE B: One column framing into the joint*

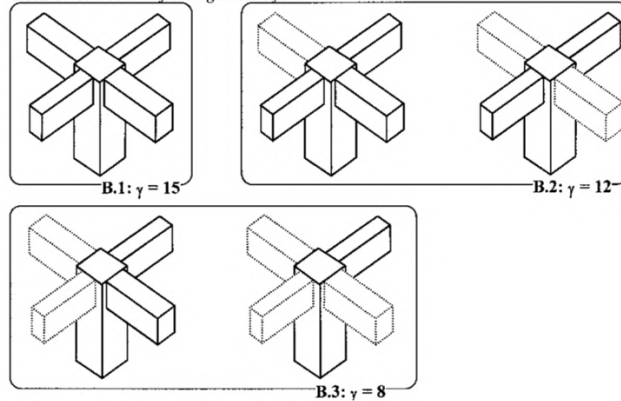
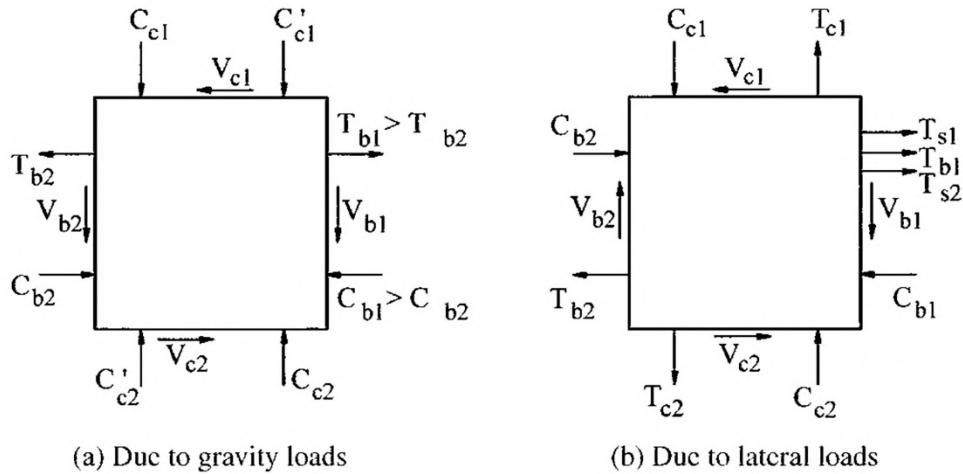


Figure 2-9. Type 2 connections  $\gamma$ -values (Joint ACI-ASCE Committee 352, 2002)

The horizontal shear demand is calculated with a free body diagram of the joint as shown in Figure 2-10.



**Figure 2-10. Joint forces at critical sections. T = tensile force; C = compressive force; V = shear force; subscript b for beam, subscript c for column; and subscript s for slab (Joint ACI-ASCE Committee 352, 2002)**

For a special moment frame, the beams are expected to provide the predominant yielding mechanism. Consequently, the beam forces acting on the faces of the joint are those corresponding to inelastic response in the beams. Tensile forces due to reinforcing bar yielding are to be multiplied by a factor not less than  $\alpha = 1.25$  for type 2 joints to consider material overstrength and strain hardening due to high inelastic demands. Additional requirements exist for the development of reinforcing bars terminating at a joint. Hooks or headed bars must pass through the joint and terminate no more than 2 in. from the far end of the hoops as shown in Figure 2-11.

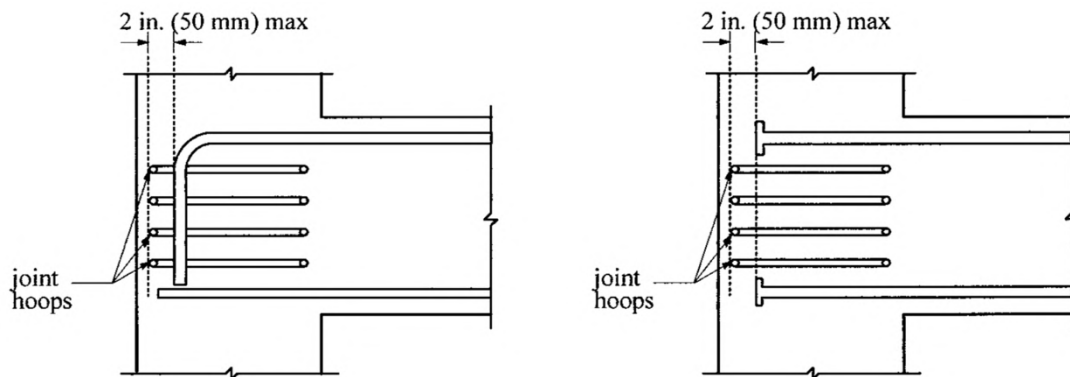


**Figure 2-11. Location of hooks and headed bars (Joint ACI-ASCE Committee 352, 2002)**



Also, the development length of hooks measured from the critical section must be at least:

$$l_{dh} = \frac{\alpha f_y d_b}{75 \sqrt{f'_c}} \quad (20)$$

The development length for headed reinforcement  $l_{dt}$  shall be at least  $\frac{3}{4}$  of the value calculated with equation (20). Additional restrictions exist depending on the spacing of developed bars and amount of confining reinforcement.

ACI 352 does not restrict the aspect ratio of beam-column joints. ACI 318-14, however, has some restrictions on the joint dimensions. The depth  $h$  of the joint (defined in Figure 2-12) shall not be less than one-half of depth  $h$  of any beam framing into the joint and generating joint shear as part of the seismic-force-resisting system. This restriction based on concerns about strength of a joint that resists joint shear through an excessively steep strut through the joint.

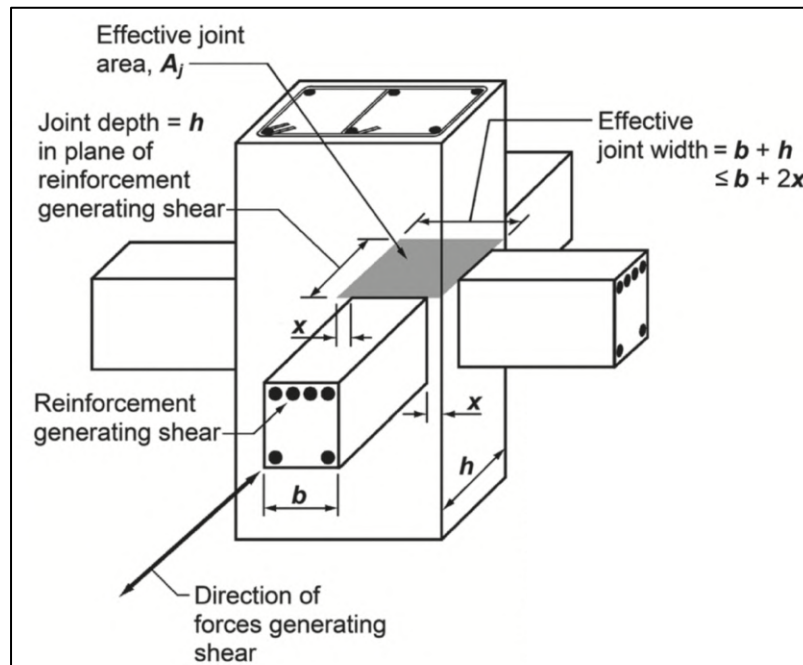


**Figure 2-12. Effective joint area (ACI 318-14 R18.8.4)**

Also, for the particular case of headed reinforcement terminating in an edge joint, the commentary of ACI 318-14 indicates that if the headed reinforcing bar is developed a distance greater than or equal to  $d/1.5$  (see Figure 2-13), then breakout is precluded and it is not required to check for breakout failure using Chapter 17.

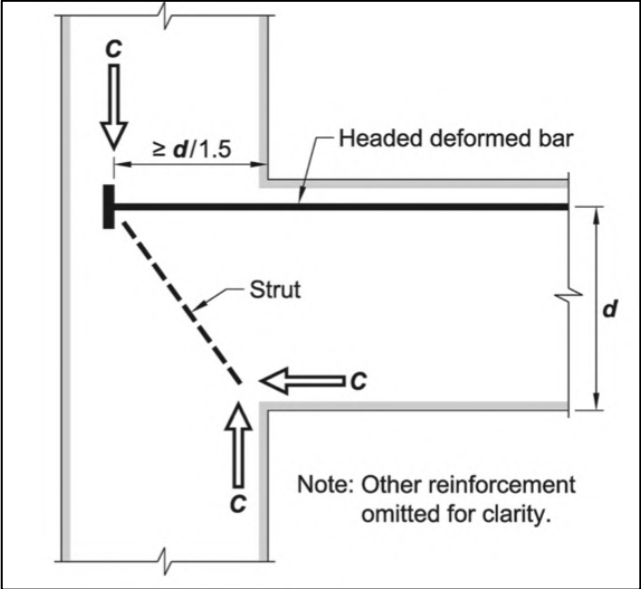


Figure 2-13. Breakout failure precluded in joint by keeping anchorage length greater than or equal to  $d/1.5$  (ACI 318-14 R25.4.4.2c)

## 3 SPECIMEN DESIGN

### 3.1 SPECIMEN REQUIREMENTS

A main purpose of the test specimen is to determine the failure mechanism and the moment transfer strength of a full-scale, column-foundation connection with cast-in-place headed anchors located away from the foundation edges. The main design considerations in selecting the test specimen details are as follows:

- All secondary failure modes will be designed to resist the expected yield capacity of the column. This includes all failure modes except concrete breakout, beam-column joint shear failure, and strut-and-tie failure.
- Specimen design will resemble as closely as possible some aspects of current practice on the West Coast of the United States.
- An ordinary concrete mixture will be used with no special additives (local materials will be used in accordance with the mixture design in APPENDIX B).
- A seismically compact wide-flanged section will be used for the column.
- No axial load will be applied to the column to isolate the effect of moment loading.
- The concrete slab will be large enough to allow breakout failure to occur without interference of boundary supports or slab edges.
- The specimen will be loaded cyclically and quasi-statically with a displacement driven loading protocol.
- The slab will not rest on the laboratory floor but will be simply supported (considered to be a more critical case without soil support).
- The column will be loaded in one lateral direction only.

### 3.2 SPECIMEN GEOMETRY AND DESIGN

Figure 3-1 shows a schematic representation of the test specimen and the loading frame. The footing slab is prestressed to the laboratory strong floor with nine 1-3/4" 150 ksi Williams Rods loaded to 170 kips each. The prestressing rods and supports are located at opposite ends of the footing with the footing spanning freely between the supports. Two actuators are attached to the column head at an angle of about 45° relative to the principal axis of the column cross section; these are programmed to displace the column in a unidirectional horizontal direction parallel to the web of the column.

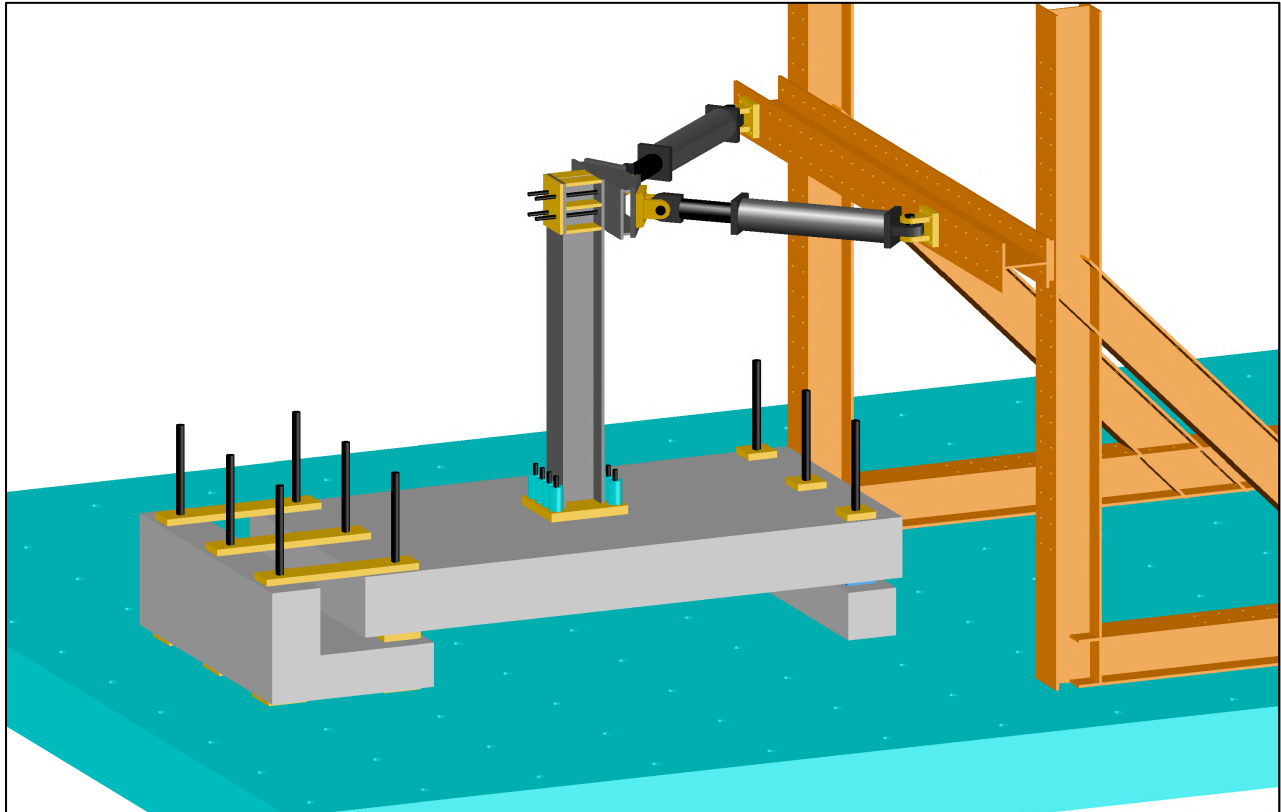


**Figure 3-1. Isometric view of specimen and loading frame**

Figure 3-2, Figure 3-3, Figure 3-4, Figure 3-5, Figure 3-6, and Figure 3-7 show the finalized specimen design. For complete as-built drawings see APPENDIX C.

As shown in Figure 3-2, the column consists of an A992 Grade 50 W12 x 112 steel section. The column is welded to a 24 in. by 21.5 in. by 2-3/4 in. A529 G50 steel base plate with a 5.25 in. by 5.25 in. by 2 in. A529 G50 shear lug (Figure 3-5). The base plate and shear lug are grouted in place to the concrete foundation. Four 1-1/2 in. diameter G105 anchor bolts on each side of the column pass through 1-5/8 in. (Figure 3-6) diameter holes in the base plate and are anchored in the concrete using heavy hex nuts an effective depth of 14.3 in.. The anchor bolts extend above the base plate a distance of 10 in. to accommodate placement of a load cell on each anchor bolt and to provide additional stretch length.

The foundation slab was designed such that the slab would have sufficient shear and moment strength to resist the expected connection moment transfer strength. Longitudinal reinforcement was designed assuming the reinforcement was Grade 60. However, to ensure that extensive flexural yielding would not occur if moment transfer strength was underestimated, the provided bars are Grade 100. Longitudinal and transverse reinforcement is provided at both the top and bottom of the slab. Details are in Figure 3-2.

The joint formed by the boundaries of the anchor bolts was confined by #4 Grade 60 hoops as shown in Figure 3-2, Figure 3-3, and Figure 3-7. Provision of hoops is consistent with the requirement of ACI 352 for hoops in beam-column joints, as well as requirements for distributed reinforcement in the ACI 318-14 strut-and-tie method.

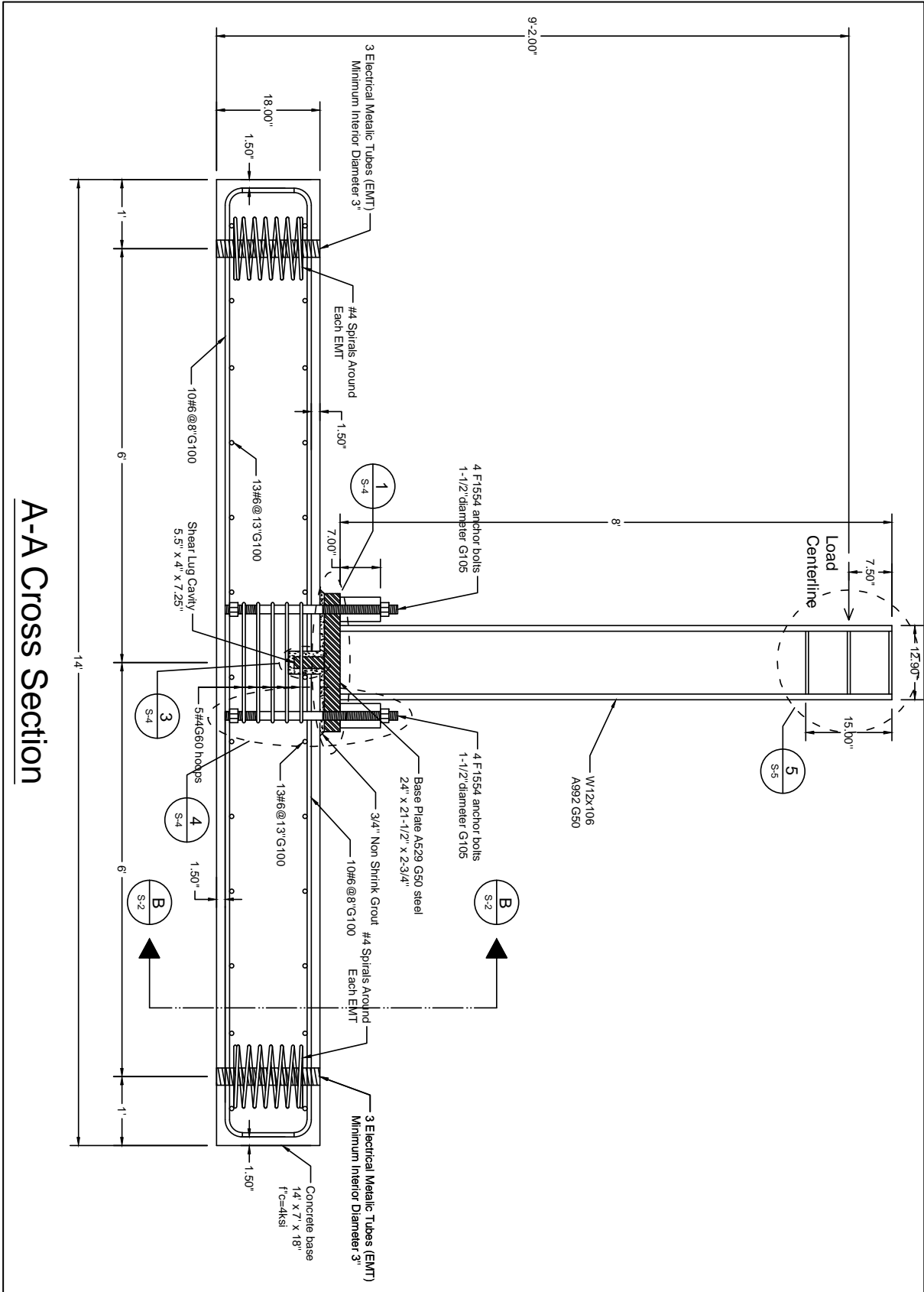


Figure 3-2. Elevation view of longitudinal cross section of specimen

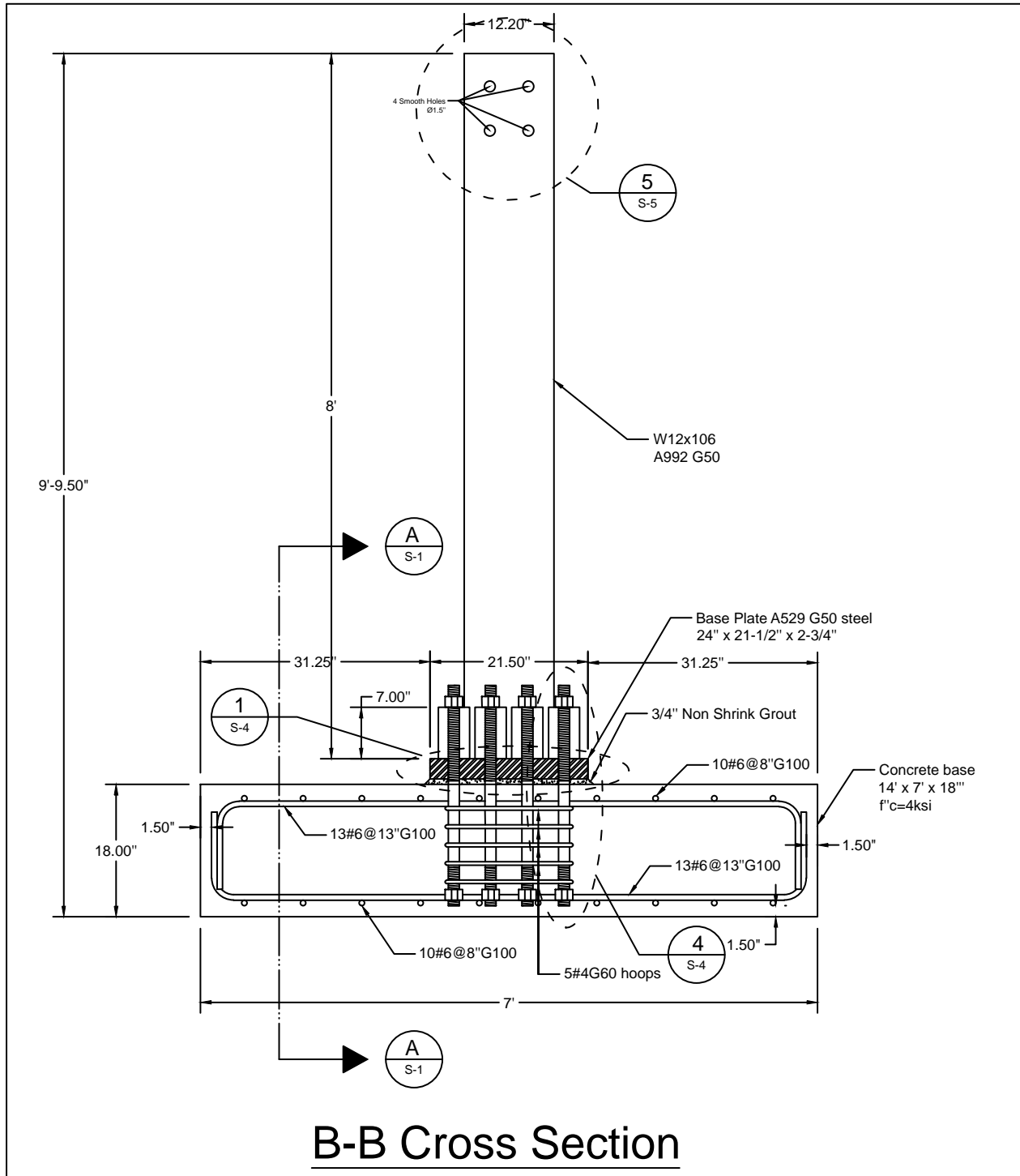


Figure 3-3. Elevation view of transverse cross section of specimen





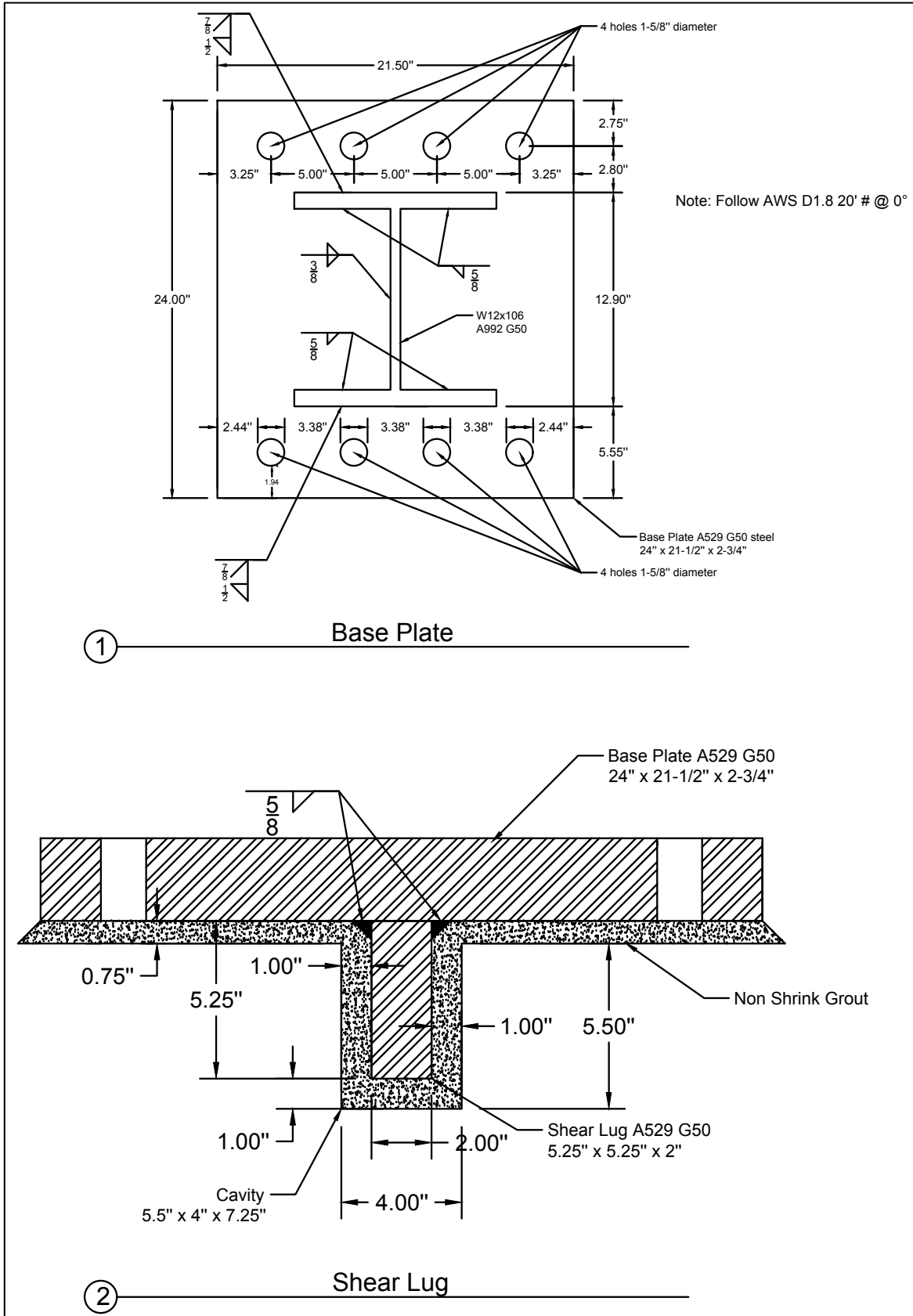
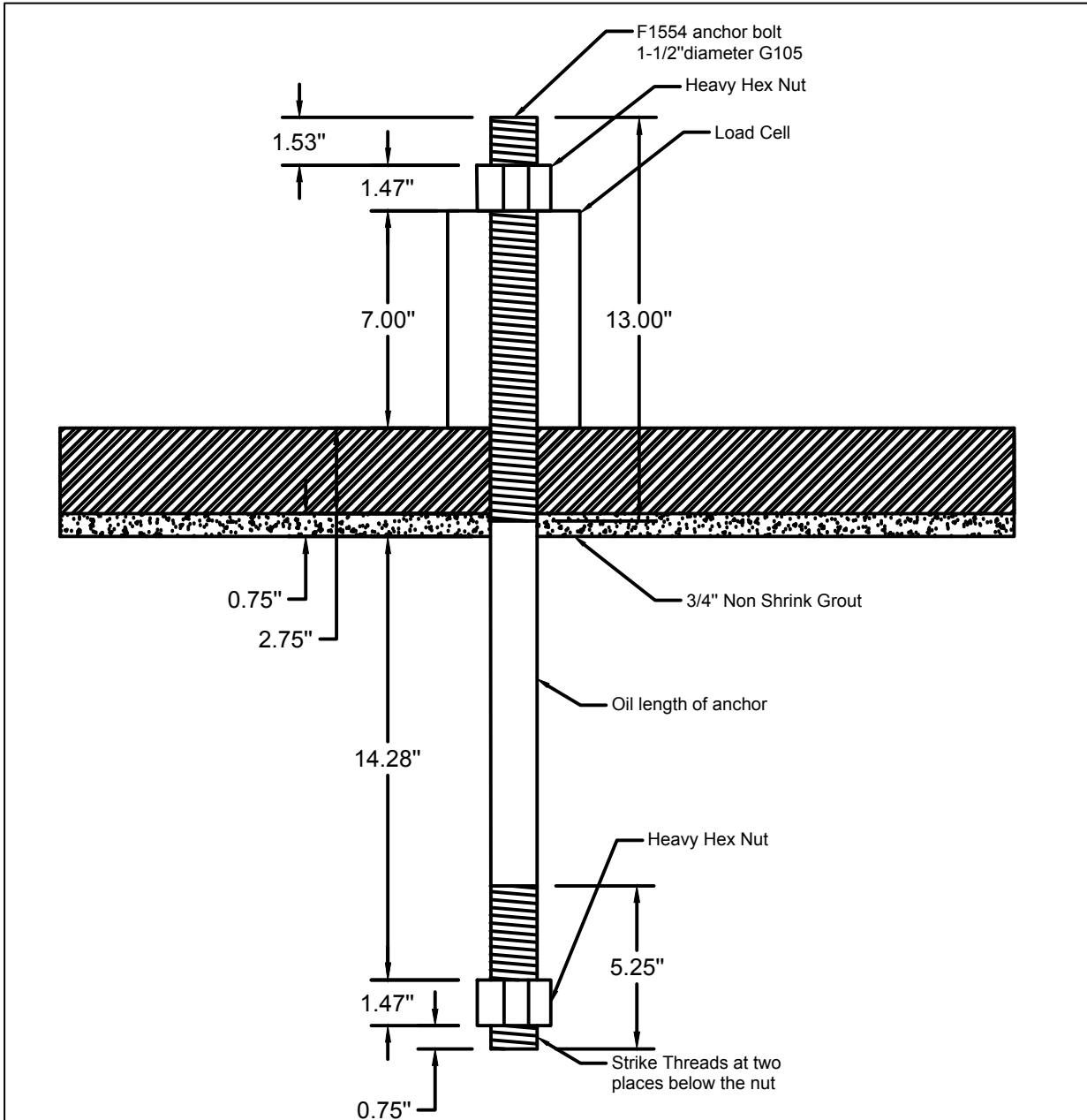
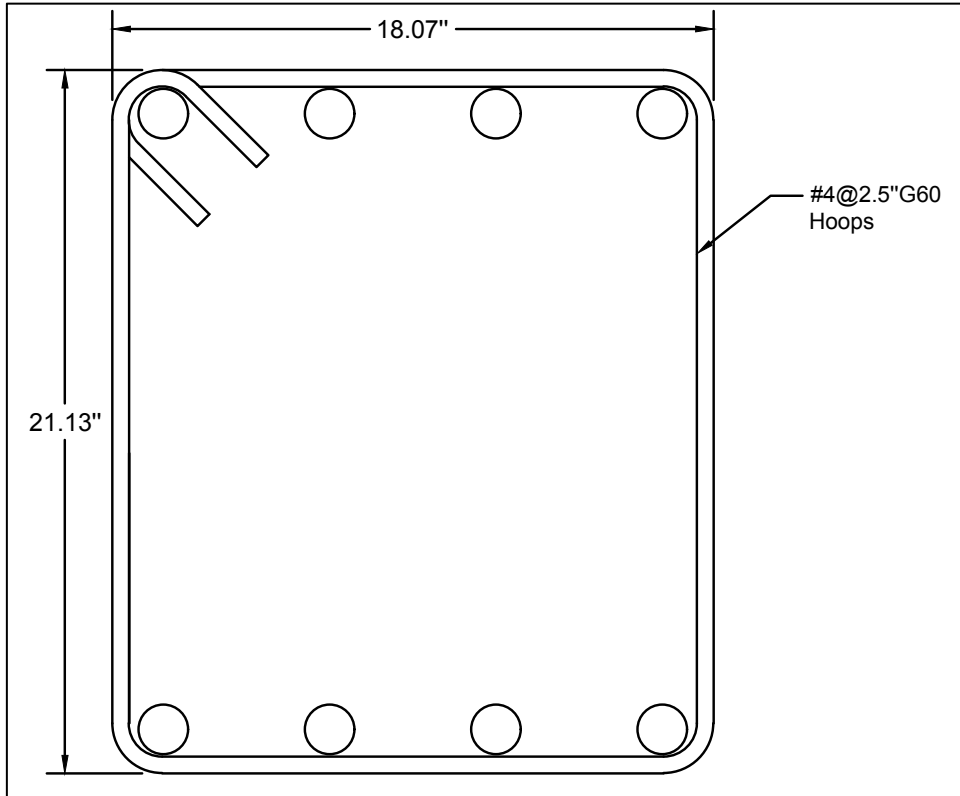


Figure 3-5. Details of specimen base plate and shear lug



**Figure 3-6. Detail of specimen anchor**



**Figure 3-7. Detail of specimen hoops**

### 3.3 CALCULATIONS OF CONNECTION STRENGTH

Detailed calculations of the strength of the column-foundation connection are presented below. Mean predictor equations and measured material properties are used. Also, the strength reduction factor for LRFD calculations is set as  $\phi = 1$  for all methods shown below. With the exception of moment transfer strength within the column-footing joint, all other strengths (for example, base plate yield, support failure, anchor yield, column failure, etc.) are designed such that the column will yield first. Detailed calculations for all other failure modes are shown in APPENDIX D.

#### 3.3.1 Concrete Breakout Equations (ACI 318-14 Ch.17 Anchoring to Concrete)

##### 3.3.1.1 Unmodified Concrete Breakout Equations

**Chap 17 ACI 318-14 Concrete Failure**

Notation

Input  

Output  

Condition check  

Input Data

<span style="background-color: yellow; border: 1px solid black; padding: 2px;"><math>f'c := 3700</math> psi</span>	Measured concrete strength on test day
<span style="background-color: yellow; border: 1px solid black; padding: 2px;"><math>nb := 4</math></span>	Number of bolts in tension
<span style="background-color: yellow; border: 1px solid black; padding: 2px;"><math>dia := 1.5</math> in.</span>	Anchor rod diameter
<span style="background-color: yellow; border: 1px solid black; padding: 2px;"><math>hef := 14</math> in.</span>	Anchor rod effective depth
<span style="background-color: yellow; border: 1px solid black; padding: 2px;"><math>kc := 24</math></span>	Preinstalled rods
<span style="background-color: yellow; border: 1px solid black; padding: 2px;"><math>\lambda a := 1</math></span>	Normal weight concrete

Group Factor

$$AN_{co} := 9 \cdot hef^2 = (1.76 \cdot 10^3) \text{ in.}^2$$

$$AN_c := (1.5 \cdot hef \cdot 2) \cdot (1.5 \cdot hef \cdot 2 + 15 \text{ in.}) = (2.39 \cdot 10^3) \text{ in.}^2$$

$$\frac{AN_c}{AN_{co}} = 1.36 \quad \text{Group factor}$$

Single anchor capacity

$$Nb1 := 24 \lambda a \cdot \sqrt{\frac{f'c}{\text{psi}}} \left( \frac{hef}{\text{in.}} \right)^{1.5} \frac{\text{kips}}{1000} = 76.5 \text{ kips}$$

$$Nb2 := 16 \lambda a \cdot \sqrt{\frac{f'c}{\text{psi}}} \left( \frac{hef}{\text{in.}} \right)^{\frac{5}{3}} \frac{\text{kips}}{1000} = 79.1 \text{ kips} \quad \text{If } 11 \text{ in.} < hef < 25 \text{ in. this equation is allowed}$$

$$Nb := \max(Nb1, Nb2) = 79.1 \text{ kips}$$

### ACI318-14 Modification Factors

$\psi_{ecN} := 1.0$  Eccentric loading for rods in tension

$\psi_{edN} := 1.0$  Not close to edge

$\psi_{cN} := 1.25$  Assumed uncracked

$\psi_{cpN} := 1.0$  For post-installed anchor rods only

### Breakout Capacity: ACI318-14 without any additional modifications

$$N_{cbg} := \frac{ANc}{ANco} \psi_{ecN} \cdot \psi_{edN} \cdot \psi_{cN} \cdot \psi_{cpN} \cdot Nb = 134 \text{ kips}$$

### Breakout Capacity: ACI318-14 mean prediction without additional modification factors

$f_{mean} := 1.33$  Factor to obtain mean predictor

$$N_{cbg}' := \frac{ANc}{ANco} \psi_{ecN} \cdot \psi_{edN} \cdot \psi_{cN} \cdot \psi_{cpN} \cdot Nb \cdot f_{mean} = 179 \text{ kips}$$

In the previous calculation, the factor for uncracked concrete is used ( $\psi_{cN} = 1.25$ ). This factor is based on research by Eligehausen and Balogh (1995). Normally, the concrete is considered as “uncracked” if service loads applied to the concrete prior to applying the anchor force are insufficient to crack the concrete. It could be argued, however, that the anchors in the test slab provide the main loading for the foundation slab and that these loads are sufficient to crack the concrete in the region of the anchors, and therefore the breakout strength should be based on cracked concrete. The breakout capacity calculation is repeated below considering the concrete to be cracked ( $\psi_{cN} = 1.00$ ).

### ACI318-14 Modification Factors

$\psi_{ecN} := 1.0$  Eccentric loading for rods in tension

$\psi_{edN} := 1.0$  Not close to edge

$\psi_{cN} := 1.25$  Assumed uncracked

$\psi_{cpN} := 1.0$  For post-installed anchor rods only

### Breakout Capacity: ACI318-14 without any additional modifications

$$N_{cbg} := \frac{ANc}{ANco} \psi_{ecN} \cdot \psi_{edN} \cdot \psi_{cN} \cdot \psi_{cpN} \cdot Nb = 134 \text{ kips}$$

### Breakout Capacity: ACI318-14 mean prediction without additional modification factors

$f_{mean} := 1.33$  Factor to obtain mean predictor

$$N_{cbg}' := \frac{ANc}{ANco} \psi_{ecN} \cdot \psi_{edN} \cdot \psi_{cN} \cdot \psi_{cpN} \cdot Nb \cdot f_{mean} = 179 \text{ kips}$$

### 3.3.1.2 Concrete Breakout Equations modified with Herzog (2015)

Through numerical studies, Herzog (2015) proposed a modification factor that considers the benefit of the compressive bearing of the base plate against the concrete cone surface. Mahrenholtz et al. (2014) reports laboratory tests that support the use of this modification factor. Calculations are shown below for the case of uncracked concrete.

**Herzog (2015) Compression Factor**

$z := 20 \text{ in.}$       Lever arm measured from anchor bolts to centroid of bearing pressure assuming uniform pressure distribution. (See base plate design in appendices)

$$\psi M := \max\left(2.5 - \frac{z}{h_{ef}}, 1\right) = 1.07$$

$$N_{cbg'} := \frac{AN_c}{AN_{co}} \psi_{ecN} \cdot \psi_{edN} \cdot \psi_{cN} \cdot \psi_{cpN} \cdot Nb \cdot f_{mean} \cdot \psi M = 191 \text{ kips}$$

Calculations are shown below for the case of cracked concrete.

**Herzog (2015) Compression Factor**

$z := 20 \text{ in.}$       Lever arm measured from anchor bolts to centroid of bearing pressure assuming uniform pressure distribution. (See base plate design in appendices)

$$\psi M := \max\left(2.5 - \frac{z}{h_{ef}}, 1\right) = 1.07$$

$$N_{cbg'} := \frac{AN_c}{AN_{co}} \psi_{ecN} \cdot \psi_{edN} \cdot \psi_{cN} \cdot \psi_{cpN} \cdot Nb \cdot f_{mean} \cdot \psi M = 153 \text{ kips}$$

### 3.3.2 Strut-and-Tie Model (ACI 318-14 Ch. 23 Strut-and-Tie Models)

A strut-and-tie model was developed to calculate the strength of the column-foundation connection. The model, shown in Figure 3-8, shows the force flow of the tensile load in the anchors ( $T_{anchors}$ ) and the base plate bearing pressure ( $C_{bp}$ ) into the slab. The tensile force in the anchors is kept in vertical equilibrium by struts spanning diagonally across the joint from the anchor heads to the base plate compressive bearing zone. The top node is kept in horizontal equilibrium by the tensile force from the surface reinforcing bars ( $T_{top}$ ). The bottom node cannot be kept in horizontal equilibrium directly by the tensile force in the bottom reinforcing bars ( $T_{bottom}$ ) because the anchor heads are not deep enough. Instead, the two bottom hoops serve as ties to keep the node in horizontal equilibrium. The tensile force in the hoops is transferred to the bottom slab reinforcing bars by a noncontact lap splice. The hoops are considered effectively anchored in the bottom node due to the fact that they are closed hoops with 135° hooks.

For this particular connection, tie failure of the hoops governs the design. The strut-and-tie model could be improved if the anchor head extended deeper into the slab, so as to place the bottom node at the same height as the bottom reinforcing bars. This way the load could follow a more direct path to the bottom reinforcing bars, avoiding the hoop ties which are the weakest link of the model. The slab would have to be thickened in this zone (forming a “pocket”) to accommodate the deeper anchors. The flexural compression zone in the slab is about 1 in. deep. This is considered insufficient to contribute in a significant way to the strut-and-tie model as it is small and far from the strut-and-tie nodes.

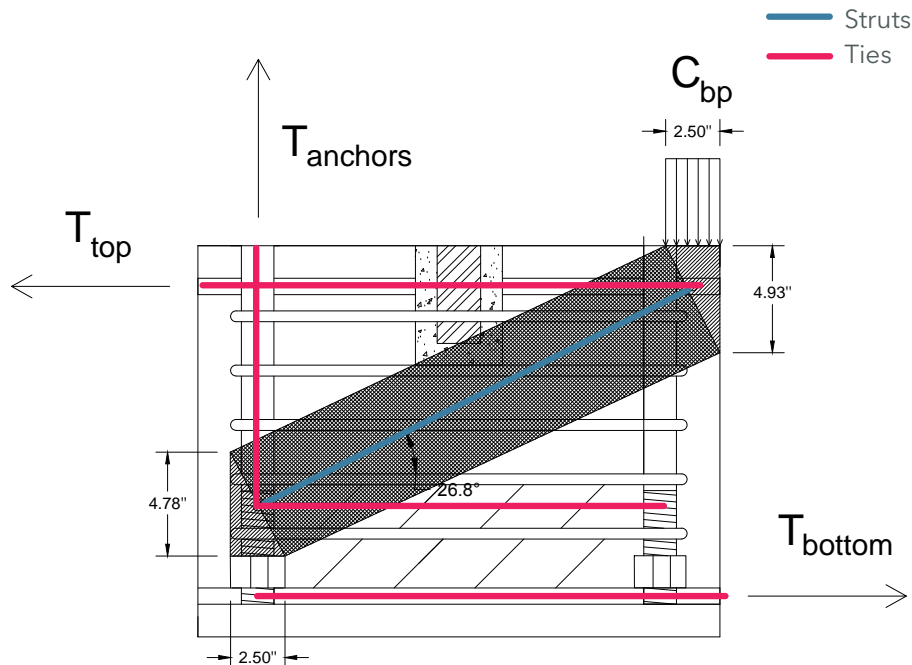


Figure 3-8. Strut-and-tie Model 1



The width of the struts is limited by the size of the anchor heads. Detailed calculations are shown below.

Input	Output	Condition Check
<u>Equilibrium</u>		
$T_{anchor} := C_{bp}$		
$T_{anchor} := Fns \cdot \sin(\theta)$		
$T_{top} := T_{bot}$		
$T_{top} := Fns \cdot \cos(\theta)$		
With:		
$T_{anchor}$	:	Total tensile force in anchor group
$C_{bp}$	:	Base plate bearing pressure
$\theta$	:	Angle between diagonal strut and horizontal ties
$Fns$	:	Compressive force in strut
$T_{top}$	:	Tensile force in top reinforcing bars
$T_{bot}$	:	Tensile force in bottom reinforcing bars
<u>Input Data</u>		
$D := 2.51 \text{ in.}$		Node depth out of plane. Taken as the average width of an anchor nut.
$\theta := 26.7^\circ$		Angle between strut and horizontal ties
<u>Hoop Confining</u>		
$As := 5 \cdot 0.2 \text{ in.}^2 = 1 \text{ in.}^2$		Total area of hoops legs confining an outer strut
$s := 2.8 \text{ in.}$		Hoop vertical spacing
$\frac{\left(\frac{As}{D \cdot s} \sin(\theta)\right)}{0.003} = 21.3$		Hoops are effective when this ratio is greater than 1

$\beta_{s1} := 0.75$  Outer struts are supported by hoops

$\beta_{s2} := 0.60$  Inner struts are not supported by hoops

### Strut Capacity

$wt := 4.78$  in. Height of bottom node

$wa := 2.51$  in. Width of bottom node

$ws := wt \cdot \cos(\theta) + wa \cdot \sin(\theta) = 5.4$  in. Strut width

$Acs := ws \cdot D = 13.5$  in.<sup>2</sup> Strut cross sectional area

$f'c := 3700$  psi Concrete measured strength

$Fns1 := 0.85 \cdot \beta_{s1} \cdot f'c \cdot Acs = 32$  kips Capacity of single outer strut

$Fns2 := 0.85 \cdot \beta_{s2} \cdot f'c \cdot Acs = 25.6$  kips Capacity of single inner strut

$T_{anchor} := \sin(\theta) (Fns1 + Fns2) \cdot 2 = 51.7$  kips Load in anchor group at strut failure

### Hoop Horizontal Ties

$T_{bot} := \cos(\theta) (Fns1 + Fns2) \cdot 2 = 103$  kips Horizontal component of strut force +

$Ats := 4 \cdot 0.2$  in.<sup>2</sup> = 0.8 in.<sup>2</sup> Tie area resisting horizontal force

$fy := 60000$  psi Tie nominal yield strength

$Fnt := Ats \cdot fy = 48$  kips Capacity of horizontal ties

The capacity of the hoop ties governs the design. Load in elements shown below.

$T_{bot} := Fnt = 48$  kips

$T_{anchor} := T_{bot} \cdot \tan(\theta) = 24.1$  kips

$T_{top} := T_{bot} = 48$  kip

$Fns := \frac{T_{anchor}}{\sin(\theta)} = 53.7$  kips

## Bottom Node

$$\beta_n := 0.80 \quad \text{C-C-T node}$$

$$f_{ce} := 0.85 \cdot \beta_n \cdot f'_c = (2.516 \cdot 10^3) \text{ psi}$$

### 1. Strut face

$$A_{nz} := D \cdot w_s = 13.5 \text{ in.}^2$$

$$F_{nn} := f_{ce} \cdot A_{nz} = 34.1 \text{ kips}$$

$$\frac{F_{nn} \cdot 4}{F_{ns}} = 2.54 \quad \text{Must be greater than 1}$$

### 2. Bottom face

$$A_{nz} := D \cdot 2.51 \text{ in.} = 6.3 \text{ in.}^2$$

$$F_{nn} := f_{ce} \cdot A_{nz} = 15.9 \text{ kips}$$

$$\frac{F_{nn} \cdot 4}{T_{\text{anchor}}} = 2.63 \quad \text{Must be greater than 1}$$

### 3. Left face

$$A_{nz} := D \cdot 4.78 \text{ in.} = 12 \text{ in.}^2$$

$$F_{nn} := f_{ce} \cdot A_{nz} = 30.2 \text{ kips}$$

$$\frac{F_{nn} \cdot 4}{F_{nt}} = 2.52 \quad \text{Must be greater than 1}$$

## Top Node

$$\beta_n := 0.80 \quad \text{C-C-T node}$$

$$f_{ce} := 0.85 \cdot \beta_n \cdot f'_c = (2.516 \cdot 10^3) \text{ psi}$$

### 1. Strut face

$$A_{nz} := D \cdot 5.53 \text{ in.} = 13.9 \text{ in.}^2$$

$$F_{nn} := f_{ce} \cdot A_{nz} = 34.9 \text{ kips}$$

$$\frac{F_{nn} \cdot 4}{F_{ns}} = 2.6 \quad \text{Must be greater than 1}$$

### 2. Top face

$$A_{nz} := D \cdot 2.51 \text{ in.} = 6.3 \text{ in.}^2$$

$$F_{nn} := f_{ce} \cdot A_{nz} = 15.9 \text{ kips}$$

$$\frac{F_{nn} \cdot 4}{T_{\text{anchor}}} = 2.63 \quad \text{Must be greater than 1}$$

### 3. Right face

$$A_{nz} := D \cdot 4.93 \text{ in.} = 12.4 \text{ in.}^2$$

$$F_{nn} := f_{ce} \cdot A_{nz} = 31.1 \text{ kips}$$

$$\frac{F_{nn} \cdot 4}{F_{nt}} = 2.59 \quad \text{Must be greater than 1}$$

### 3.3.3 Horizontal Joint Shear Equations (ACI 352R-02 Design of Beam-Column Connections)

The ACI 352-02 (2002) provisions were developed for design of beam-column joints in moment frames. Here we follow an engineering practice of extending the application of the provisions to the design of column-foundation connections in which the flexural tension forces from the column are developed through cast-in-place headed anchors. The ACI 352 design procedure requires definition of the dimensions of the concrete column entering the joint. Here we replace the actual steel column with a pseudo-concrete column. The outer column dimensions are assumed to be the center to center distance between the outermost anchors plus anchor bar diameter plus two hoop bar diameters plus twice the nominal cover of 1.5 in., resulting in 24 in. by 20.5 in. nominal column dimensions as shown in Figure 3-9. Also, the joint is confined with hoops as if it were a special moment frame joint. Detailed calculations of joint nominal strength are shown below.

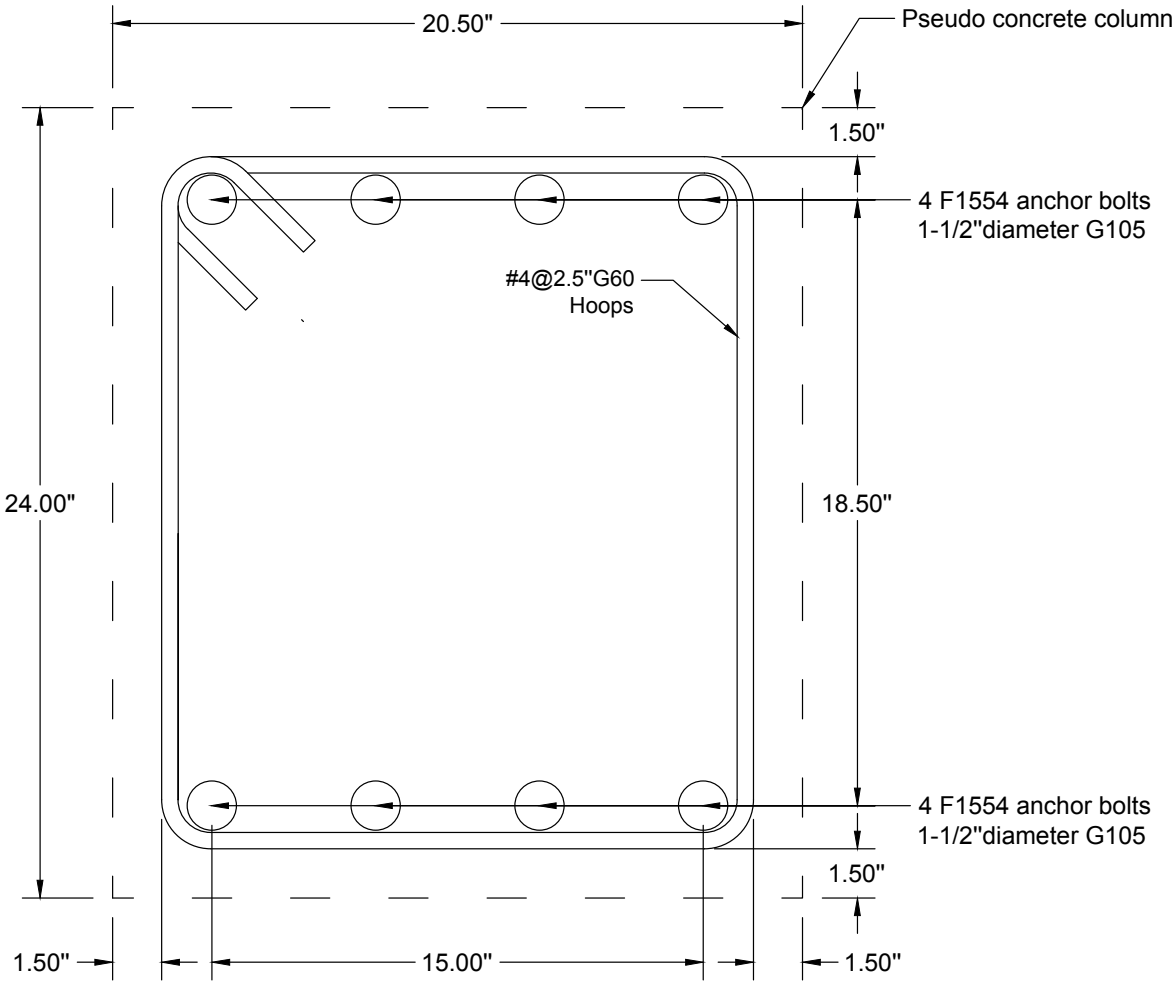


Figure 3-9. Pseudo concrete column dimensions

The nominal horizontal joint shear is calculated below:

Notation

Input

Output

Condition Check

Input Data

$P_u := 0.8$  kips

$M_u := 8700$  kips · in.

$V_u := 98.3$  kips

$f'_c := 3700$  psi

$n := 4$  Number of bolts in tension

Column Dimentions

Assumed as center to center of anchors + anchor diameter + confining steel+ 2 covers

$b_c := 15$  in. + 1.5 in. + 2 · 0.5 in. + 2 · 1.5 in. = 20.5 in. Out of plane width

$h_c := 18.5$  in. + 1.5 in. + 2 · 0.5 in. + 2 · 1.5 in. = 24 in. In plane horizontal width

$d_b := 1.5$  in. Anchor diameter

Horizontal Joint Capacity

$b'_b := 84$  in. Slab width

$b_b := \min(3 b_c, b_c + 1.5 h_c, b'_b) = 56.5$  in. Maximum width allowed by ACI-352

$b_j := \min\left(\frac{(b_b + b_c)}{2}, b_b, b_c\right) = 20.5$  in.

$\gamma := 15$  Joint coefficient for roof joint confined on all 4 sides

$V_{nh} := \gamma \cdot \sqrt{\frac{f'_c}{\text{psi}}} \cdot \frac{b_j}{\text{in.}} \cdot \frac{h_c}{\text{in.}} \cdot \frac{\text{kips}}{1000} = 449$  kips  
Nominal horizontal joint shear capacity

Using the free body diagrams in Figure 3-10, Figure 3-11, and Figure 3-12, the load in the anchor group ( $T_u$ ) can be written as a function of the horizontal joint shear as follows:

$$T_u = \frac{P*H}{L} + \frac{V_{uh}}{\alpha} * \left( \frac{Av}{Ah} \right) \quad (21)$$

Where:

$P$ : Force applied on column free end

$H$ : Vertical distance between point of load application and bottom surface of slab (see Figure 3-10)

$L$ : Horizontal distance between slab supports (see Figure 3-10)

$V_{uh}$ : Ultimate horizontal joint shear

$\alpha$ : Reinforcement yield strength factor

$Av$ : Vertical joint area (cover included)

$Ah$ : Horizontal joint area (cover included)

The force applied on the column free end ( $P$ ) can also be written as a function of the variables shown above:

$$P = \frac{V_{nh}}{\frac{2\alpha}{0.9d} \left( \frac{H(L-h_c)}{2} - \frac{t}{4} \right) + \frac{\alpha}{c} - 1} \quad (22)$$

Where:

$t$ : Slab thickness

$h_c$ : in plane horizontal joint width

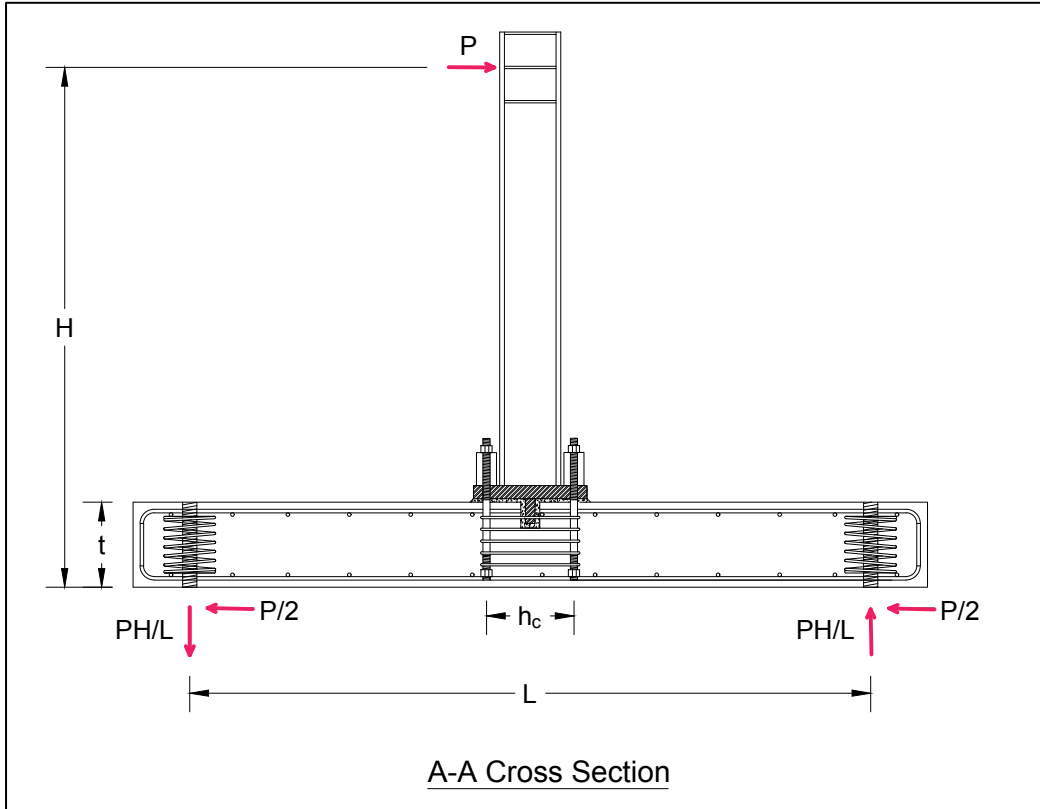


Figure 3-10. Free body diagram complete specimen

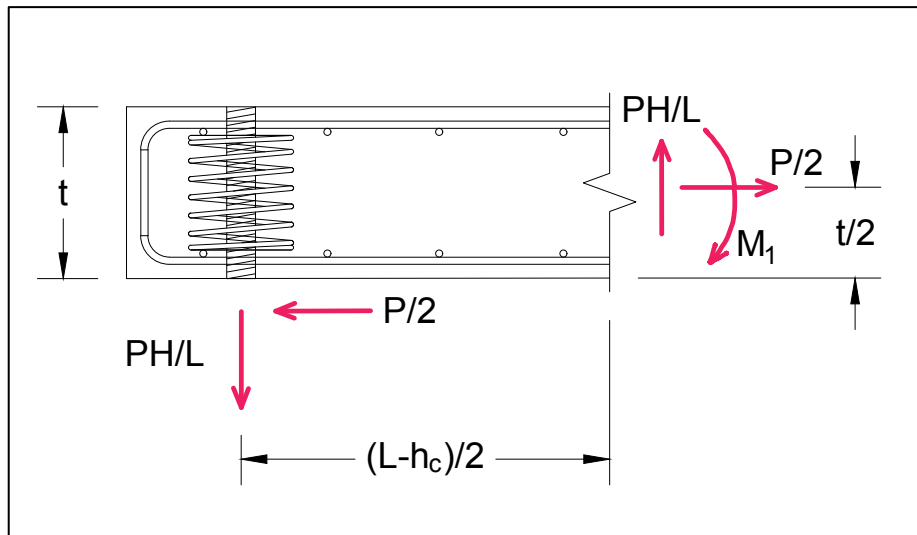


Figure 3-11. Free body diagram internal forces acting on node



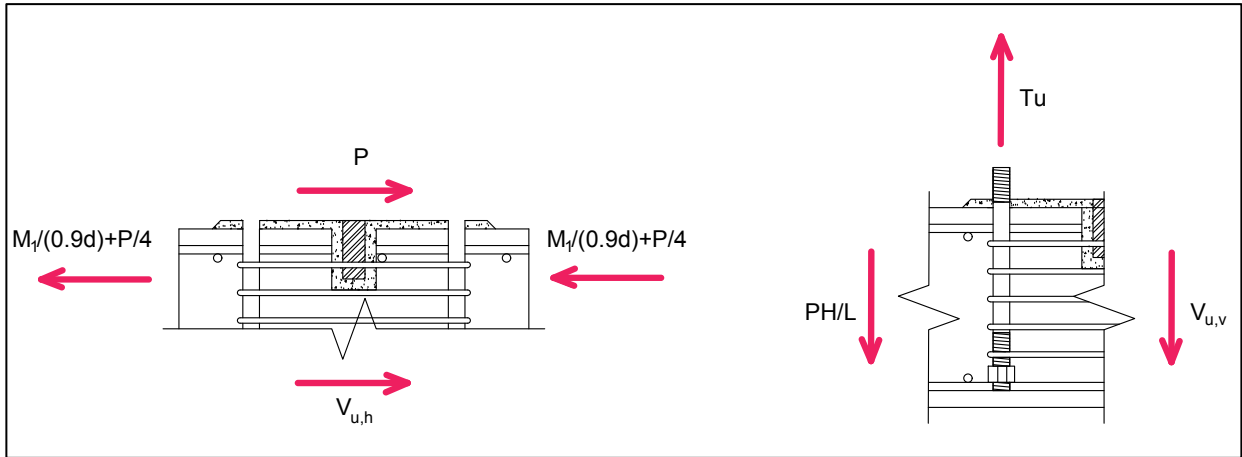


Figure 3-12. Free body diagrams for horizontal (left) and vertical joint shear (right)

The load in the anchor group at joint failure ( $T_u$ ) is calculated below using equations (21) and (22):

$H := 110 \text{ in.}$	Vertical distance between point of load application and bottom surface of slab
$L := 144 \text{ in.}$	Horizontal distance between slab supports
$t := 18 \text{ in.}$	Slab thickness
$\alpha := 1.0$	Factor for nonlinear behaviour
$h_c = 24 \text{ in.}$	In plane horizontal node width
$d := t - 1.5 \text{ in.} - 0.75 \frac{\text{in.}}{2} = 16.1 \text{ in.}$	Distance from extreme compression fiber to centroid of longitudinal reinforcement
$P := \frac{V_{nh}}{\frac{2 \alpha}{0.9 d} \left( \frac{H}{L} \frac{(L - h_c)}{2} - \frac{t}{4} \right) + \frac{\alpha}{2} - 1} = 86.4 \text{ kips}$	
	Load applied to column free end
$A_v := t \cdot 20.5 \text{ in.} = 369 \text{ in.}^2$	Vertical joint area (cover included)
$A_h := 20.5 \text{ in.} \cdot 24 \text{ in.} = 492 \text{ in.}^2$	Horizontal joint area (cover included)
$T_u := \frac{P \cdot H}{L} + \frac{V_{nh}}{\alpha} \cdot \left( \frac{A_v}{A_h} \right) = 403 \text{ kips}$	
	Load in anchor group

A load of 403 kips is expected in the anchor group when the horizontal joint shear reaches the ultimate value of 449 kips.

### 3.3.4 Summary of Connection Capacities

Table 3-1 lists the summary of the ultimate loads in the anchor group based on the different design methodologies discussed previously.

**Table 3-1. Summary of mean ultimate load in anchor group using different failure criteria with no safety factor**

Failure Criteria	Anchor Group Load (kips)	Notes
1. Breakout uncracked	179	Unmodified
1. Breakout cracked	143	Unmodified cracked
1. Breakout uncracked + Herzog (2015)	191	Modified by Herzog (2015)
1. Breakout cracked + Herzog (2015)	153	Modified by Herzog (2015) cracked
2. Strut-and-tie model	24	4 struts, one per anchor head
3. Beam-Column Joint	403	Assumed $\gamma = 15$ roof connection
Note: $\phi=1$ , mean predictor value $f_{\text{median}} = 1.33$		

## 4 TEST SET-UP

As can be seen in Figure 4-1, the 18 in. thick foundation slab was placed on concrete supports on both ends. To prevent sliding during the test, the slab was prestressed to the laboratory floor with nine 1-3/4" 150 ksi Williams Rods loaded to 170 kips each. Two actuators were attached to the column near its free end, oriented at approximately 45° from the longitudinal axis and programmed to move the column longitudinally with no transverse displacement.

Before initiation of loading, each anchor was prestressed to a torque of 60 lb-ft in the following order: one, eight, four, five, two, seven, three, and six (see Figure 4-5 for anchor numbering). Each anchor was then prestressed to a torque of 120 lb-ft following the same order. The initial load in the anchor groups can be seen in Figure 5-12 before the external loading begins.

See Figure 3-1 to Figure 3-6 for drawings with dimensions. See APPENDIX G for photographs of the construction process and test set-up.



Figure 4-1. Specimen set-up and instrumentation

## 4.1 INSTRUMENTATION

A total of 80 instruments measuring at a frequency of 5 Hz were used to measure the specimen behavior during testing. Figure 4-1 shows the final test set-up and instrumentation. The instruments used were:

- 41 strain gages attached to reinforcing steel
- 3 wire pots
- 10 load cells
- 26 linear potentiometers

Fourteen strain gages were placed on longitudinal reinforcing bars. Of these, seven were placed on the top layer and seven on the bottom layer of the foundation slab as can be seen in the sketches in Figure 4-2. Five strain gages were placed on the transverse reinforcement on the top layer only (Figure 4-3). Finally, eight strain gages were placed on the hoops confining the anchors. The second hoop from the top and the second hoop from the bottom were instrumented (Figure 4-2). One gage was placed on each leg of the hoop (Figure 4-4). The main goal of the gages was to determine if reinforcement yielding occurred before the failure of the connection.

Three wire pots were used to track the movement of the free end of the column at the elevation of the actuators in the X, Y, and Z directions to monitor and enforce unidirectional movement (Figure 4-2 and Figure 4-3).

A load cell was placed on each anchor (Figure 4-5).

Twenty linear potentiometers were placed on the slab surface to measure the vertical displacements during cyclic loading (Figure 4-6). Finally, six linear potentiometers were used to monitor support movement as a check that the test specimen was fixed to the laboratory strong floor as intended. Specimen horizontal movement was measured relative to the supports and relative to the laboratory strong floor, while support uplift was measured at the supports.



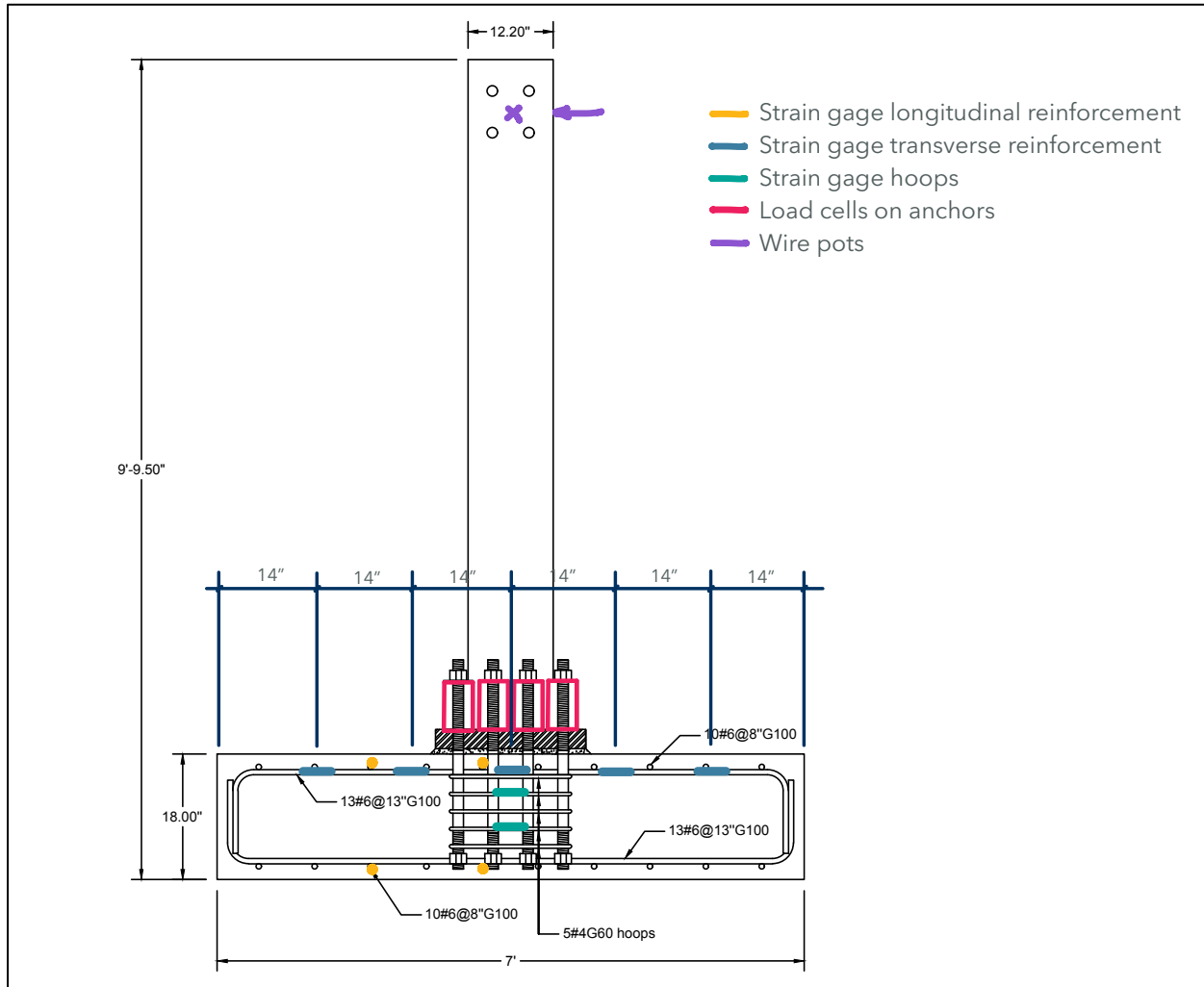


**Figure 4-3. Cross section B-B of specimen showing instrumentation**

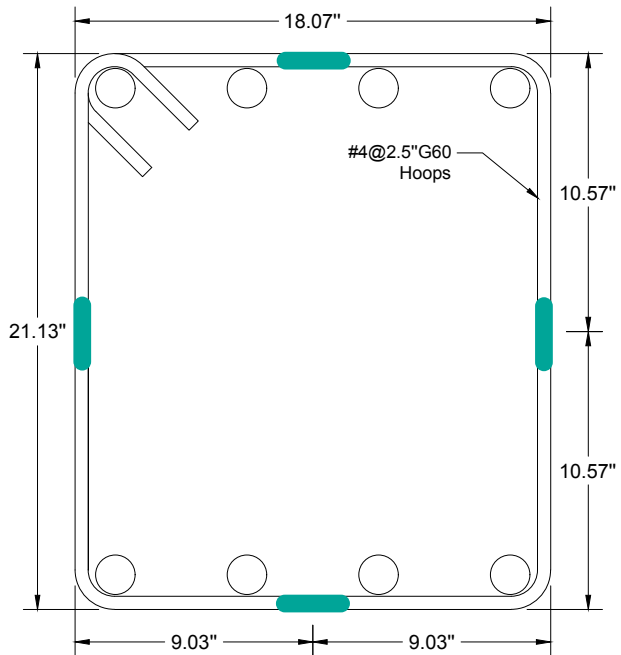


Figure 4-4. Sketch of strain gages on second-from-top and second-from-bottom hoops

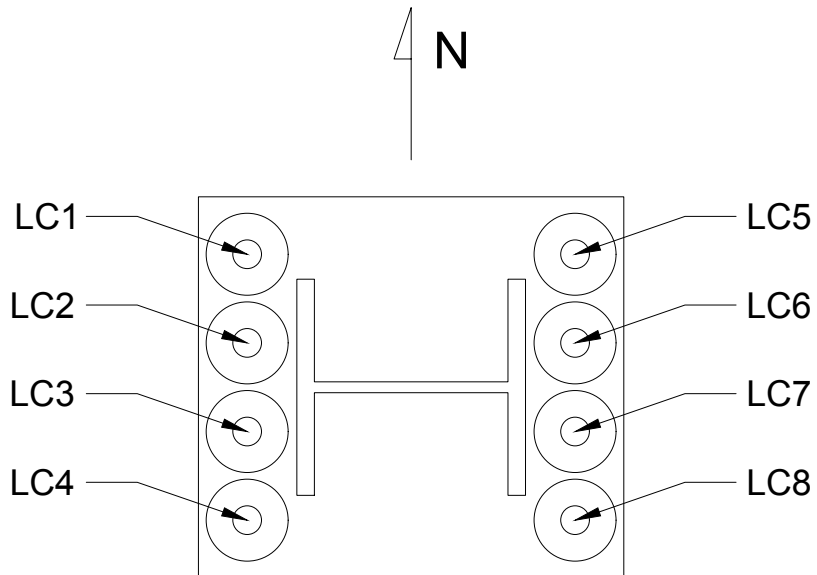


Figure 4-5. Plan view of base plate showing numbering of anchors and load cells





## 4.2 LOADING PROTOCOL

The loading protocol was derived from the recommendation of FEMA-461 (2007). The top of the column was subjected to cycles of imposed displacement in the longitudinal direction of increasing amplitudes shown in Table 4-1. Two 45° actuators attached to the column were programmed to minimize transverse displacements. Displacements were imposed at a uniform rate, traveling from zero to maximum displacement in 30 s. As can be seen in Figure 4-7, two complete cycles were applied at each amplitude before continuing to the next amplitude.

**Table 4-1. Amplitude of displacement-controlled loading protocol**

Cycle	$\delta$ (in.)
1	0.11
2	0.15
3	0.21
4	0.29
5	0.41
6	0.58
7	0.81
8	1.13
9	1.58
10	2.05
11	2.53
12	3.00
13	3.48
14	3.95

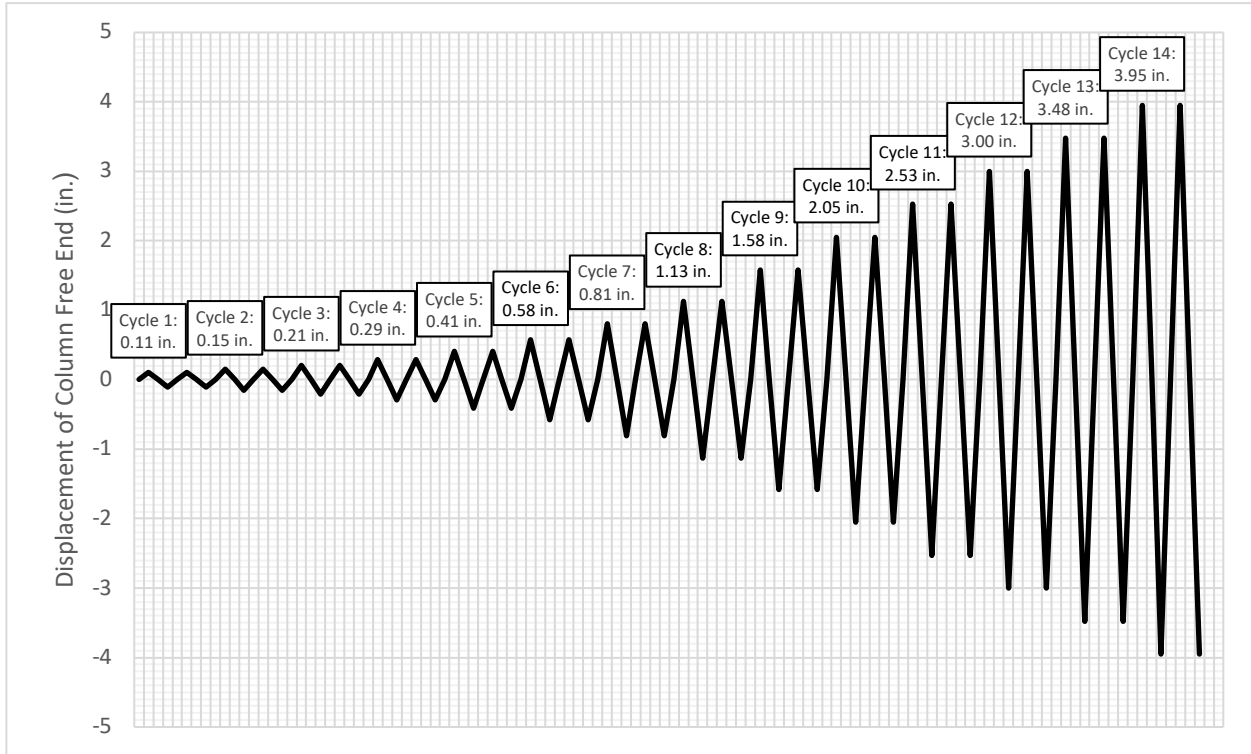


**Figure 4-7. Loading protocol imposed to column free end modified from FEMA-461 (2007)**

The loading was paused at the first positive and negative peak of each new displacement target to document crack size and propagation. After large cracks had formed, the loading was paused not at the peaks but post-peak at about 80% of the maximum displacement. Figure 4-8 shows how the loading progressed with time showing the pauses.

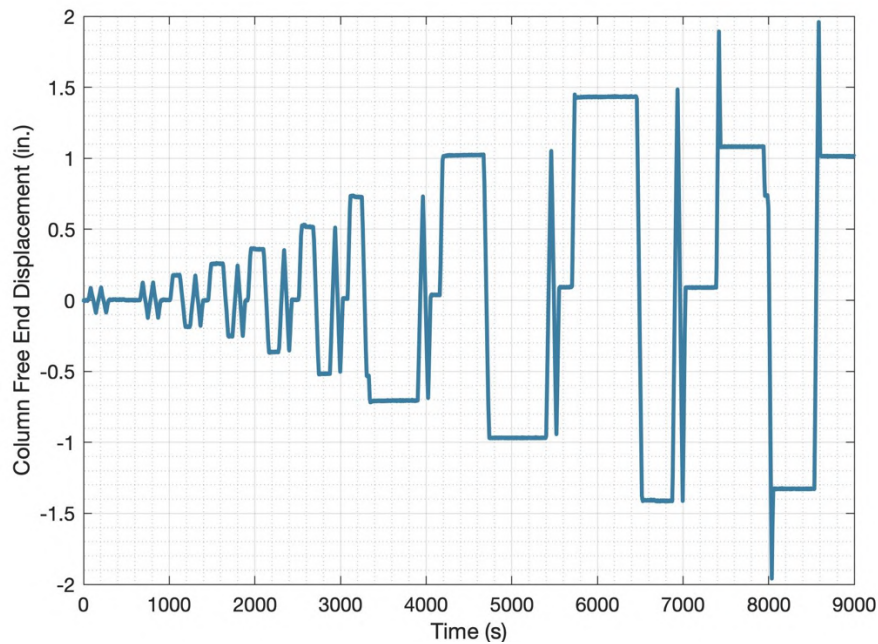


**Figure 4-8. Column free end displacement versus time triangulated with wire pots attached to the column free end, pauses in loading appear as horizontal lines**

# 5 RESULTS

## 5.1 CRACK PATTERNS

As was described in section 4.2, the test was paused at peak displacements to draw the emerging crack patterns. The cracks formed at each load cycle were identified with different colors. Figure 5-1 shows the crack patterns at the end of the test on the top surface of the slab and the north and south lateral faces of the slab.

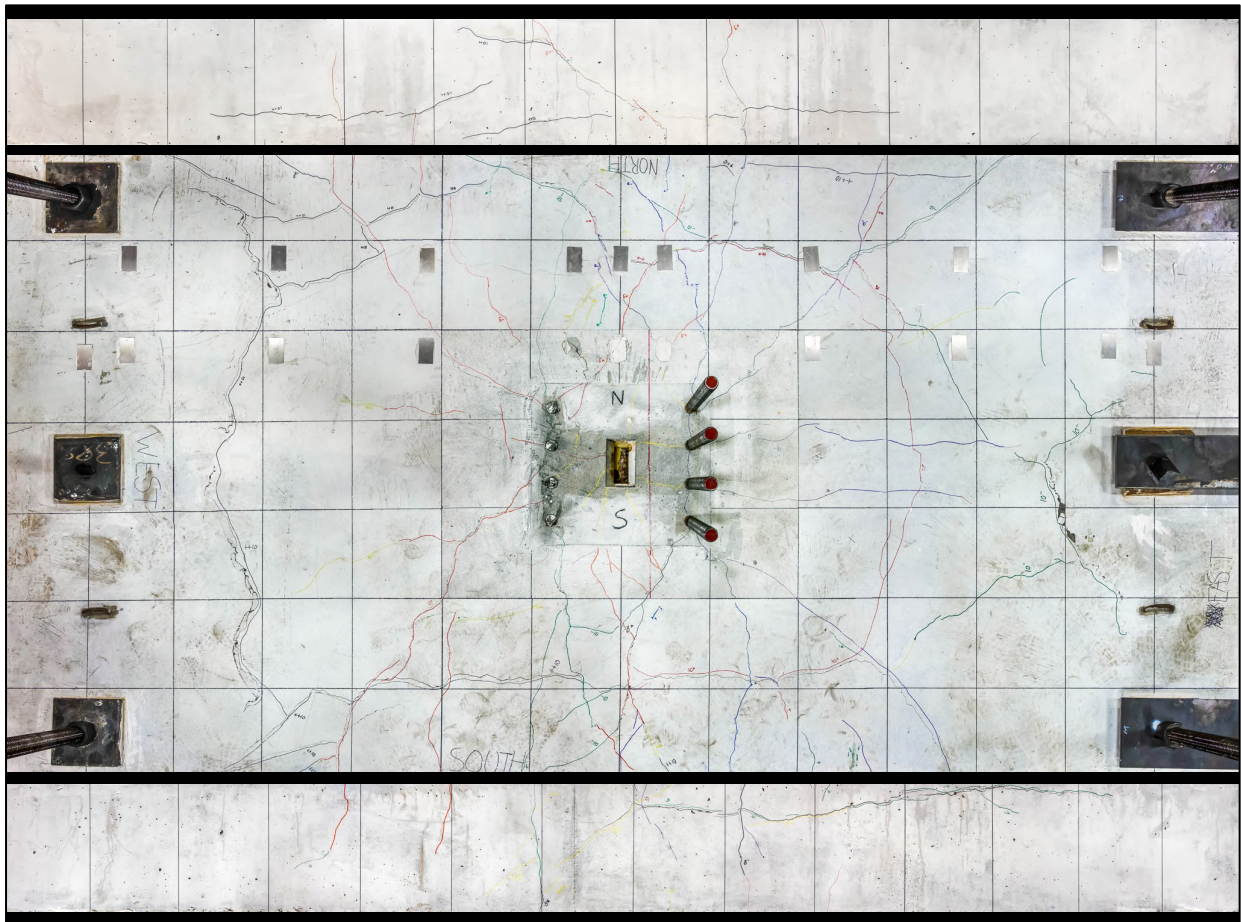
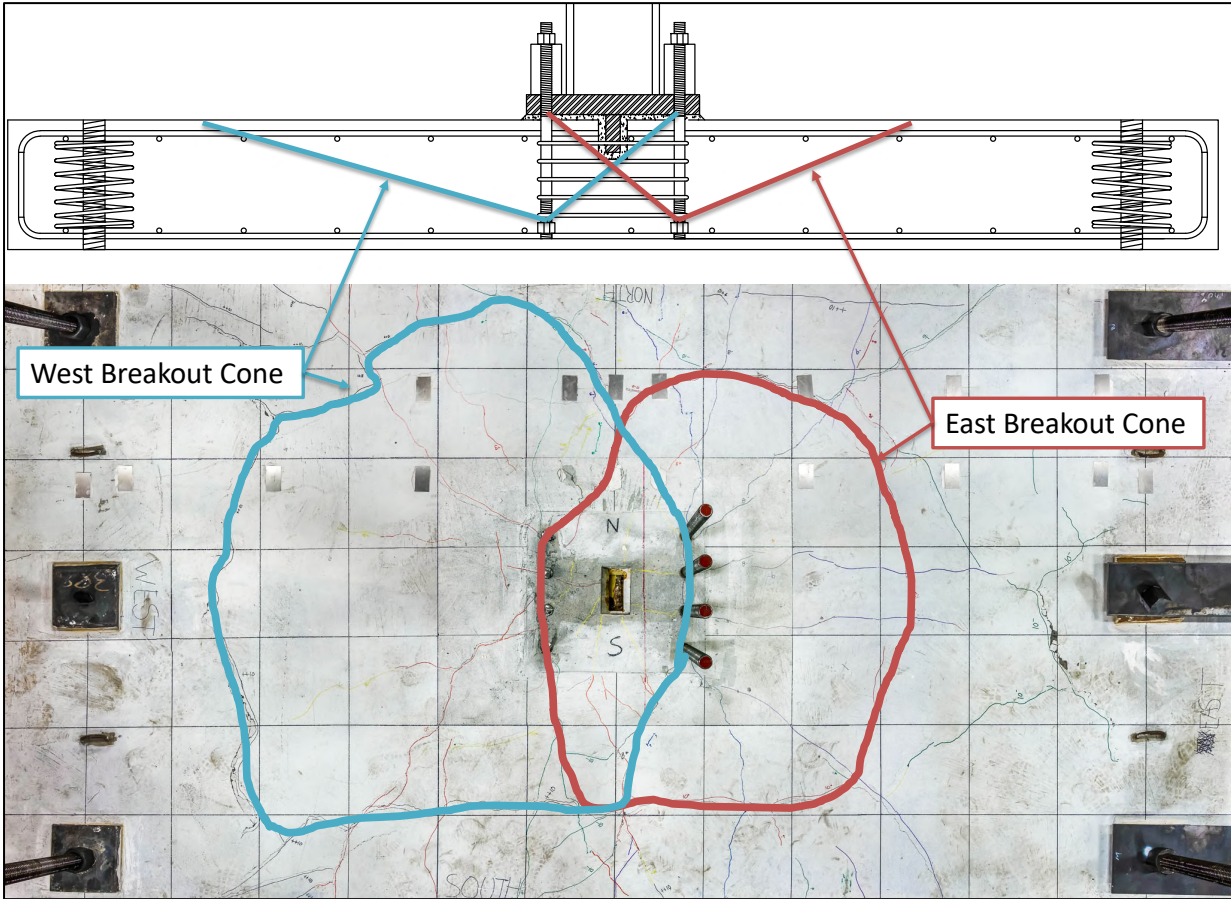


Figure 5-1. Specimen crack pattern after failure, 12 in. x 12 in. grid, top view and two lateral views

Breakout cones are observed on the top surface of the slab around each anchor group as identified in Figure 5-2. The cones are observed to be asymmetric with a much steeper slope towards the interior of the joint.



**Figure 5-2. Specimen crack pattern after failure, 12 in. x 12 in. grid, east and west breakout cones identified**

After testing, the foundation slab was saw cut approximately in half in the transverse direction as shown in Figure 5-3. The exposed cross section of the east half is shown in Figure 5-4. Two horizontal cracks can be observed along the length of the cross section, which correspond to the two intersecting breakout cones.

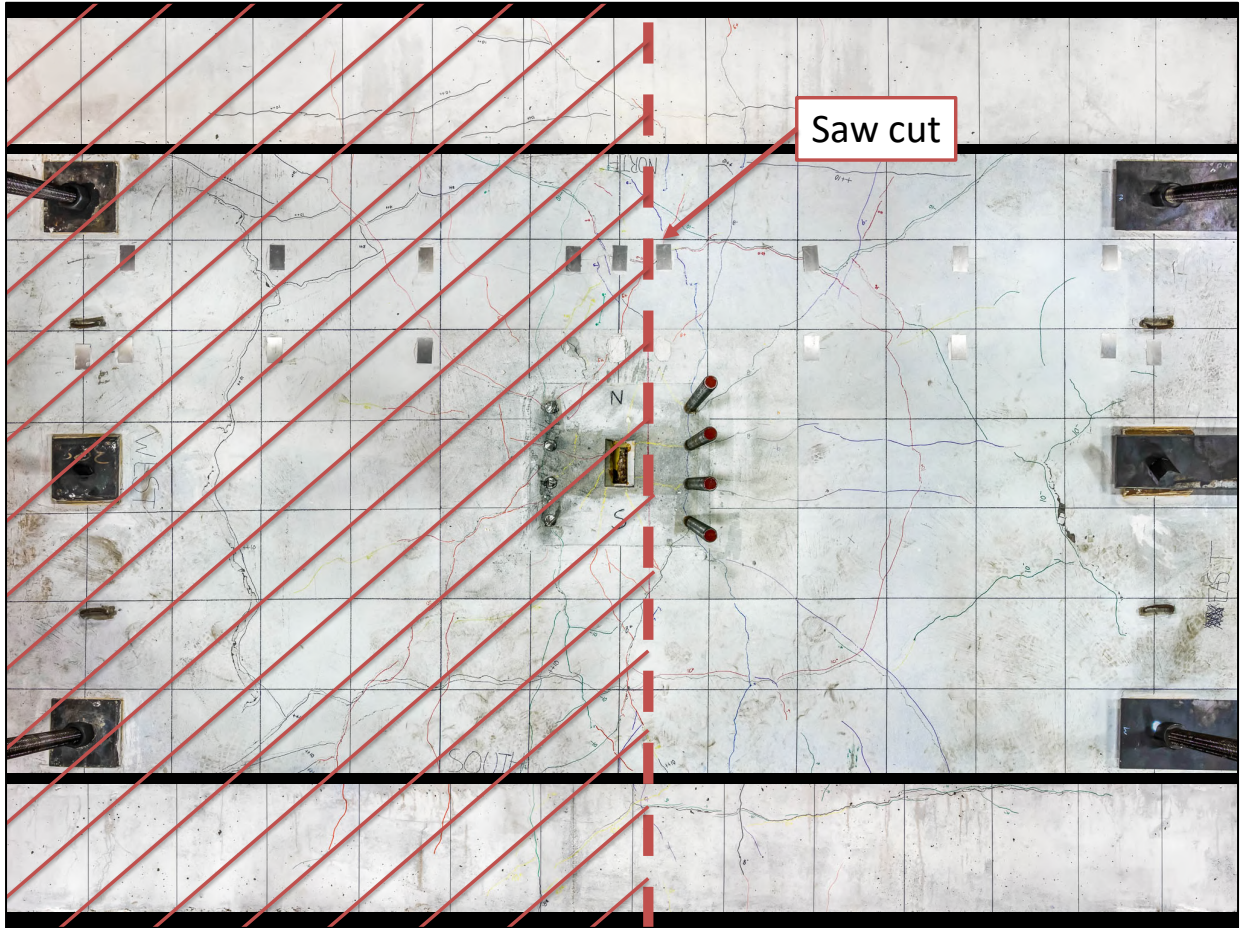


Figure 5-3. Location of specimen saw cut

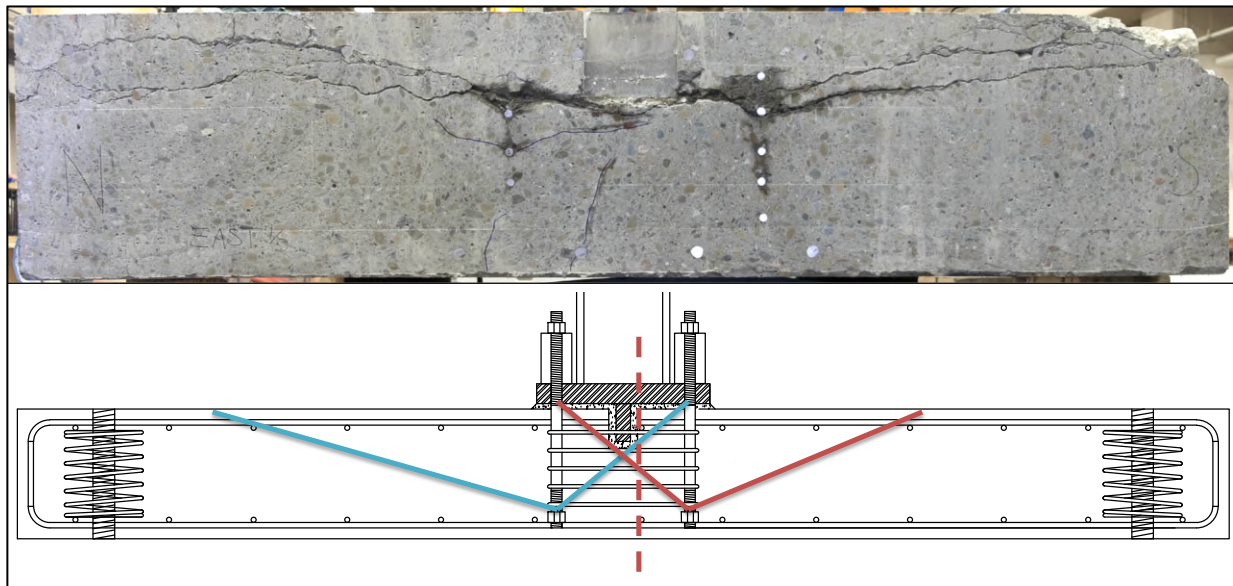


Figure 5-4. Slab cross section of east section showing two horizontal cracks corresponding to the two breakout cones indicated in the bottom drawing

To verify that the cracks observed in the saw-cut cross section are part of a breakout cone (and not evidence of a pullout or shear lug failure), sections of the cone were removed with a jack hammer to expose the bottom surface of the crack. As can be seen in Figure 5-5, this surface was steeply sloped towards the anchor heads as would be expected of a breakout-type failure. The crack surface did not cut through aggregate. Crack pattern observations from this section support the conclusion that concrete breakout failure occurred for both breakout groups.

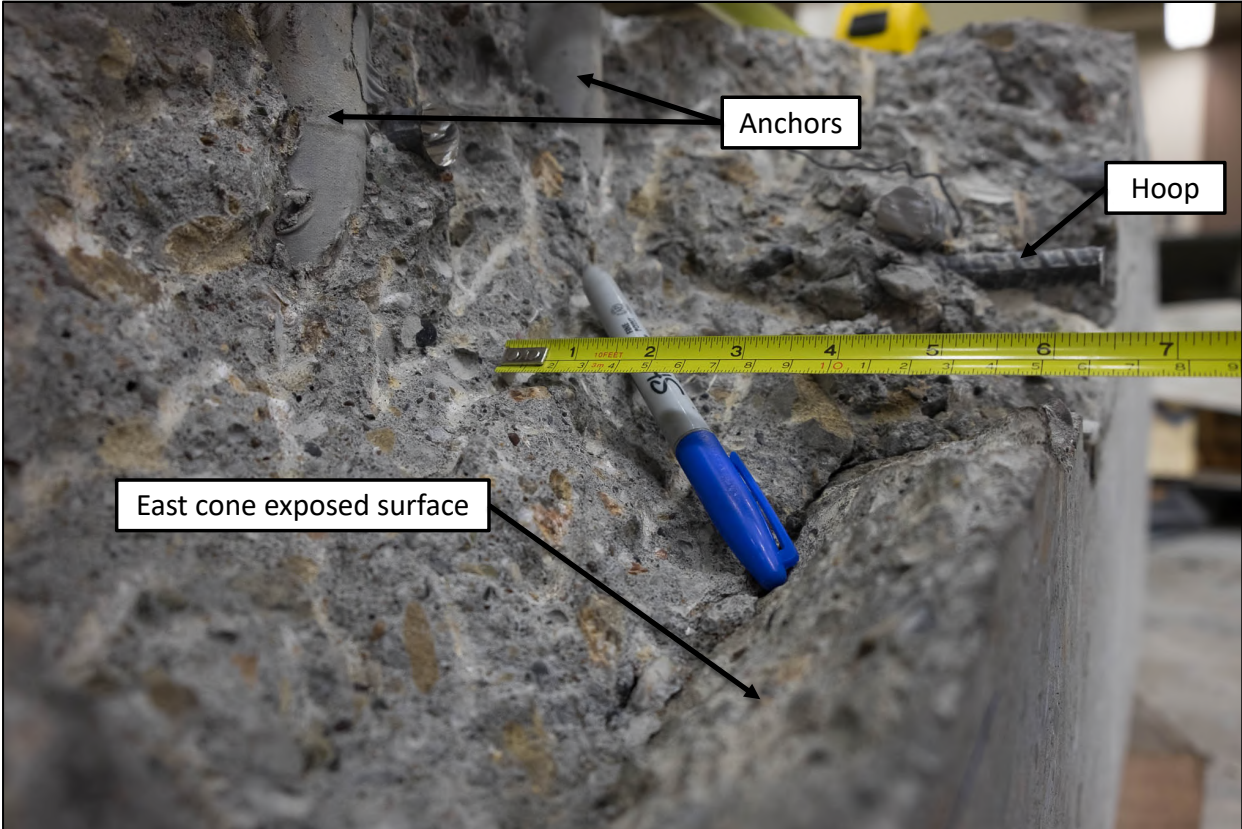


Figure 5-5. Exposed bottom surface of east breakout cone inside joint

Minimum cracking and damage were observed on the bottom surface of the foundation slab (Figure 5-6). Punching of the anchors through the bottom of the slab was not observed.



**Figure 5-6. Minimal damage observed on specimen bottom surface as seen from the east**



### 5.2 INSTRUMENTATION READINGS

As described in section 4.1, 80 different instruments were used to measure the specimen behavior:

- 26 linear potentiometers
- 10 load cells
- 41 strain gages on reinforcement
- 3 wire pots

The force – displacement relationship of the column free end (shown in Figure 5-7) plots each load cycle (displacement goal from Table 4-1) with a different color and highlights the instant of failure. After breakout, the connection resistance drops to about 50% of the maximum resistance. This residual capacity is likely attributable in part to the presence of surface reinforcement in the foundation slab, which kept the concrete cones from displacing significantly. Also, relaxation of the specimen is observed when the loading is paused. Figure 5-7 highlights the load and displacement at the end of each pause. Finally, the specimen stiffness is slightly higher when loading the east anchor group as opposed to loading the west anchor group.

Table 5-1 shows the maximum force and displacement of the column free end for each cycle compared with the displacement goal for each cycle. The measured displacements tend to be lower than the displacement goal for each cycle; but the maximum measured displacements in each direction of loading tend to be similar to each other.

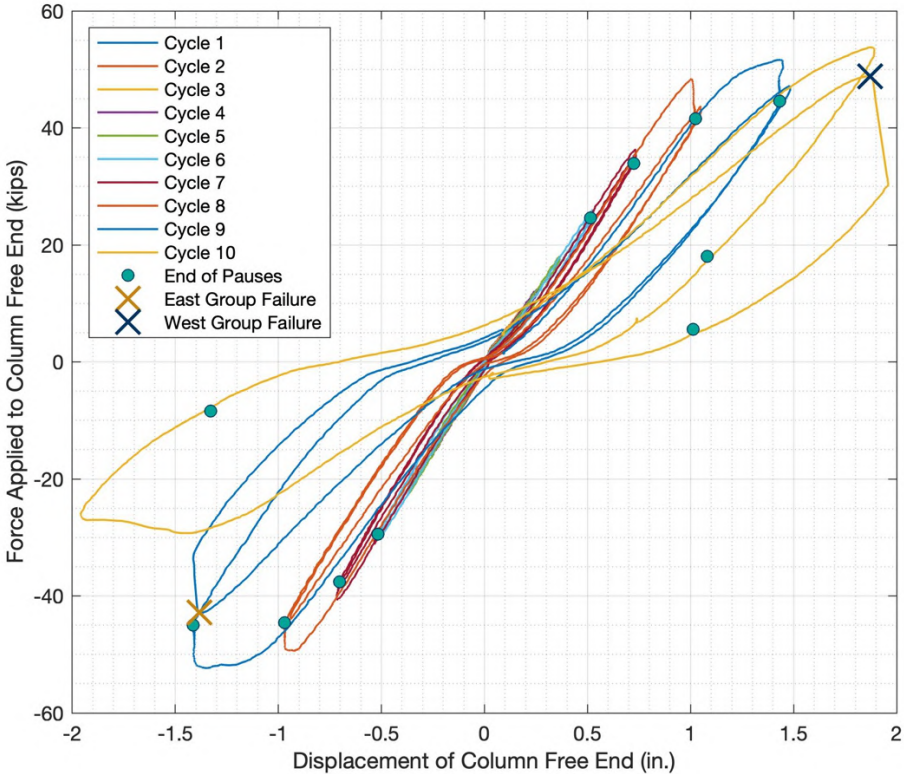


**Figure 5-7. Longitudinal force – displacement relationship of the column free end as measured by actuator load cells and the triangulation of wire pot attached to column free end (positive displacement east movement)**

**Table 5-1. Maximum displacement and force applied to column free end per cycle**

Cycle	Goal $\delta$ (in)	West Anchor Group		East Anchor Group	
		$\delta$ Max (in)	Force Max (in)	$\delta$ Max (in)	Force Max (in)
1	0.11	0.09	4.99	0.09	6.43
2	0.15	0.13	6.34	0.12	8.48
3	0.21	0.18	8.84	0.19	12.0
4	0.29	0.26	12.5	0.26	16.1
5	0.41	0.37	18.0	0.37	22.5
6	0.58	0.53	26.0	0.52	30.5
7	0.81	0.74	36.3	0.72	40.7
8	1.13	1.05	48.3	0.97	49.4
9	1.58	1.48	51.6	1.42	52.3
10	2.05	1.96	53.8	1.96	29.3

The connection begins to show pronounced nonlinear behavior in both loading directions during cycle eight (see Figure 5-7) and shows ductile behavior through cycles nine and ten until failure. Taking the yield displacement as the maximum displacement where linearity is conserved and the maximum displacement as the displacement at the instant of breakout failure, an approximate displacement ductility capacity can be calculated as:

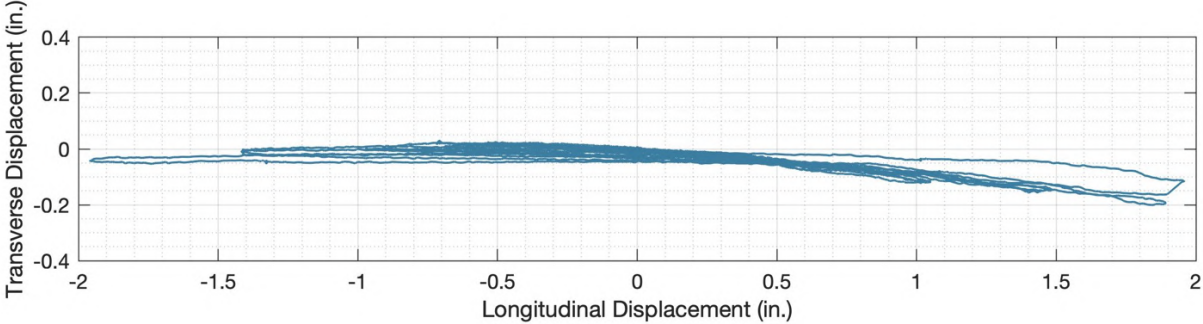
$$\mu = \frac{d_{max}}{d_y}$$

Averaging the behavior in both directions, an approximate displacement ductility capacity for the connection is found to be 1.64 (see Table 5-2). This value is of interest because no ductility was expected for a breakout-type failure. It is possible that the surface reinforcement, which intersected the concrete cone, provided some additional resistance to the failure plane, resulting in the observed ductility.

**Table 5-2. Approximate ductility capacity calculation per loaded anchor group**

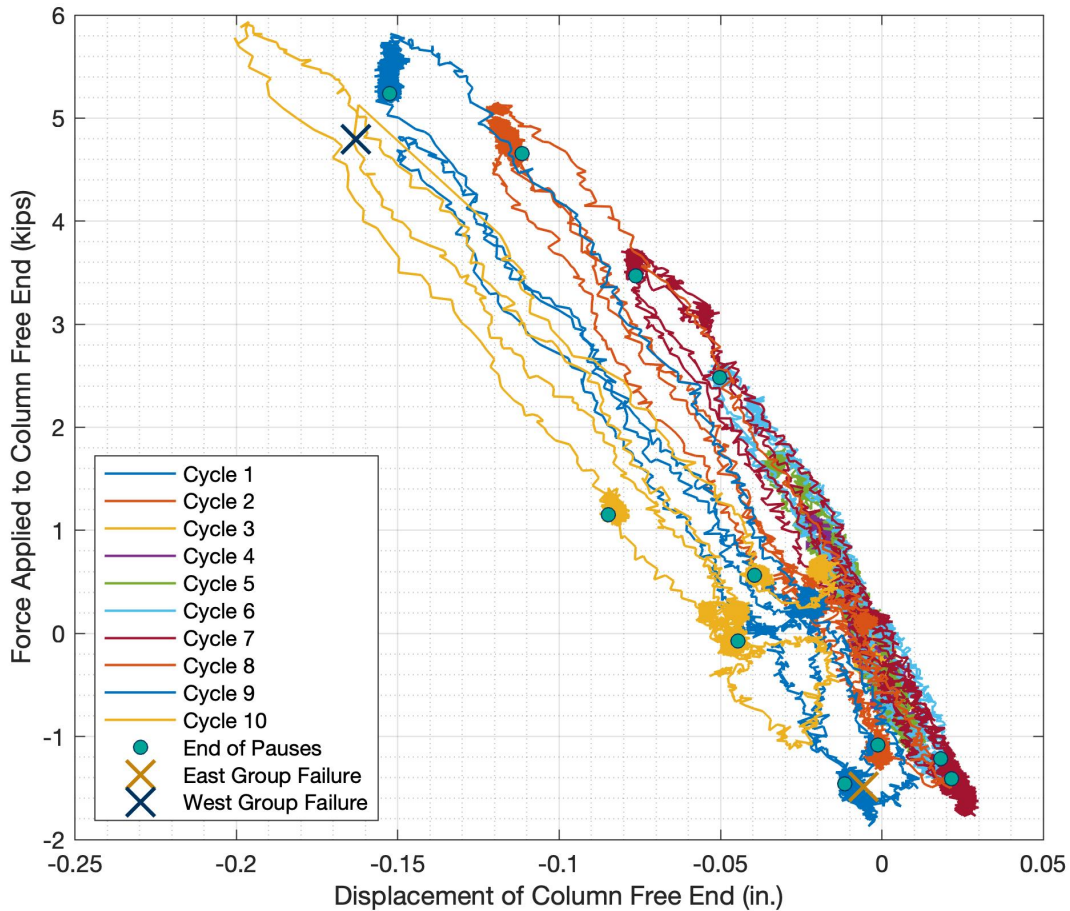
Anchor Group	$\delta_y$ (Max cycle 8) (in.)	$\delta_{max}$ (in.)	$\mu$
West	1.05	1.87	1.78
East	0.92	1.38	1.50
Average	-	-	1.64

Figure 5-8 shows a plan view of the movement of the column free end. As described in section 4, two actuators were attached to the column free end at 45° and programmed to limit movement to the longitudinal direction only. Figure 5-8 shows about a 10% sway in the transverse direction when pushing the column towards the east, with somewhat lower transverse sway for loading towards the west.



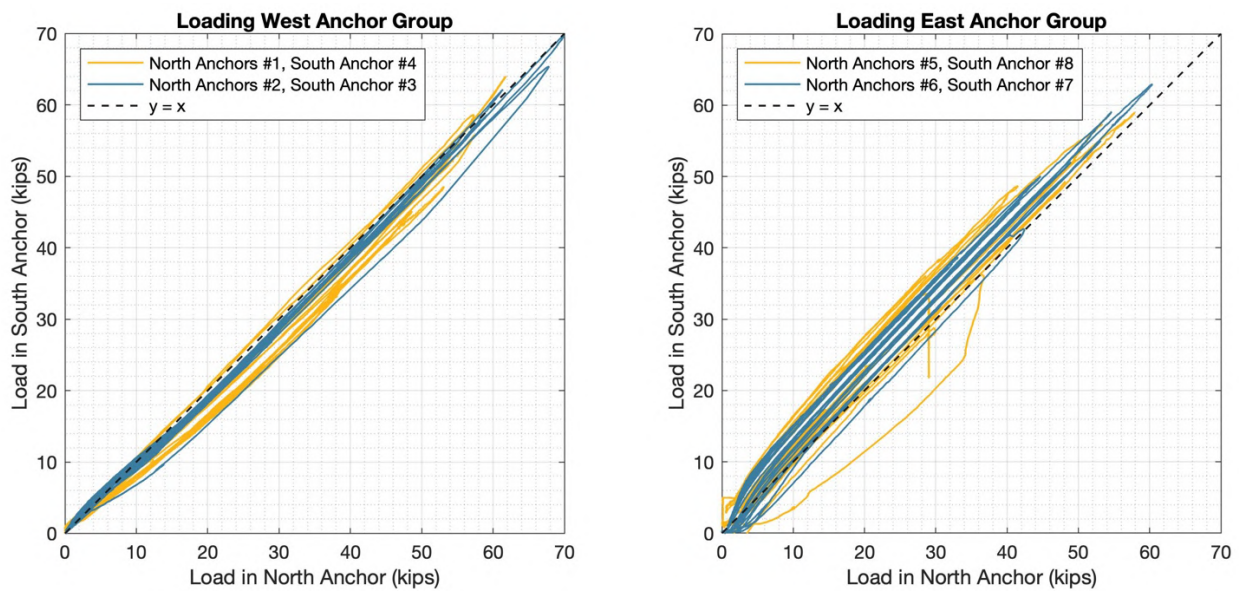
**Figure 5-8. Plan view of the displacement of the column free end triangulated with measurements from wire pots 1 and 3 attached to the column free end (positive displacement is north and east)**

Figure 5-9 plots the force – displacement relationship for the column free end in the transverse direction. The two actuators attached to the column free end were programmed to move the column solely in the longitudinal direction. Both the maximum transverse force and maximum transverse displacement are about 10% of the corresponding values in the longitudinal direction. A downward slope is observed because when the column displaced transversely to the south (negative displacement), the actuators applied a force to the north (positive force) to minimize transverse movement. Also, the transverse movement increased as the test progressed and was the largest after the first breakout failure (that is, cycle 10).



**Figure 5-9. Transverse force – displacement relationship of the column free end as measured by actuator load cells and the triangulation of wire pot attached to column free end (positive displacement east movement)**

If the specimen were perfectly symmetric along the longitudinal axis (creating symmetric north and a south halves), and if the loading were applied perfectly in the longitudinal direction with no transverse loading, then the readings from the load cells on the anchors would be identical to the corresponding symmetric anchor of the other half. Figure 5-10 plots the load in each north anchor against the load in the corresponding symmetric south anchor for each anchor group separately (see Figure 4-5 for anchor numbering). When loading the west anchor group, a higher load is measured in the north anchors than in the corresponding symmetric south anchors. This asymmetry can be attributed to the transverse loading observed in the column free end displacements shown in Figure 5-8. On the other hand, when loading the east anchor group, a higher load is measured in the south anchors than in the corresponding symmetric north anchors. This asymmetry must be due to the specimen geometry and material and not to the loading because when loading the east group, the transverse loading is small and is in the opposite direction (see Figure 5-8).



**Figure 5-10. Plot of the load in each north anchor versus the load in the corresponding symmetric south anchor for the east and west anchor groups separately**

During the loading some asymmetry in the anchor loads was observed. The inner anchors (number 2, 3, 6, and 7) consistently registered a larger load than the outer anchors (number 1, 4, 5, and 8). See Figure 4-5 for anchor numbering scheme. The difference is more pronounced in the west anchor group.

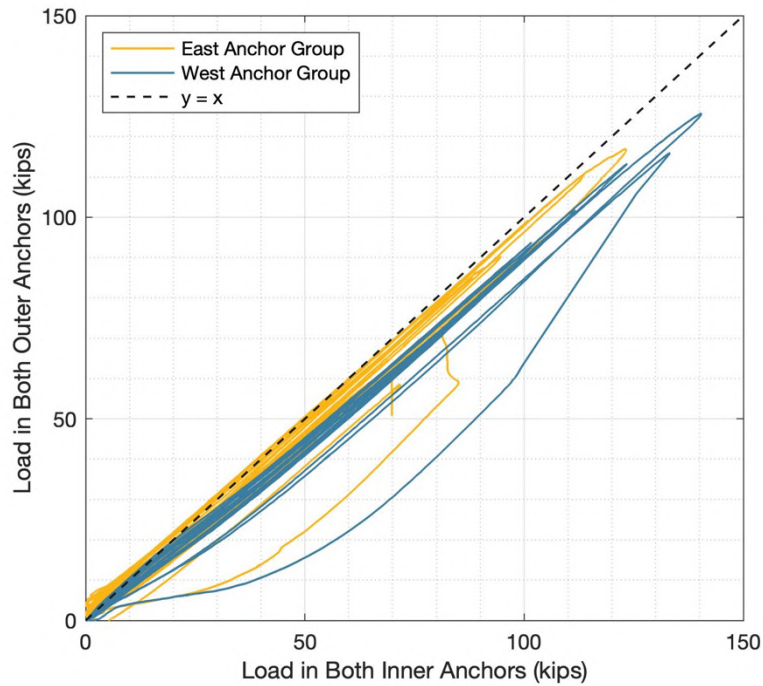


**Figure 5-11. Plot of the load in the two inner anchors against the load in the two outer anchors for the east and west anchor groups**

Figure 5-12 shows the load in each anchor group versus time as measured by the load cells on each individual anchor. The initial prestress is observed to decrease as loading progresses. Also, relaxation of the specimen is observed when the loading is paused at maximum displacements. The load at breakout failure is highlighted for both the west and east anchor groups. It is noted that the load at breakout was not the maximum load resisted by the anchor groups. The specimen failed when trying to load back up to the maximum load of the previous cycle. Table 5-3 indicates the maximum load and the load at breakout on both anchor groups. In this report the term “breakout load” will refer to the maximum load resisted by an anchor group at any time during testing and not the load at the instant of breakout failure.

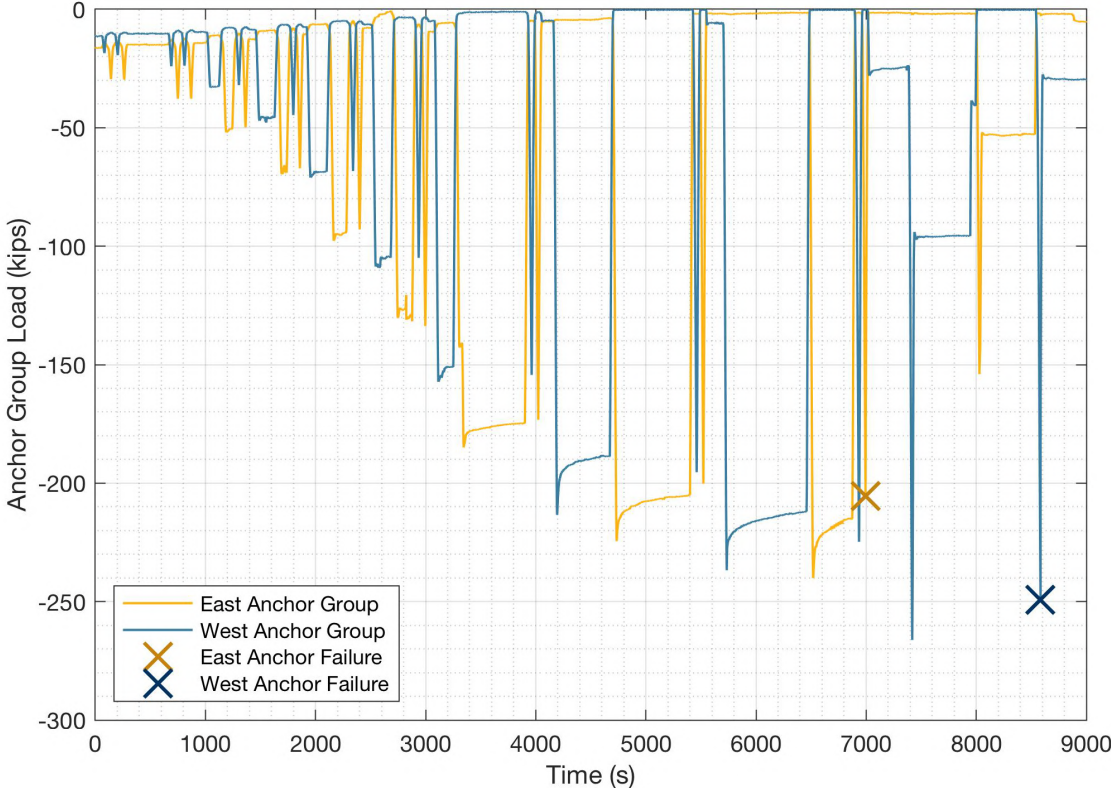


**Figure 5-12. Load in each anchor group as measured by load cells on each anchor (negative load represents a compressive force)**

**Table 5-3. Maximum load and load at breakout for east and west anchor groups (kips)**

Anchor Group	Max Load (kips)	Anchor Group Load at Failure (kips)
West	266	249
East	240	205

Figure 5-13 plots the anchor group load versus the base plate uplift. The base plate uplift was measured as the difference between the linear potentiometer reading placed vertically on the base plate and slab beside the anchors. The east group behaves more nearly linearly while the west group shows a more pronounced hardening behavior that intensifies as the loading progresses. When loading the west group, the base plate initially lifts off the slab with only minor loading of the anchor group, but then hardens to a stiffness nearly equal to that of the east group but offset from it. This difference in stiffness may be due to the fact that the actuator was attached to the column before the anchors were prestressed. The actuator may have held the column at a slight angle keeping the base plate from being flush against the slab surface. The prestress in the anchors tried to pull the base plate down towards the slab surface but was not able to do so fully leaving a gap on the side of the west anchor group. This difference in behavior of the base plate partially explains the stiffness difference between the two directions as observed in the force-displacement diagram for the column free end (Figure 5-7).

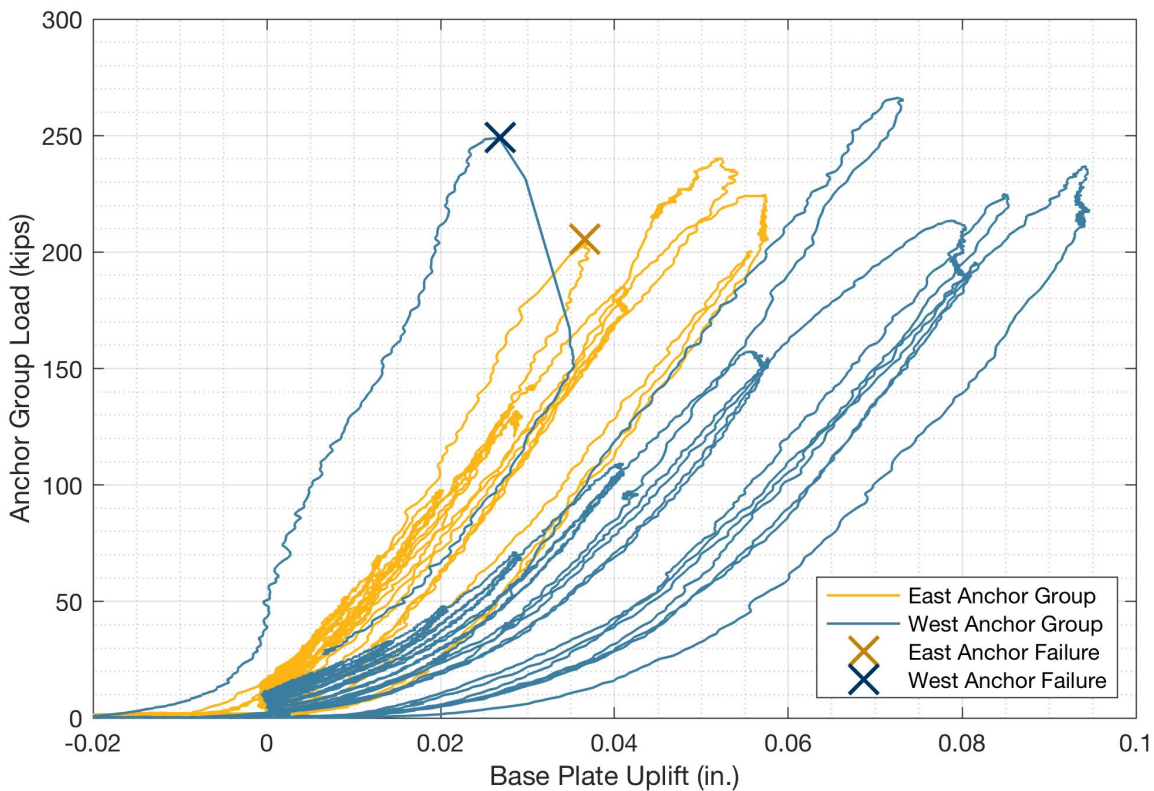


**Figure 5-13. Anchor group load against base plate uplift as measured by load cells on each anchor and linear potentiometers on base plate and slab**



Figure 5-14 plots the hoop strains of each leg versus time for the second-from-top and second-from-bottom hoops, respectively. For the second-from-top hoop, the only legs to yield ( $2000 \mu\epsilon$  for G60 reinforcement) were the longitudinal legs H6 and H8 (long legs). The longitudinal legs cross the cone failure plane. The short legs did not yield. These did not cross the cone failure plane but simply remained in the cone volume and moved with it. In the second-from-bottom hoop, no yielding occurred. These results seem to indicate that not all hoops along the joint height are equally effective at confining this type of joint and may not fully support the diagonal strut running through the joint as proposed in the strut-and-tie model.

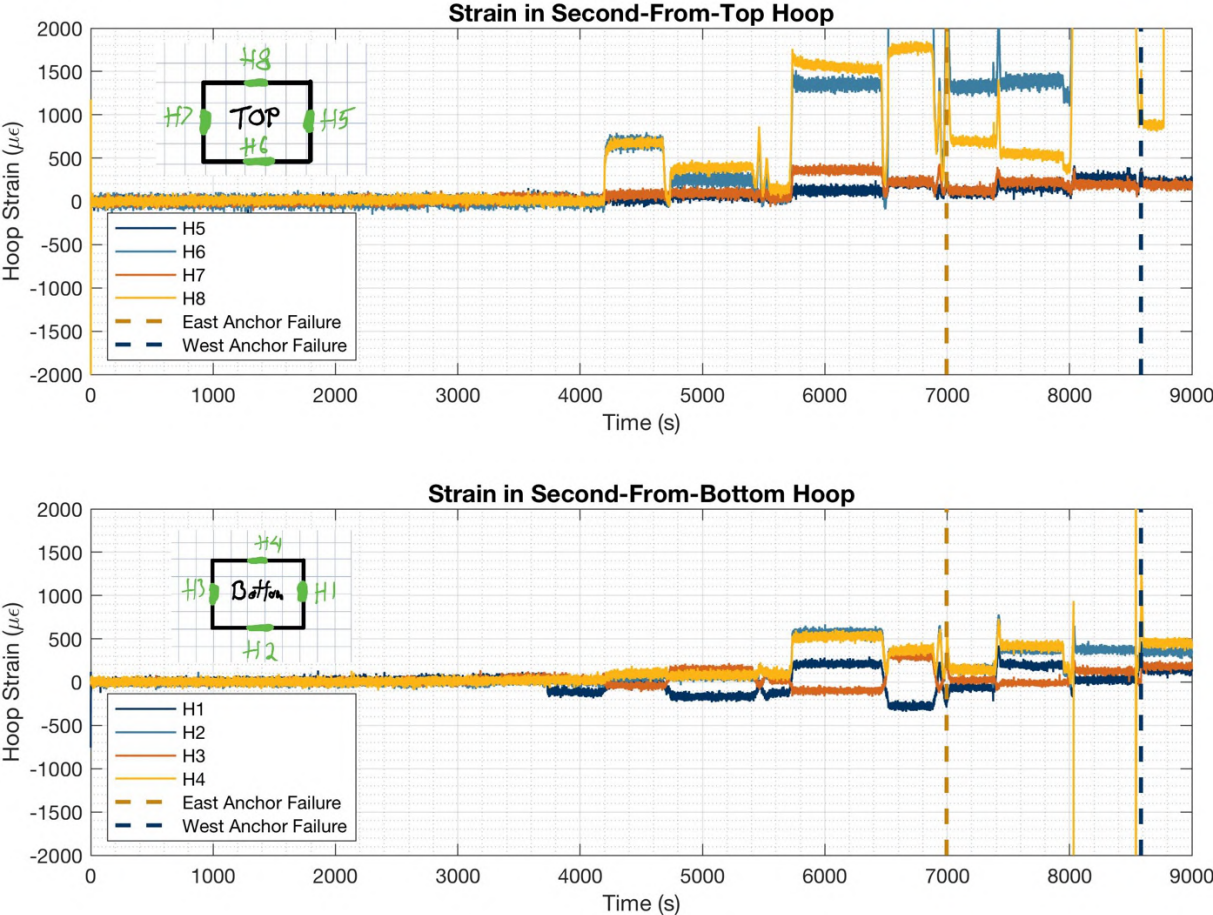


**Figure 5-14. Strains in four legs of hoops plotted versus time; second-from-top and second-from-bottom hoops are plotted**

Figure 5-15 graphs the absolute rotation of the slab and the base plate from horizontal versus time at the slab-column interface. It is observed that initially the slab barely rotates and most of the rotation happens in the base plate due to extension of the anchors and slipping between anchor and base plate (see Figure 5-13). As the test progresses, damage spreads in the concrete and the slab rotates more. In the final cycle (after both groups failed), the slab rotates more than the base plate. This is consistent with the breakout type failure mode observed.

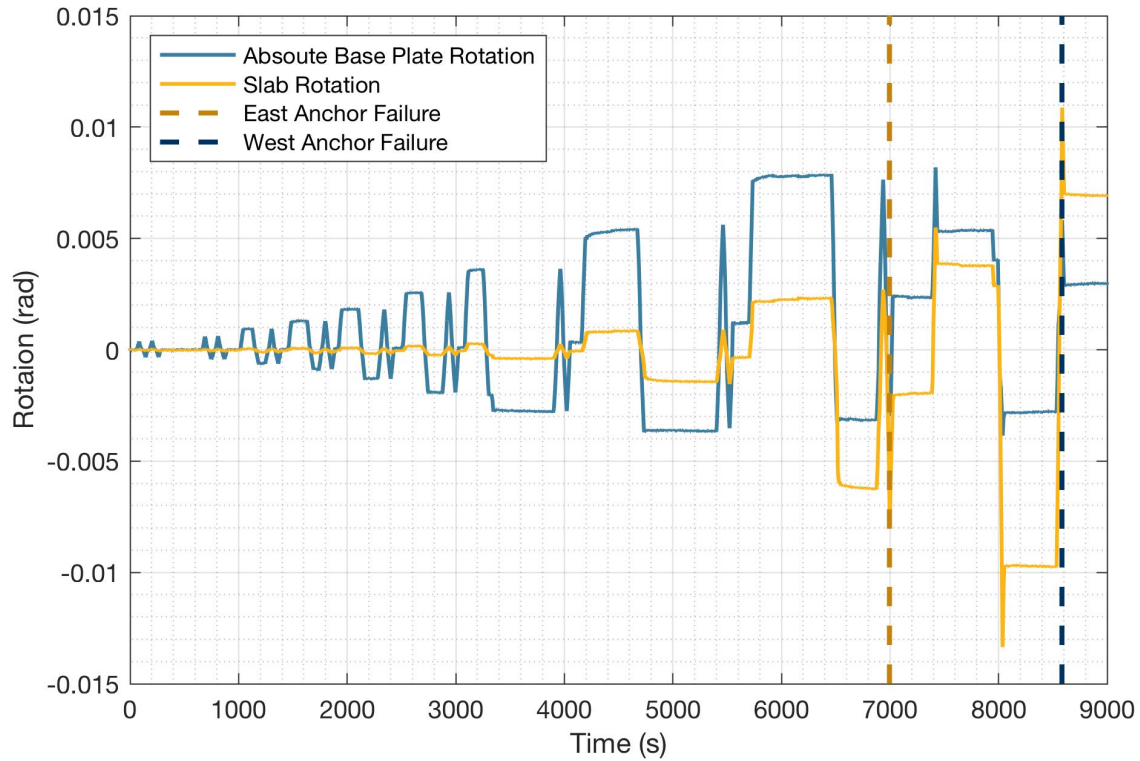
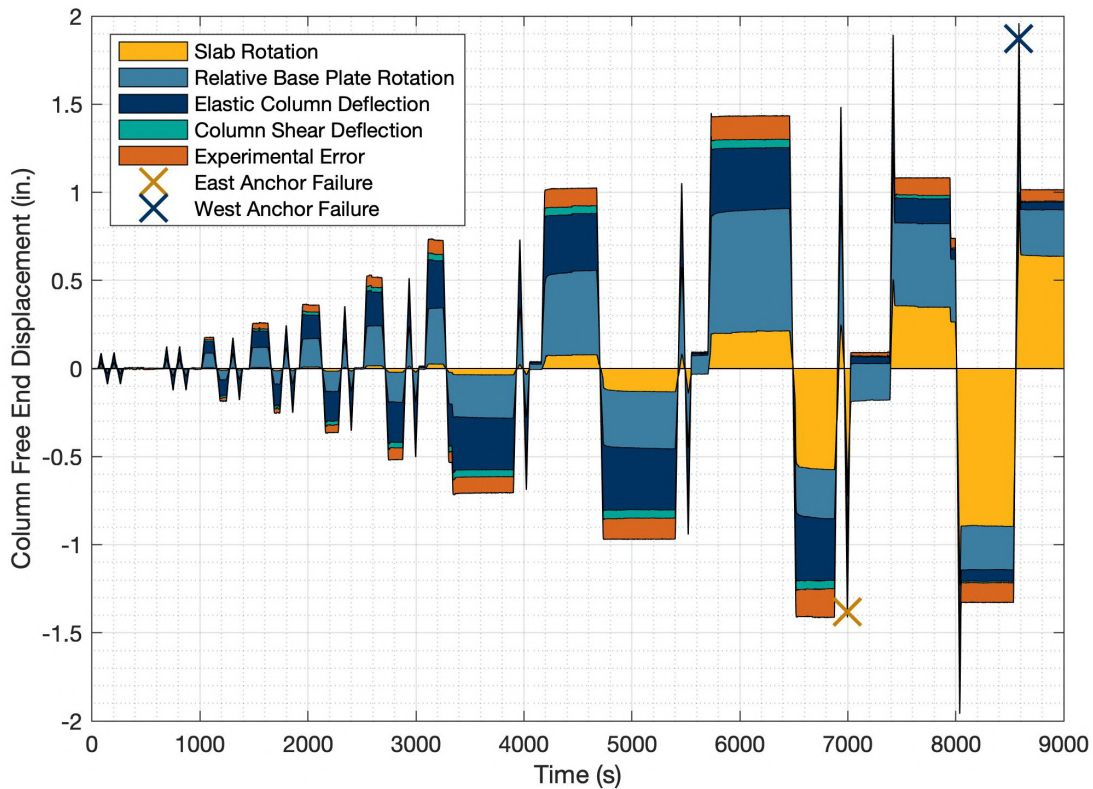


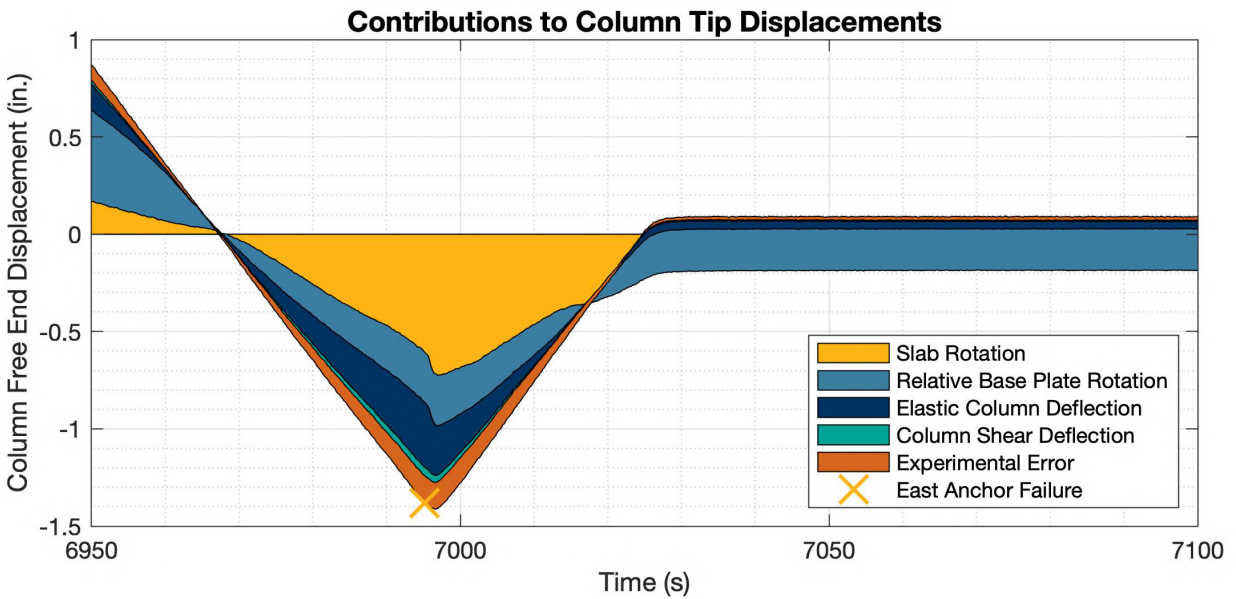
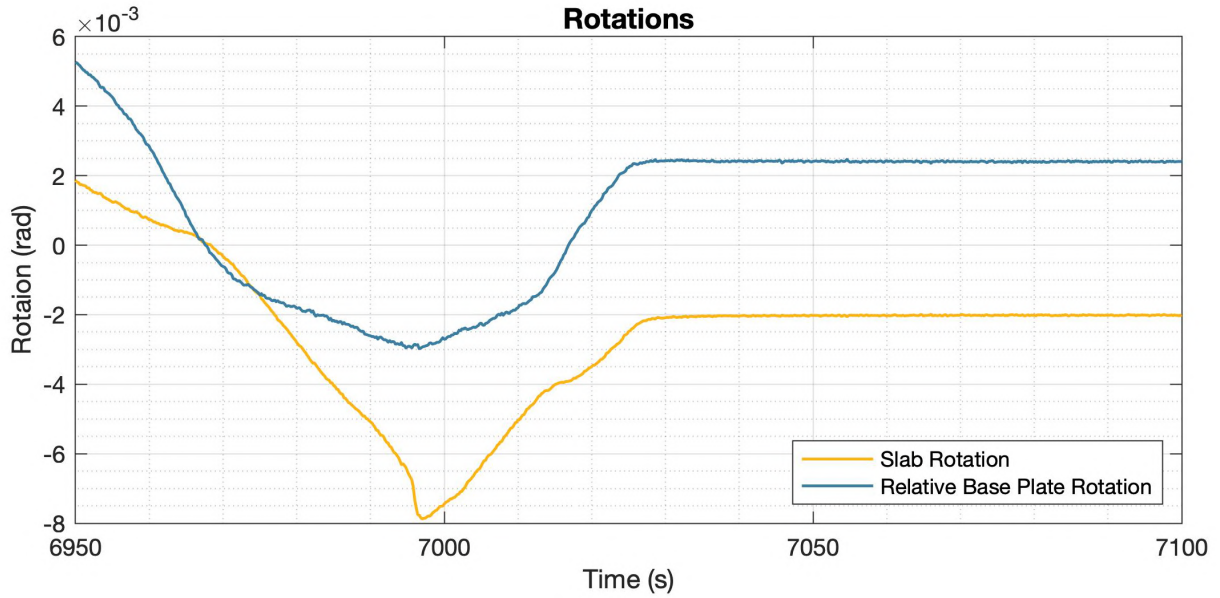
Figure 5-15. Absolute rotation of slab and base plate versus time

Figure 5-16 plots the displacement of the column free end versus time and subdivides the displacement into contributions due to slab rotation, relative base plate rotation and elastic column deflections due to moment and shear. The displacement due to the slab and the base plate rotation are calculated based on measured data. The column elastic deflection is calculated with the elastic theory knowing the load applied to the column free end. The remainder of the displacement is attributed to experimental error. Similar to the previous plot, initially the majority of the displacement is due to the elastic deformation of the column and the rotation of the base plate (anchor extension). As damage progresses in the concrete, the contribution of the slab rotation increases while the contribution of the elastic column decreases. The displacement due to elastic column deflection decreases after breakout because the column unloads. The contribution due to slab rotation after failure is relatively large because the breakout cone displaces as a solid object.



**Figure 5-16. Column free end displacement divided into contributions from the slab rotation, the relative base plate rotation, the elastic column deflection, the column shear deflection and experimental error versus time**

Figure 5-17 and Figure 5-18 present the same measurements as Figure 5-15 and Figure 5-16 but focus in on the instant of breakout failure for the east and west anchor groups respectively. At the instant of breakout failure, the contribution of the column free end displacement due to elastic deformation of the column decreases suddenly and the slab rotates suddenly. This is because the column unloads at breakout failure and the concrete cone displaces as a rigid object. The displacement due to base plate rotation is nearly constant before and after breakout. The displacement due to experimental error also seems to remain constant before and after breakout. Similar trends are observed for both breakout failures.



**Figure 5-17. At the instant of breakout of the east cone, the rotation of the slab and the base plate versus time (top) and the column free end displacement divided into contributions from the slab rotation, the relative base plate rotation, the elastic column deflection, and experimental error versus time (bottom)**

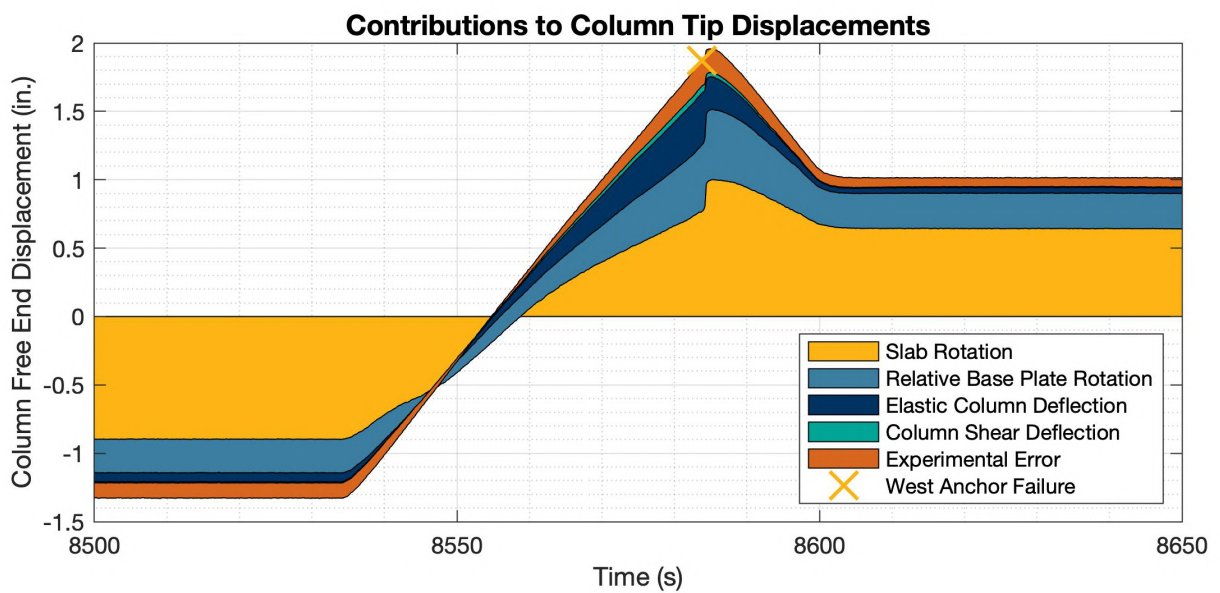
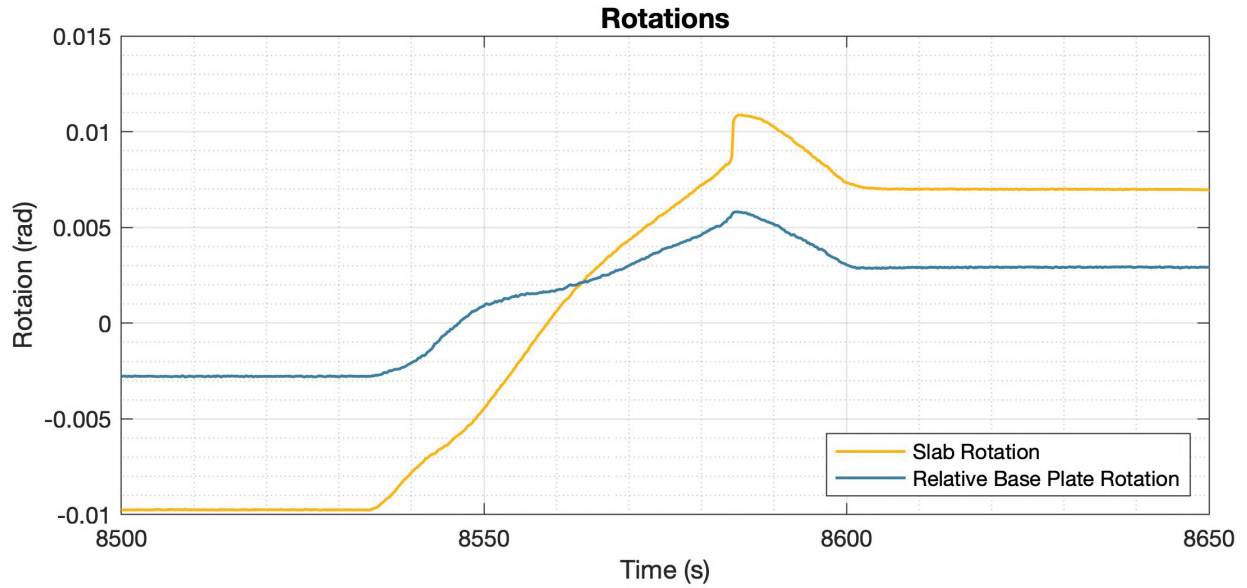


**Figure 5-18. At the instant of breakout of the west cone, the rotation of the slab and the base plate versus time (top) and the column free end displacement divided into contributions from the slab rotation, the relative base plate rotation, the elastic column deflection, and experimental error versus time (bottom)**

Design Guide 1 by AISC (Base Plate and Anchor Rod Design, 2006) was used to proportion the specimen. This document recommends assuming a uniform bearing pressure between the base plate and the slab surface as seen in Figure 5-19. To verify this design assumption, the anchor load obtained through this procedure was compared with the experimental anchor group load as measured by load cells on the anchors. There is good correspondence at low load levels as can be seen in Figure 5-20; but as the load increases and damage occurs in the slab, the experimental load tends to become larger than the theoretical load by about 10% on average. This means that the resultant of the bearing pressure is closer to the anchors than what is predicted by the AISC uniform pressure model. This can be achieved by decreasing the value of the bearing pressure or by assuming the pressure distribution is not uniform but instead is largest towards the anchors. Both effects are expected to have contributed to this effect.

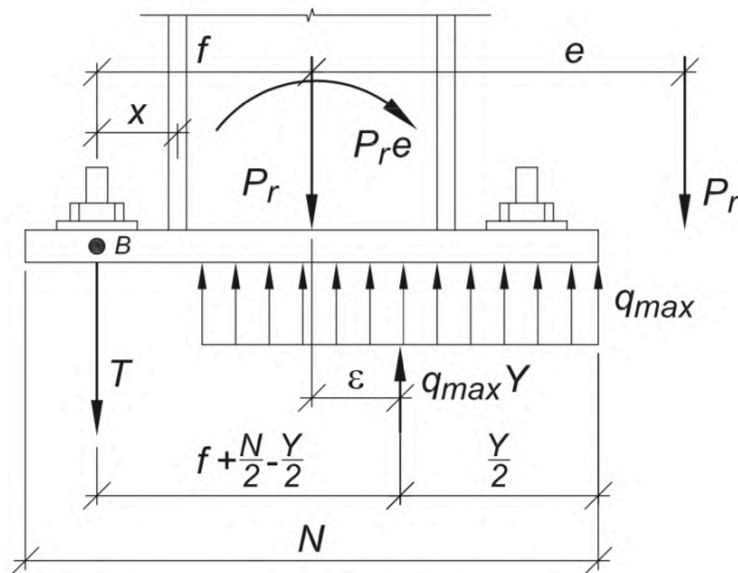
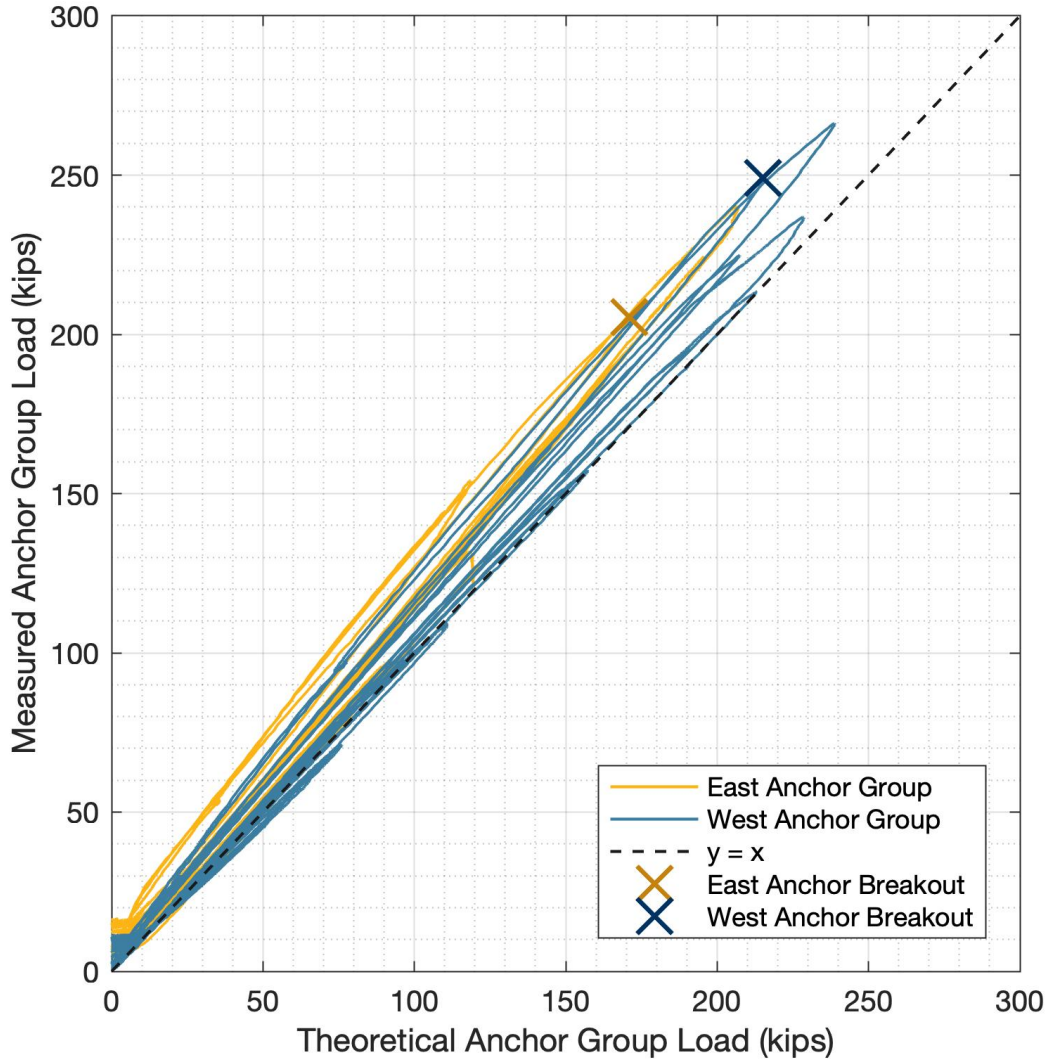
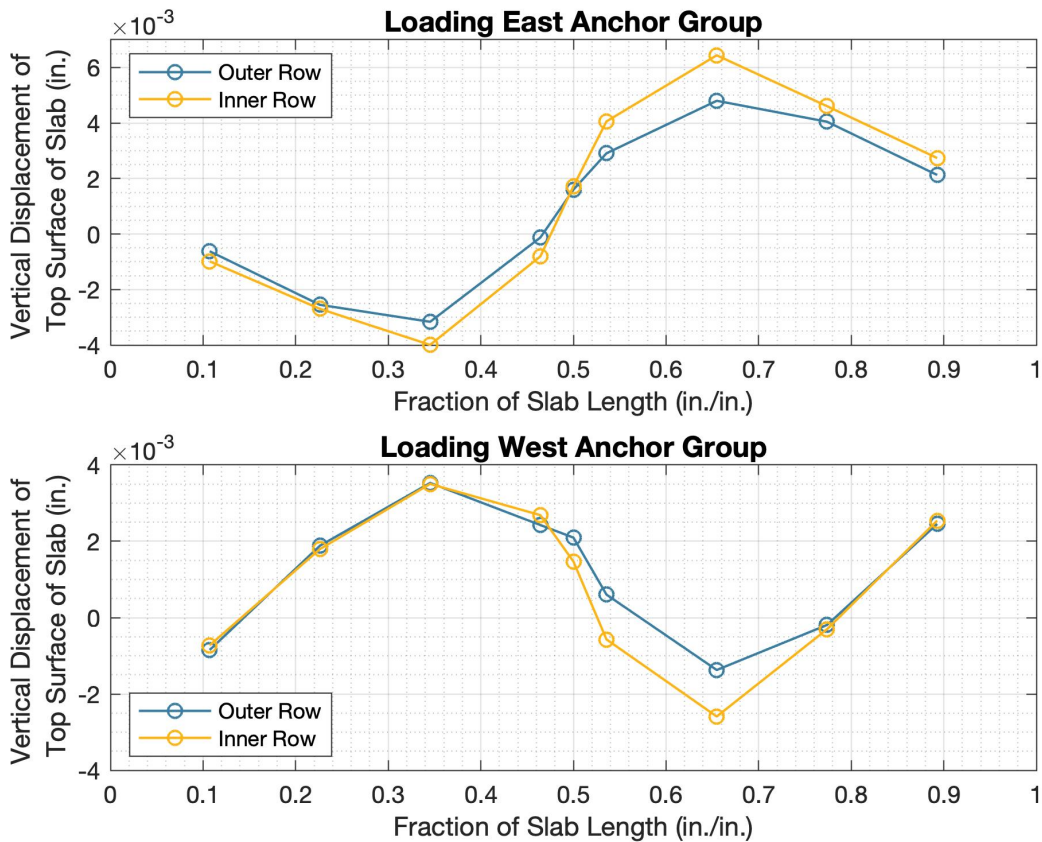


Figure 5-19. Base plate with large moment (AISC, 2006)



**Figure 5-20. Comparison between the theoretical and the measured load in both anchor groups; assuming uniform bearing pressure distribution under base plate for theoretical; taking experimental loads from load cells on anchors**

Two rows of linear potentiometers were placed along the top surface of the slab to measure vertical displacements (see arrangement of potentiometers in Figure 4-6). The rows span the longitudinal direction of the slab. Deflections due to self-weight are not included as the reference position of the instruments is the deformed shape of the simply supported slab under self-weight. The row of instruments closest to the slab centerline will be referred to as the “inner row” (15.5 in. from slab centerline) and the other as the “outer row” (27.5 in. from slab centerline). Before breakout failure occurred, the slab deformed with a double-curvature shape as can be seen in Figure 5-21. The double-curvature shape is visible when loading in both directions. This shape is consistent with what is expected from elastic beam theory.



**Figure 5-21. Vertical displacements of the top surface of the slab measured with two rows of linear potentiometers at maximum positive and negative displacement for cycle seven (before breakout).**



Figure 5-22 shows the displacement measurements by the same instruments as described above, but for 5 s before and 5 s after both breakout failures. The east anchor group failed first. The double-curvature shape is no longer observed. For both breakout failures, the inner row tends to have higher displacements than the outer row.

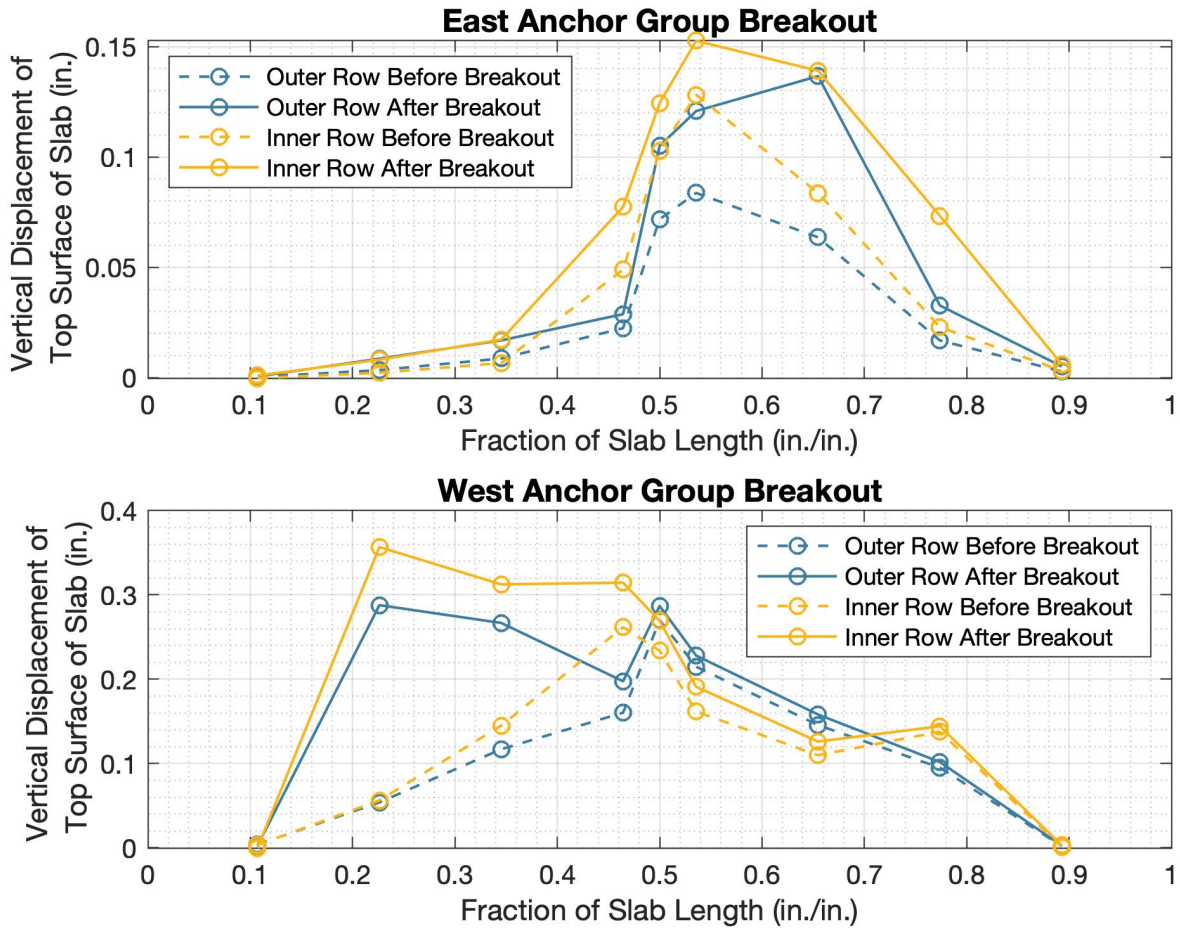
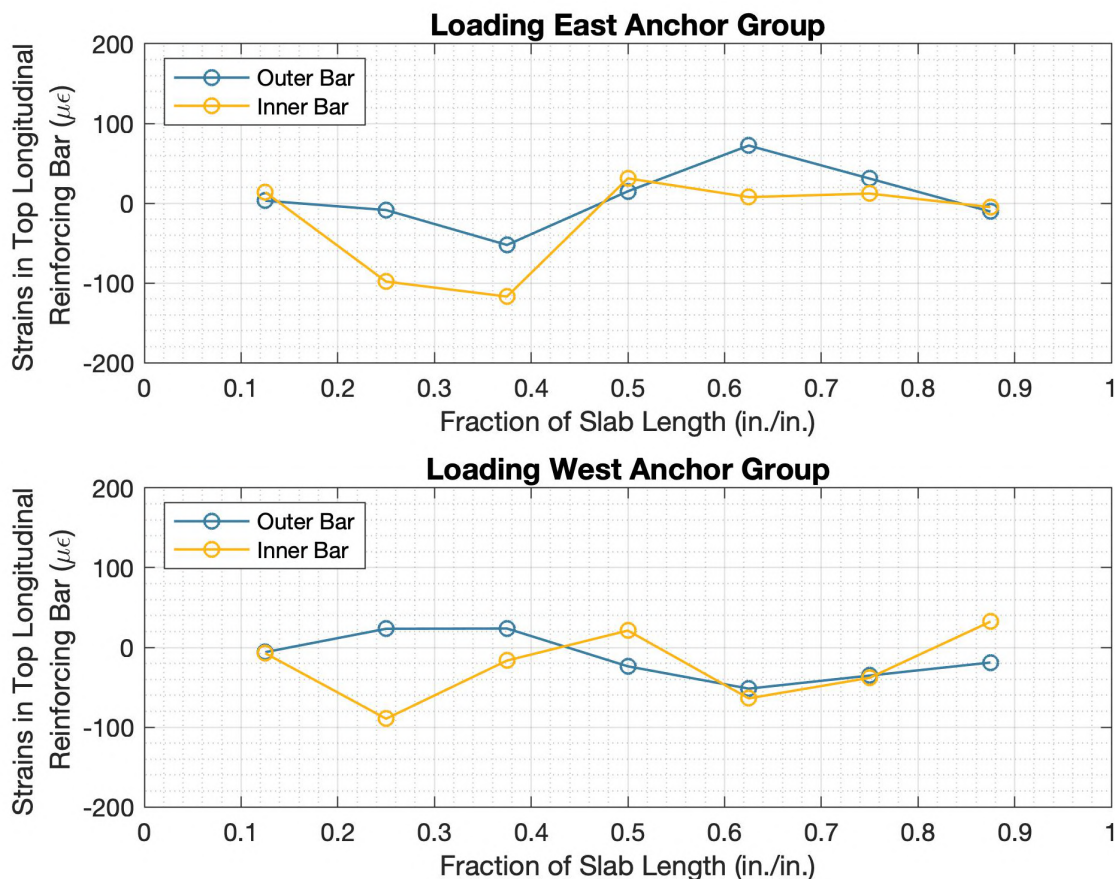


Figure 5-22. Vertical displacements of the top surface of the slab measured with two rows of linear potentiometers 5 s before and 5 s after breakout failure for both loading directions

Four longitudinal reinforcing bars were instrumented, each with seven equally spaced strain gages 21 in. on center (see arrangement of strain gages in Figure 4-2). A top and a bottom reinforcing bar, placed 4 in. from the slab centerline, were instrumented and will be referred to as the top and bottom “inner bars” (see Figure 4-3). Another top and bottom reinforcing bars, placed at 28 in. from the slab centerline, will be referred to as the top and bottom “outer bars”. Strains due to self-weight are not included because the reference position of the instruments is the simply supported slab under self-weight. Figure 5-23 plots the strains in the inner and outer top reinforcing bars at maximum positive and negative displacement for cycle seven (that is, before breakout failure). The outer bar shows a double-curvature shape for both loading directions. This shape is similar to what was observed with the linear potentiometers on the slab surface (see Figure 5-21) and is consistent with what would be expected from elastic beam theory. On the other hand, the inner reinforcing bars do not show double curvature. The inner reinforcing bars cross through the anchor group and are likely influenced by local strains around the anchors. Figure 5-24 plots the same information but for the inner and outer bottom bars. Similar trends are observed.



**Figure 5-23. Strains of the inner and outer top reinforcing bars measured with strain gages spaced 21 in. on center at maximum positive and negative displacements for cycle seven (Note: the second from the right gage of the outer bar malfunctioned, the average of the adjacent gages is plotted instead)**

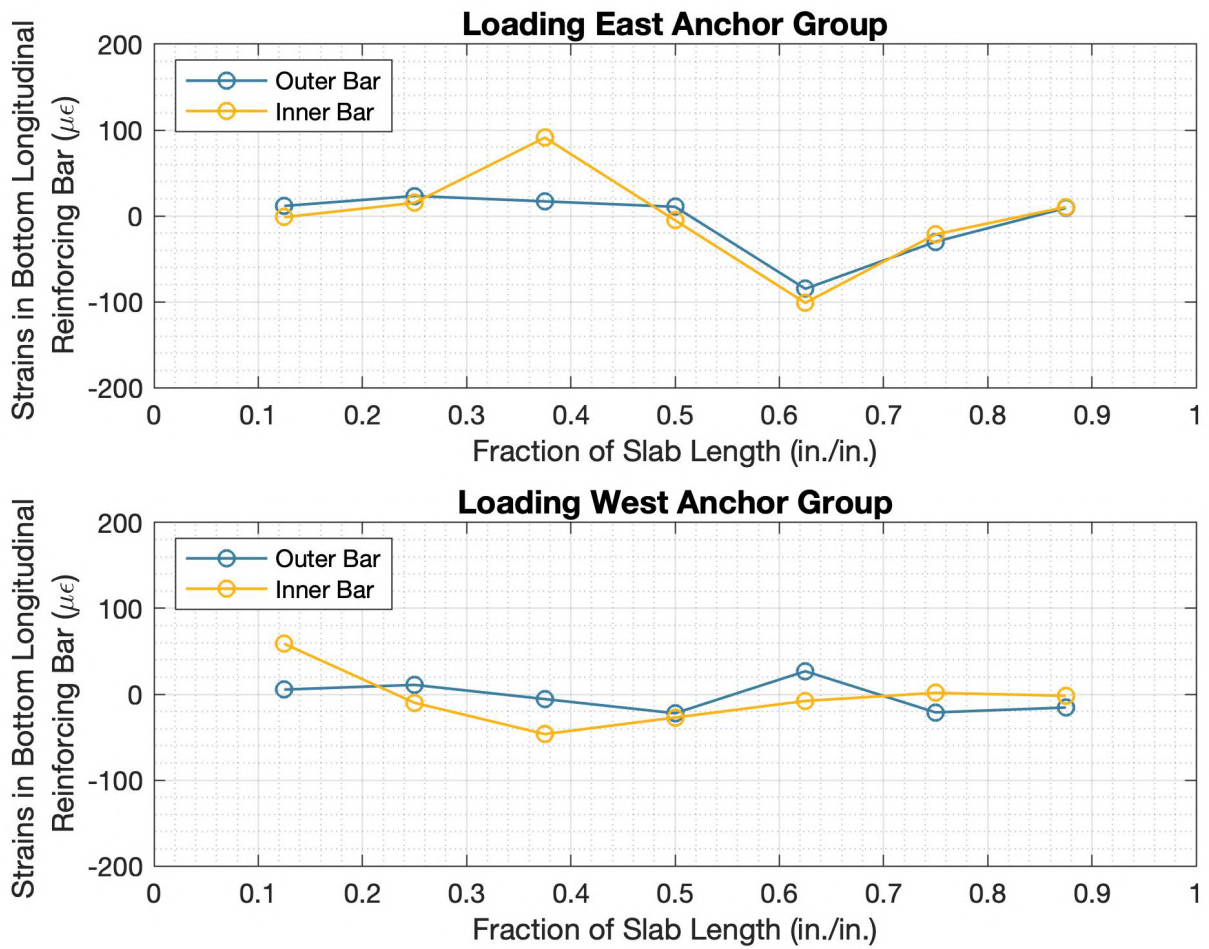


Figure 5-24. Strains of the inner and outer bottom reinforcing bars measured with strain gages spaced 21 in. on center at maximum positive and negative displacements for cycle seven (Note: the fourth from the left gage of the inner bar and the first and third from the left gage of the outer row malfunctioned, the average of the adjacent gages is plotted instead)

Figure 5-25 shows the strains of the top reinforcing bars measured 5 s before and 5 s after breakout failure for both loading directions. The east anchor group failed first. The double-curvature shape is no longer observed. Notice that at breakout of the west anchor group two strain gages malfunctioned. Also, no section of the reinforcing bar reached  $2000 \mu\epsilon$ , which is approximately the yielding strain of Grade 60 reinforcement. As described in Chapter 3, the slab reinforcement was designed to resist moments corresponding to the expected moment transfer strength assuming it was Grade 60 reinforcement. However, to avoid excessive inelastic strains in case the moment transfer capacity was underestimated, Grade 100 reinforcement was substituted for Grade 60 reinforcement.

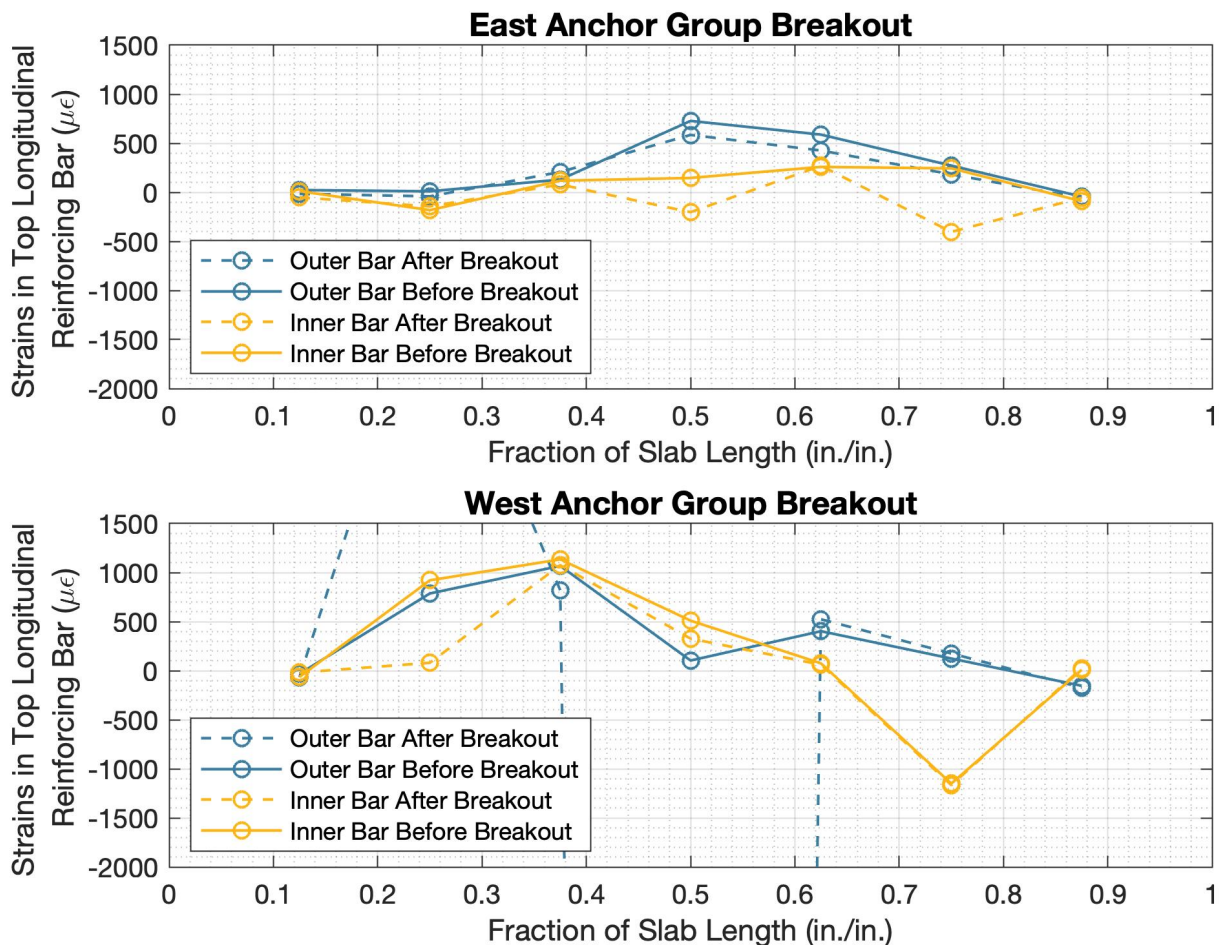
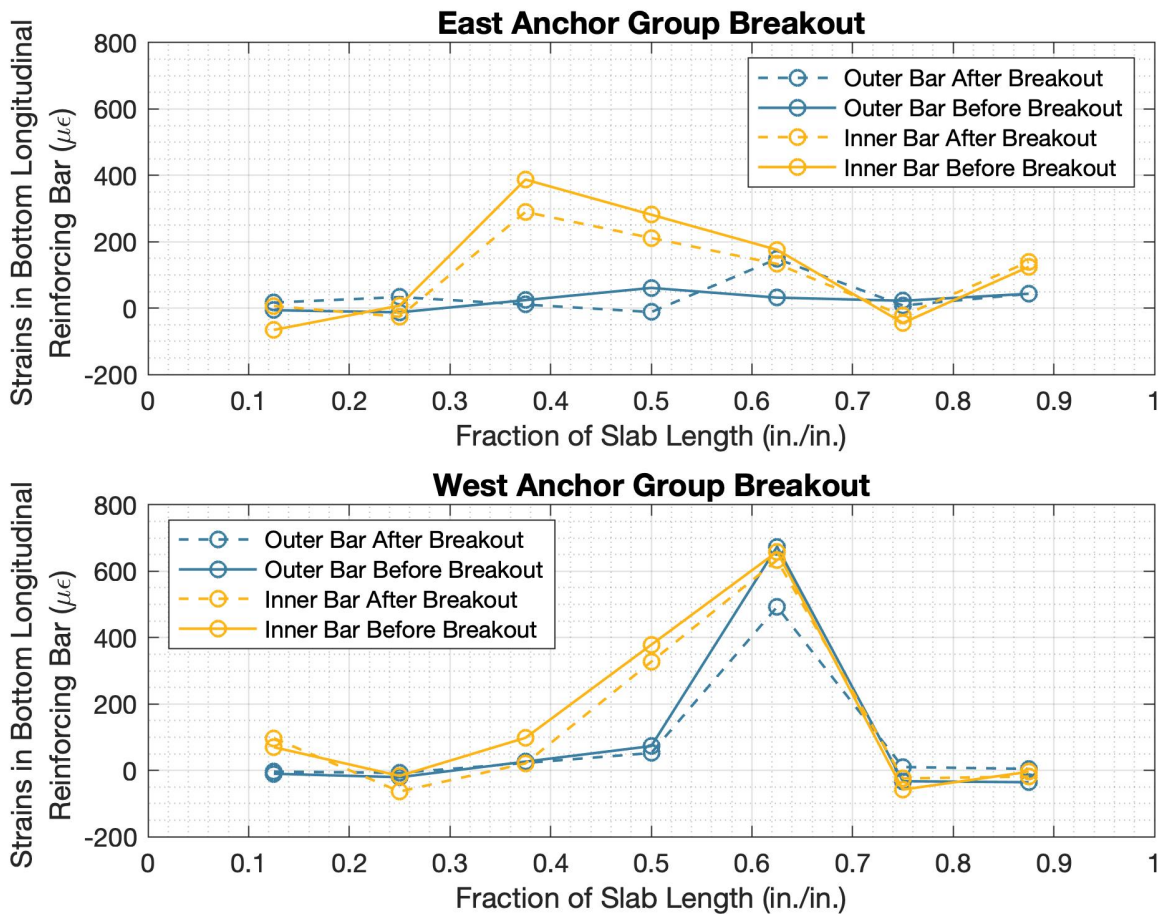


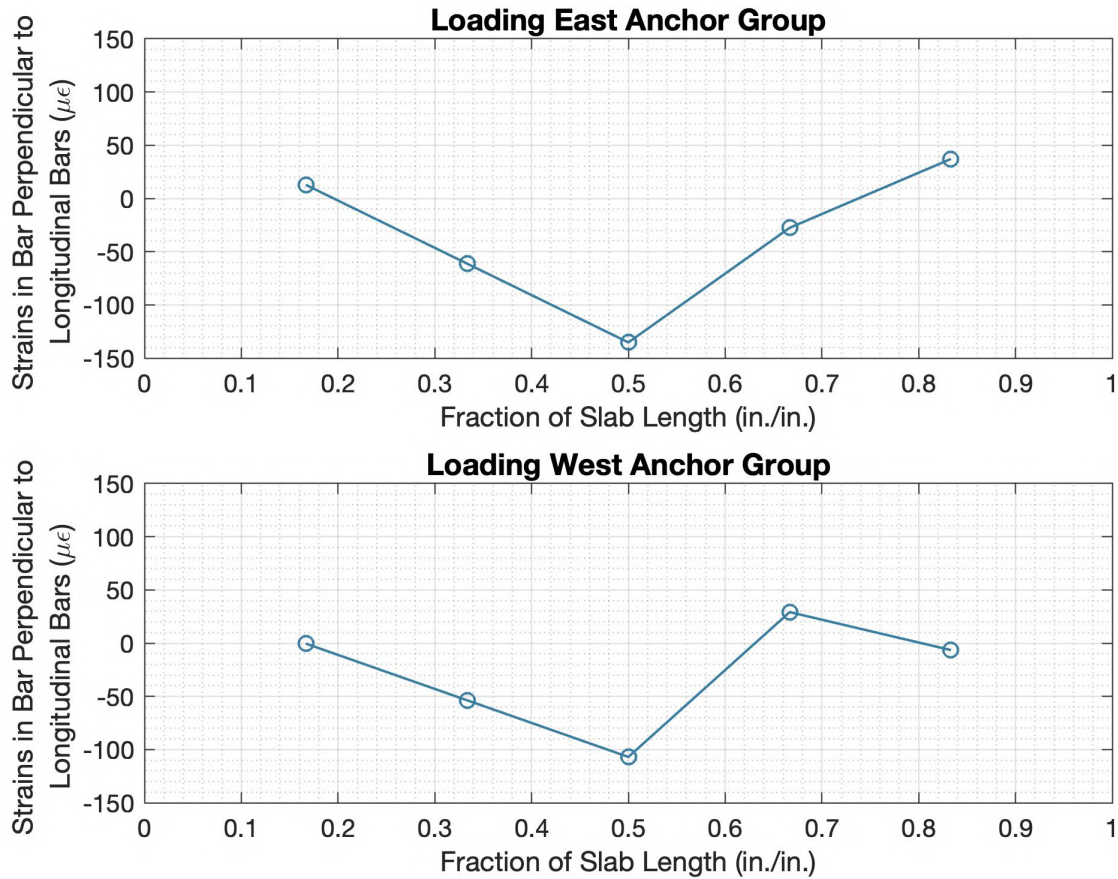
Figure 5-25. Strains of top reinforcing bars measured with strain gages spaced 21 in. on center 5 s before and 5 s after breakout failure for both loading directions (Note: two strain gages failed when the west anchor group failed)

Figure 5-26 shows the strains of the inner and outer bottom reinforcing bars measured 5 s before and 5 s after breakout failure for both loading directions. The east anchor group failed first. The strains are consistent with the strut-and-tie model proposed in section 3.3.2 where the tensile force of the horizontal ties is assumed to be carried from the hoops over a noncontact lap splice to the bottom reinforcing bars. The inner bars are, on average, more strained than the outer bars. A drop in strain is observed for most strain gages after both breakout failures. Also, no section of the reinforcing bar reached 2000  $\mu\epsilon$ , which is approximately the yielding strain of Grade 60 reinforcement.



**Figure 5-26. Strains of bottom reinforcing bars measured with strain gages spaced 21 in. on center 5 s before and 5 s after breakout failure for both loading directions (Note: the fourth from the left gage of the inner bar and the first and third from the left gage of the outer row malfunctioned, the average of the adjacent gages is plotted instead)**

One reinforcing bar perpendicular to the longitudinal bars in the top mat was instrumented with five strain gages spaced 14 in. on center (see strain gage arrangement Figure 4-2 and Figure 4-3). Figure 5-27 plots the strains in this bar at the maximum positive and negative displacements for cycle seven. The strains are slightly higher when the east anchor group is being loaded but the magnitude of the strains is, in general, small.



**Figure 5-27. Strains in the reinforcing bar perpendicular to the longitudinal bars measured with strain gages spaced 14 in. on center at maximum positive and negative displacements for cycle seven (Note: the second from the left gage malfunctioned, the average of the adjacent gages is plotted instead)**

Figure 5-28 shows the strains of the bar perpendicular to the longitudinal bars measured 5 s before and 5 s after breakout failure for both loading directions. The east anchor group failed first. The strains are small compared to the stains in the longitudinal reinforcing bars both before and after the breakout failure of the east anchor group. The cyclic loading process between the two breakout failures significantly strained the bar. This is likely due to the displacement of the dislodged east concrete cone. In both cases, breakout tended to cause the strains in the bar to shift towards tensile strains. Importantly, no section of the reinforcing bar reached 2000  $\mu\epsilon$ , which is approximately the yielding strain of Grade 60 reinforcement.

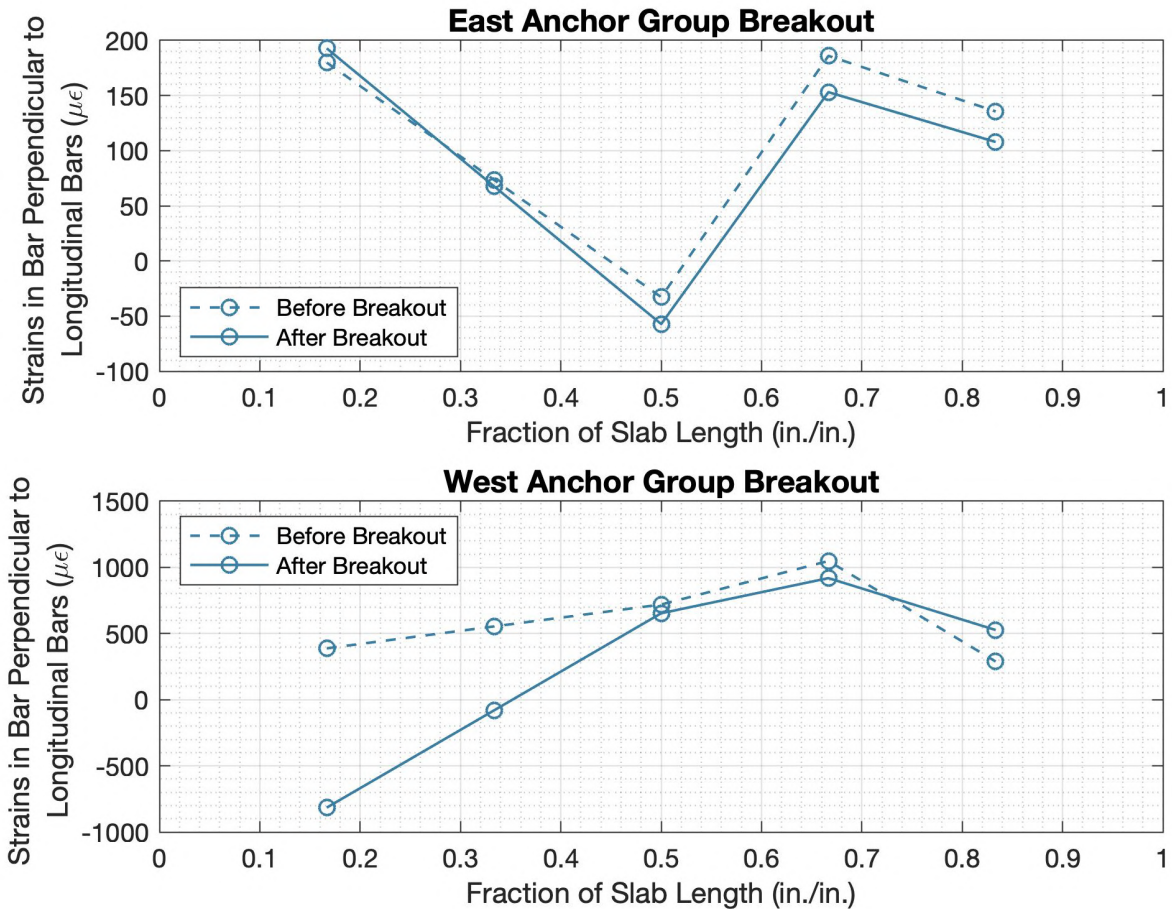


**Figure 5-28. Strains in the bar perpendicular to the longitudinal bars measured with strain gages spaced 14 in. on center 5 s before and 5 s after breakout failure for both loading directions (Note: the second from the left gage malfunctioned, the average of the adjacent gages is plotted instead)**

### 5.3 SPECIMEN SLIDING, ELONGATION AND SUPPORT UPLIFT

To prevent sliding during the test, the specimen was prestressed to the laboratory floor with nine 1-3/4" 150 ksi Williams Rods loaded to 170 kips each. Linear potentiometers were placed on the east and west faces of the slab along the slab longitudinal center line and at mid height (see section 4.1) to detect any sliding movement of the specimen relative to the laboratory floor. Figure 5-29 plots the horizontal displacement of the east and west supports as well as the east and west faces of the slab. Positive sliding is movement towards the east.

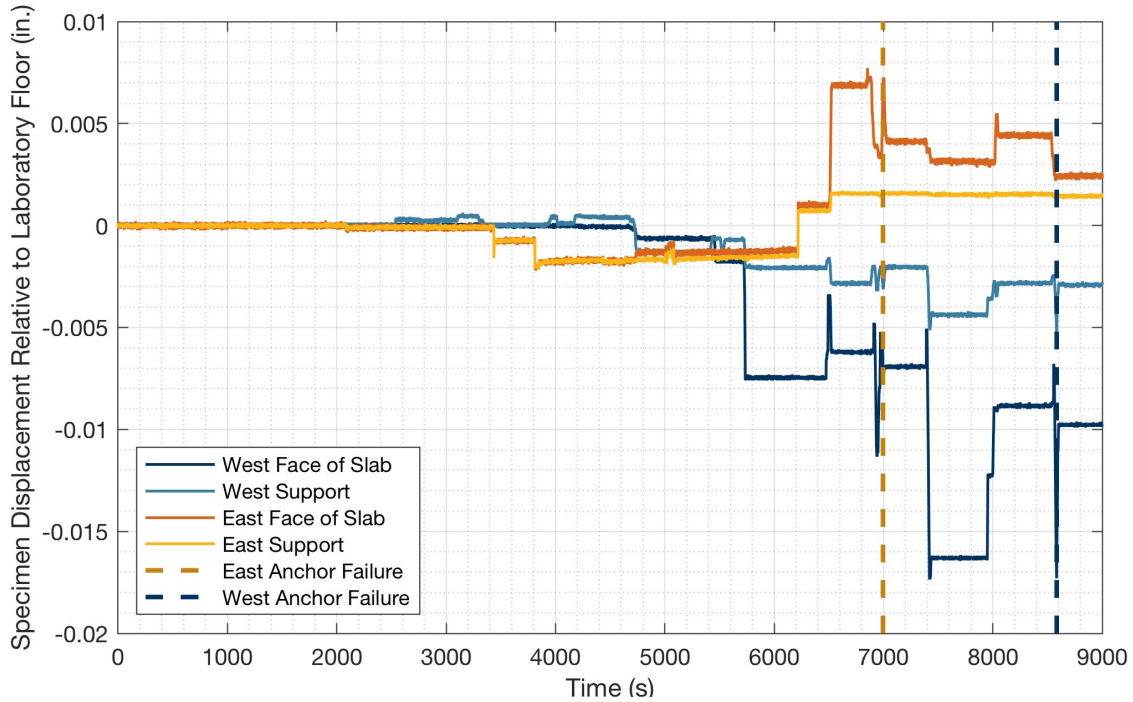


Figure 5-29. Specimen sliding measured along the slab centerline in the direction of loading relative to the laboratory floor, positive sliding is movement towards the east



The difference between the displacements of the east and west faces of the slab is the specimen longitudinal elongation which is shown in Figure 5-30. Positive elongation corresponds to the slab becoming longer.

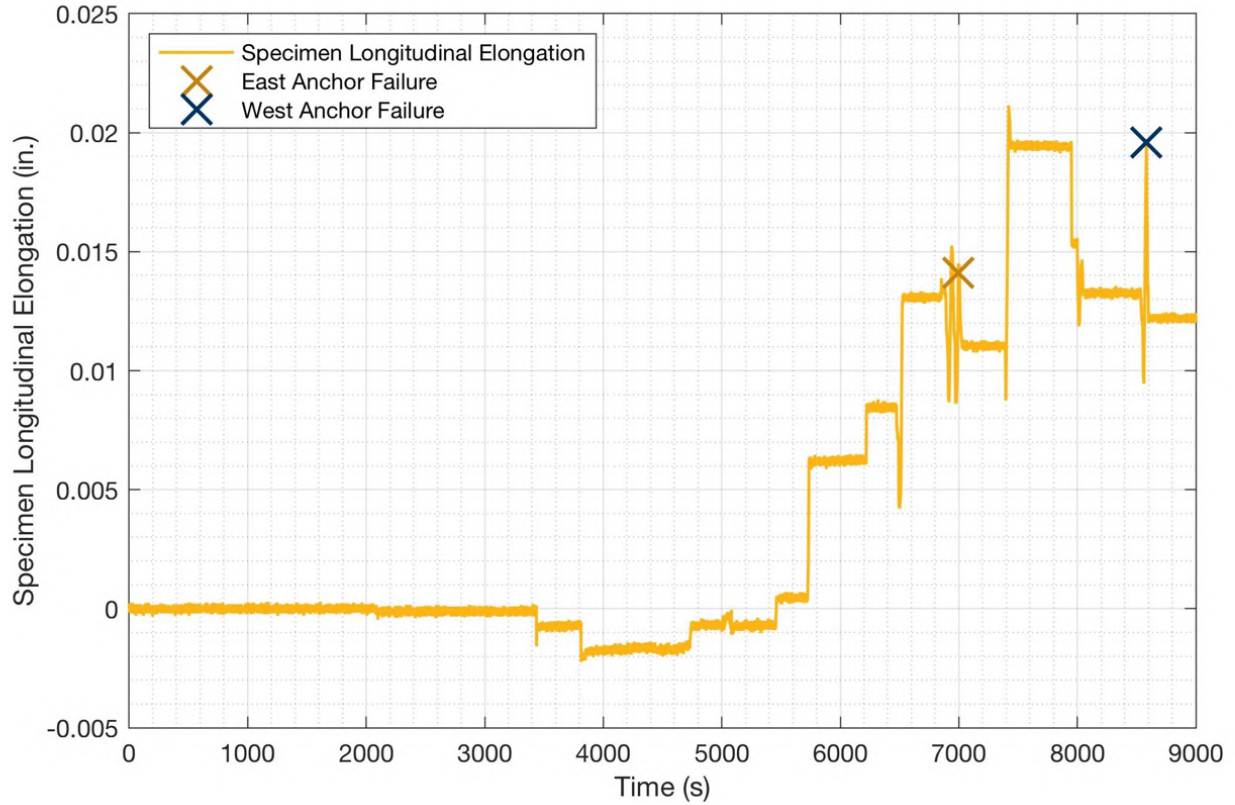
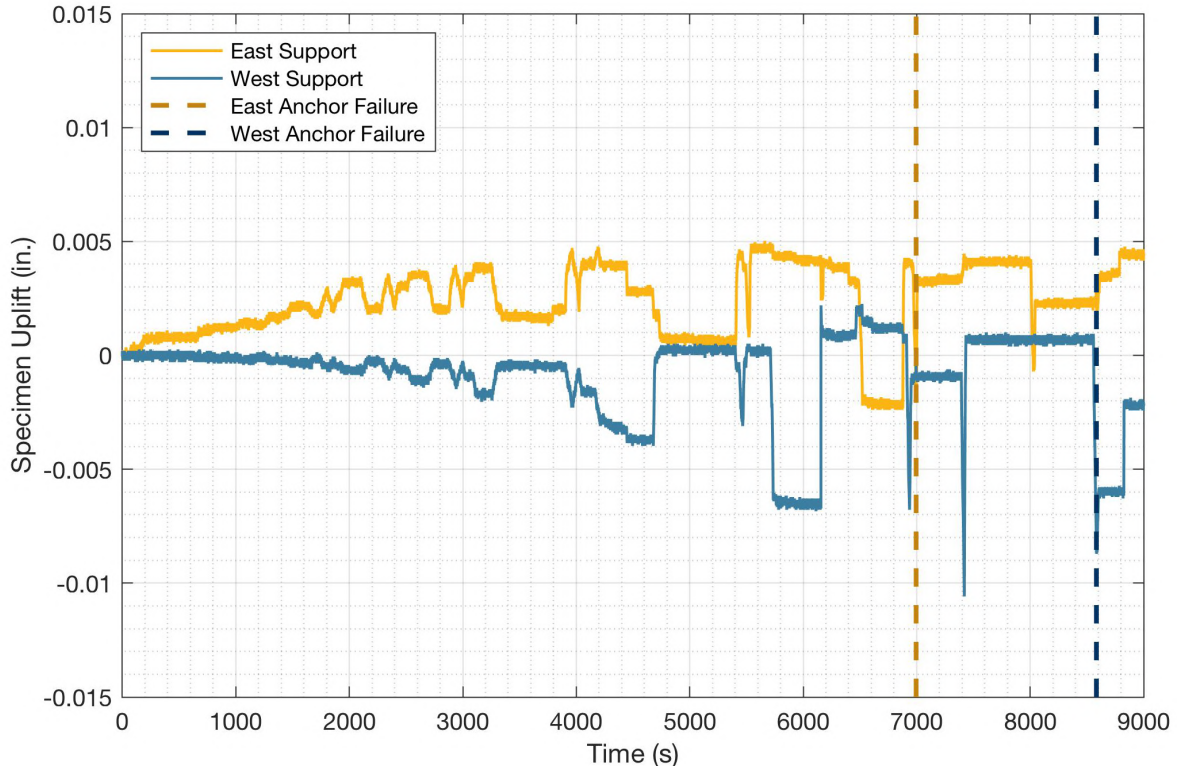


Figure 5-30. Slab longitudinal elongation during testing,

Linear potentiometers were placed in a vertical position on the top surface of the slab above the concrete supports as described in section 4.1 to measure specimen uplift at the supports. Figure 5-31 plots the uplift of both support with a positive measurement indicating uplift. During loading, the east support seems to uplift slightly while the west support mostly sinks downward.



**Figure 5-31. Specimen uplift at west and east supports**

The previous results indicate that the prestressed supports were effective in preventing both uplift and sliding of the specimen during testing.

## 6 DISCUSSION

Table 6-1 summarizes the loads in the anchor group at failure for multiple design methods. The table also shows the experimentally observed failure loads.

**Table 6-1. Summary of mean anchor group loads at failure for various design methods and the experimental results with no safety factors**

Failure Criteria	Anchor Group Load (kips)	% of Measured	Notes
1. Breakout uncracked	179	71%	Unmodified
1. Breakout cracked	143	57%	Unmodified cracked
1. Breakout uncracked + Herzog (2015)	191	75%	Modified by Herzog (2015)
1. Breakout cracked + Herzog (2015)	153	60%	Modified by Herzog (2015) cracked
2. Strut-and-tie Model 1	24	10%	4 struts, one per anchor head
3. Beam-Column Joint	403	159%	Assumed $\gamma = 15$ roof connection
East group breakout	240	95%	First/east breakout
West group breakout	266	105%	Second/west breakout

Note:  $\phi=1$ , mean predictor value  $f_{\text{median}} = 1.33$

The test specimen failure mode was clearly concrete breakout. Crack patterns on the surface of the specimen, as well as posthumous interior exploration, revealed breakout cones for both anchor groups (see Figure 5-1 to Figure 5-5). Evidence of beam-column joint failure was not observed. This failure mode would have involved concrete deterioration and joint dilation which would have caused large strains in all legs of the hoops which was not observed. Evidence of a strut-and-tie type failure was not observed. Tie failure would have involved the failure of anchors, hoops, or longitudinal reinforcing bars. Node failure would have involved the crushing of concrete at the anchor head bearing surface or along the base plate bearing surface. Strut failure would have involved the splitting or crushing of struts.

The failure load obtained from the breakout equations was the closest to the experimental failure load. Including the modification factor  $\psi_M$  proposed by Herzog (2015) improves the results. The strut-and-tie model under predicts the capacity of the connection, while the horizontal joint shear method over predicts the capacity of the connection.

The strut-and-tie model used could be improved if the anchor heads extended past the bottom reinforcing bars, so as to place the bottom strut-and-tie node at the same height as the bottom reinforcing bars. This way the load could follow a more direct path to the bottom reinforcing bars and skip the hoops which were the weakest link in the model. The slab would have to be thickened in this zone to accommodate the deeper anchors.

The horizontal joint shear method assumes beams with shear reinforcement frame into the joint. Even though the test specimen joint was confined on all sides by concrete slab material, the lack of shear reinforcement in this region could account for the lower than expected strength. Slab shear reinforcement could improve the connection strength.

Breakout failure does not seem to be precluded by placing the anchors a distance of  $d/1.5$  into the concrete as suggested in the commentary of ACI 318-14 section R25.4.4.2c.

The ACI strut-and-tie model significantly underpredicted the connection strength. This may be because the ACI strut-and-tie models ignore the tension capacity of concrete which seems to be a significant player in anchor capacity and behavior.

Figure 5-7 shows that the connection demonstrated some ductility before breakout failure occurred. This is of interest because a breakout type failure was expected to be fragile. An average ductility value of 1.64 was calculated (see Table 5-2).

Figure 5-7 and Figure 5-12 show relaxation of the specimen when the loading was paused at the peaks, particularly during the final three load cycles.

The peak measured displacements were on average 11% below the displacement goals of the loading protocol (see Table 5-1). The average difference between the peak measured displacements in the east and west loading directions was about 3%. Even though the measured displacements were less than the desired displacements, this was not a significant issue as there was east-west symmetry.

Two actuators at  $45^\circ$  to the loading direction were attached to the column free end and programmed to minimize out-of-plane motion. Some out-of-plane motion was detected, particularly when loading the west anchor group (see Figure 5-8). The maximum transverse displacement was about 10% of the longitudinal displacement. Figure 5-10 shows some asymmetry in the loads of the north anchors compared to the symmetric south anchors, which can be attributed to asymmetric material properties and to the slight asymmetric loading. Figure 5-11 shows that the inner anchors consistently carried a higher load than the outer anchors. This may be because the load path to the inner anchors is stiffer than the load path to the outer anchors due to the flexibility of the base plate.

The initial prestressing load in the anchors was lost as the cyclic loading progressed (see Figure 5-12). The anchors were not re-stressed during the test.

Some stiffness asymmetry was observed between the east and west anchor groups (see Figure 5-7). Figure 5-13 shows that when loading the east anchor group, the anchors begin to carry load the moment the base plate lifts off the slab. For the west group, on the other hand, the base plate initially lifts off the slab with only minor loading of the anchor group. The group then hardens to a stiffness nearly equal to that of the east group, but offset from it. The failure loads of both groups are similar and seem to be unaffected by this initial stiffness asymmetry.

The confining hoops placed near the top of the joint were more effective than those placed towards the bottom of the joint as they were strained more (see Figure 5-14). Also, only the legs of the hoops that crossed the concrete cone failure planes were observed to carry any significant load.

Figure 5-15 and Figure 5-16 show that during the elastic loading cycles, the column free end displacement was due mostly to the elastic deflection of the column and the anchor elongation. As the cycling loading progressed and damage spread in the concrete, the slab rotation became the

dominant contributor to the column free end deflection. Also, at the instant breakout failure occurred, the slab rotated suddenly and the column unloaded (see Figure 5-17 and Figure 5-18).

The AISC uniform bearing pressure model for the design of base plates from Design Guide 1, under predicts the anchor group load at large loads by about 10%. (see Figure 5-20). The lever arm between the loaded anchors and the resultant of the bearing pressure is shorter than what is obtained using the AISC uniform pressure model.

Section 5.3 shows that the specimen supports performed as designed. The specimen sliding, elongation and uplift were all less than 0.025in., which is considered acceptable.

When using the ACI-318 breakout equations, the concrete is considered “uncracked” if the service loads applied to the concrete prior to applying the anchor force are insufficient to crack the concrete. It could be argued, however, that the anchors in the test slab provide the main loading for the foundation slab and that these loads are sufficient to crack the concrete in the region of the anchors. Therefore, the breakout strength for this type of column-foundation connections should be based on cracked concrete using a cracked concrete factor of  $\psi_{cN} = 1.00$  and not  $\psi_{cN} = 1.25$ . When using the ACI-318 breakout equations, a 25% drop in capacity when using the factor for cracked concrete ( $\psi_{cN} = 1.00$  instead of  $\psi_{cN} = 1.25$ ) might be too severe a punishment for headed anchors in the configuration tested.

As the specimen design intended, none of the instrumented reinforcing bars from the top or bottom meshes surpassed  $2000 \mu\epsilon$  which is approximately the yielding strain of Grade 60 reinforcement (see Figure 5-23 to Figure 5-28).

Before breakout failure, the top surface of the slab deflected in a double curvature shape as would be expected from traditional elastic beam theory (see Figure 5-21).

## 7 CONCLUSIONS

A full-scale test specimen of an interior (not close to the foundation edges) steel-column-to-concrete-foundation connection with cast-in-place headed anchors was designed, built, and tested under quasi-static cyclic loading. No axial load was applied to the column so as to isolate the effect of moment loading. The applicability of various design methods was investigated.

The test specimen clearly failed in a concrete breakout mode. No evidence of horizontal joint shear failure or strut-and-tie type failure was observed.

The breakout equations (ACI 318-14 Chap. 17) seem to be the most appropriate design method for column-foundation connections with cast-in-place headed anchors of the geometry tested. This is consistent with the observation of a breakout type failure. The addition of the modification factor  $\Psi_M$ , as proposed by Herzog (2015), improves the results. This factor is not included in ACI 318-14. The breakout cones were observed to be asymmetric with a much steeper slope towards the interior of the joint, which is consistent with Herzog (2015) in that the base plate bearing pressure impedes the formation of a full breakout cone.

The strut-and-tie model proposed does not seem to be appropriate for the design of column-foundation connections of the geometry tested as it severely underestimated the connection strength. The behavior of anchors depends largely on the tensile capacity of concrete which strut-and-tie models ignore. The model could be improved if the anchor heads extended past the bottom reinforcing bars allowing for a more direct load path. The slab would have to be thickened in this zone to accommodate the deeper anchors.

The horizontal-joint-shear method (ACI 352R-02) does not seem to be appropriate for the design of column-foundation connections of the geometry tested as it overestimates the connection strength. Slab shear reinforcement could improve the connection capacity bringing the experimental capacity closer to that obtained with the horizontal-joint-shear method as this method assumes beams with shear reinforcement frame into the joint.

Breakout failure does not seem to be precluded by placing the anchors a distance of  $d/1.5$  into the concrete as suggested by the commentary of ACI 318-14 section R25.4.4.2c.

The AISC uniform bearing pressure model for the design of base plates from Design Guide 1 (2006), underestimates the anchor group load for connections of the geometry tested.

## 8 REFERENCES

- ACI Committee 318. (2014). *Building Code Requirements for Structural Concrete and Commentary (ACI 318-14)*. Farmington Hills, MI: American Concrete Institute.
- ACI Committee 349. (2013). *Code Requirements for Nuclear Safety Related Concrete Structures*. Farmington Hills, MI: American Concrete Institute.
- ACI Committee 374. (n.d.). *ACI 374, Performance-Based Seismic Design of Concrete Buildings*.
- AISC. (2006). *Design Guide 1: Base Plate and Anchor Rod Design*.
- ASTM. (2014). *ASTM C469, Standard Test Method for Static Modulus of Elasticity and Poisson's Ratio of Concrete in Compression*.
- ASTM. (2017). ASTM A370 - 17, Standard Test Methods and Definitions for Mechanical Testing of Steel Products. In *ASTM International*. West Conshohocken, PA.
- ASTM. (2017). *ASTM C496, Standard Test Method for Splitting Tensile Strength of Cylindrical Concrete Specimens*.
- ASTM. (2018). ASTM C39 / C39M - 18, Standard Test Method for Compressive Strength of Cylindrical Concrete Specimens. In *ASTM International*. West Conshohocken, PA.
- Eligehausen, R., and Balogh, T. (1995). Behaviour of Fasteners Loaded in Tension in Cracked Reinforced Concrete. *ACI-Structural Journal*, 92(3), 365-379.
- Eligehausen, R., and Mallee, R. (2000). *Befestigungstechnik im Beton- und Mauerwerksbau*. Berlin, Germany: Ernst and Sohn.
- Eligehausen, R., and Sawade, G. (1989). *A Fracture Mechanics based Description of the Pull-Out Behaviour of headed Studs embedded in Concrete*. (L. Elfgren, Ed.) London: Chapman and Hall.
- Eligehausen, R., Bouska, P., Cervenka, V., and Pukl, R. (1992). Size Effect of the Concrete Cone Failure Load of Anchor Bolts. In Z. P. Bazant (Ed.), *Fracture Mechanics of Concrete Structures* (pp. 517-525). London, New York: Elsevier Applied Science.
- Eligehausen, R., Fuch, W., Ick, U., Mallee, R., Reuter, M., Schimmelpfenning, K., and Schomal, B. (1992). Behaviour of headed anchors under concentric tension. *Bauingenieur*, 68, 183-196.
- Eligehausen, R., Mallee, R., and Silva, J. F. (2006). *Anchorage in Concrete Construction*. Berlin: Ernst and Sohn.

- FEMA-461. (2007). *Interim Testing Protocols for Determining the Seismic Performance Characteristics of Structural and Nonstructural Components*.
- Fuchs, W., Eligehausen, R., and Breen, J. (1995). Concrete Capacity Design (CCD) Approach for Fastening to Concrete. *ACI Structural Journal*, 73-94.
- Herzog, M. (2015). *Beitrag zur Vereinheitlichung der Bemessung im Stahlbetonbau und in der Befestigungstechnik (Contribution to the standardization of design in reinforced concrete construction and fastening technology)*. Stuttgart, Germany: Institut für Werkstoffe im Bauwesen der Universität Stuttgart.
- Joint ACI-ASCE Committee 352. (2002). *Recommendations for Design of Beam-Column Connections in Monolithic Reinforced Concrete Structures*. American Concrete Institute.
- Mahrenholtz, C., Akguzel, U., Eligehausen, R., and Pampanin, S. (2014, September - October). New Design Methodology for Seismic Column-to-Foundation Anchorage Connections. *ACI Structural Journal*.
- Moehle, J. P. (2015). *Seismic Design of Reinforced Concrete Buildings* (1st ed.). McGraw-Hill Education.
- Nilforoush, R., Nilsson, M., and Elfgren, L. (2017). Experimental Evaluations of Influence of Member Thickness, Anchor-Head Size, and Reinforcement on the Tensile Capacity of Headed Anchors in Uncracked Concrete. *Journal of Structural Engineering*.
- Nilforoush, R., Nilsson, M., Elfgren, L., Ozbolt, J., Hofmann, J., and Eligehausen, R. (2017). Influence of Surface Reinforcement, Member Thickness and Cracked Concrete on Tensile Capacity of Anchor Bolts. *ACI Structural Journal*, 1543-1556.
- Nilforoush, R., Nilsson, M., Elfgren, L., Ozbolt, J., Hofmann, J., and Eligehausen, R. (2017). Tensile Capacity of Anchor Bolts in Uncracked Concrete: Influence of Member Thickness and Anchor's Head Size. *ACI Structural Journal*, 1519-1530.
- Ozbolt, J., Eligehausen, R., Periskic, G., and Mayer, U. (2007). 3D FE Analysis of Anchor Bolts with Large Embedments. *Engineering Fracture Mechanics*, 74(1-2), 168-178.
- Ozbolt, J., Eligehausen, R., and Periskic, G. (2007). 3D FE Analysis of Anchor Bolts with Large Embedments. *Engineering Fracture Mechanics*, 74(1-2), 168-178.
- Rehm, G., Eligehausen, R., and Mallee, R. (1988). *Befestigungstechnik (Fixing technology)*. Berlin, Germany: Ernst and Sohn.
- RILEM TC. (1994). FMC 2 Size-effect method for determining fracture energy and process zone size of concrete, 1990. *RILEM Recommendations for the Testing and Use of Construction Materials*, 102-106.



Wight, J., and MacGregor, J. (2009). *Reinforced Concrete*. New Jersey: Pearson Prentice Hall.

# APPENDIX A. MATERIAL PROPERTIES

## A.1 Concrete Compressive Strength ASTM-C39

Table A- 1 and Figure A- 1 summarize the results of compressive strength tests performed according to ASTM-C39. The column-foundation test specimen was tested on day 21.

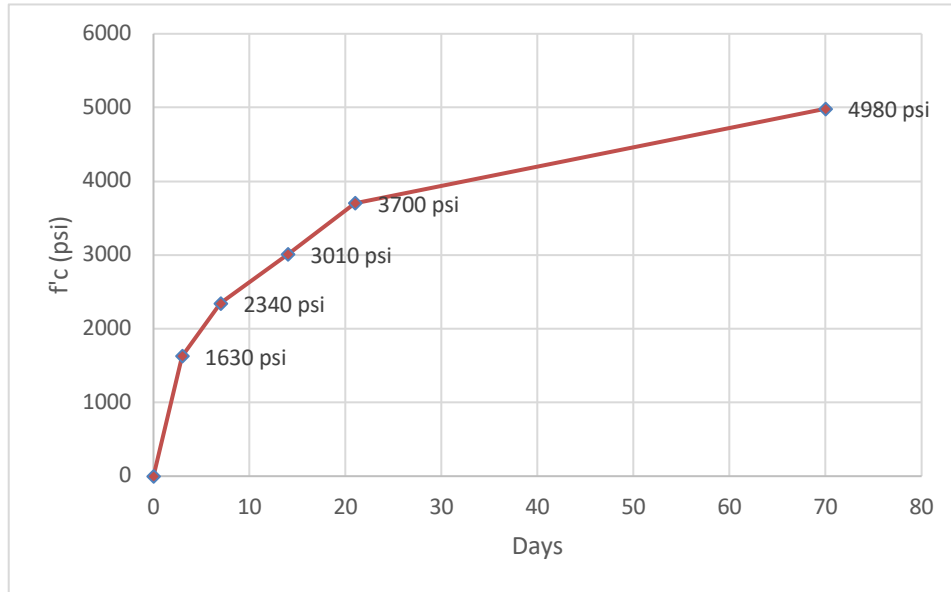


Figure A- 1. Concrete compressive strength growth

Table A- 1. Concrete compressive strength results

Date	Days since cast	f'c (psi)	Average f'c (psi)
24-Nov-17	3	1630	1630
		1660	
		1600	
28-Nov-17	7	2250	2340
		2380	
		2410	
5-Dec-17	14	3150	3010
		2870	
		3010	
12-Dec-17 (Test Day)	21	3860	3700
		3490	
		3610	
		3630	
		3800	
		3810	
30-Jan-17	70	5010	4980
		4990	
		4950	

## A.2 Concrete Modulus of Elasticity and Stress-Strain Curve ASTM-C469

Three concrete cylinders were tested according to ASTM-C469 to determine the stress - strain curve of the concrete on testing day (21 days from casting) (Figure A- 2).

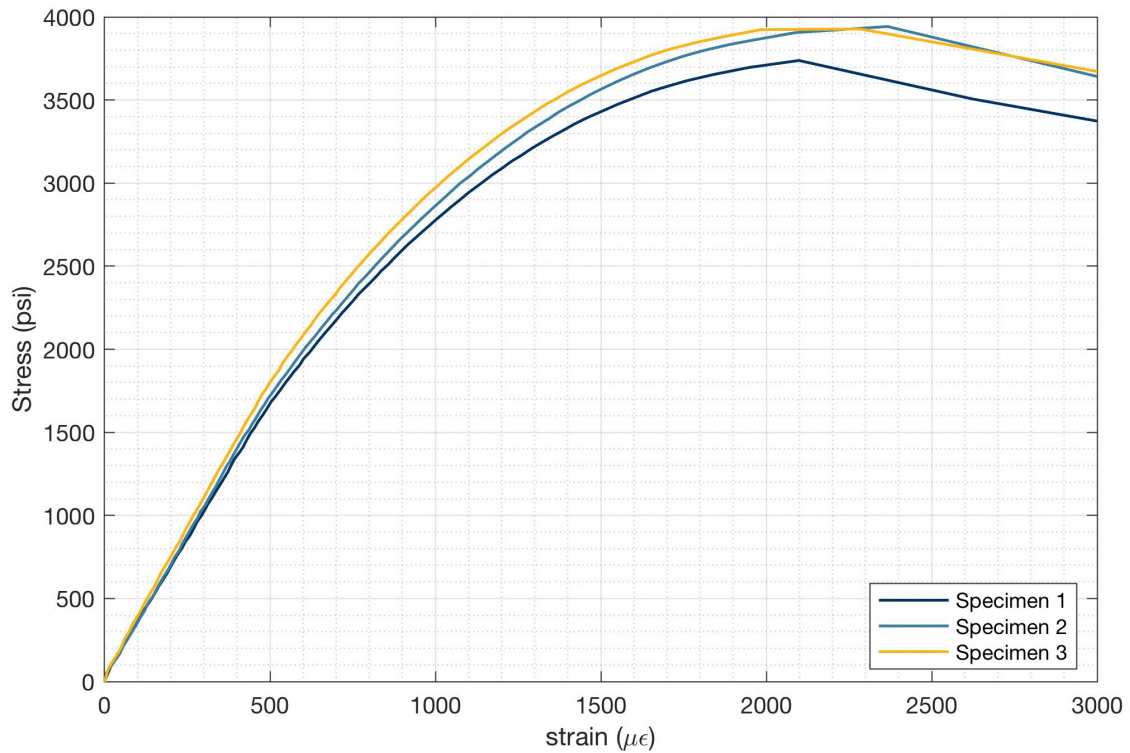


Figure A- 2. Concrete stress - strain results on testing day (21 days from casting)

Table A- 2. Concrete modulus of elasticity test results

Specimen	1	2	3	Average
Initial Concrete Modulus of Elasticity E (psi)	3,360,000	3,440,000	3,620,000	3,470,000

### A.3 Concrete Splitting Tensile Strength ASTM-C496

Splitting tensile strength tests on the concrete were performed on test day (21 days from casting) following the procedures of ASTM-C496-17. Results are shown in Table A- 3.

**Table A- 3. Concrete splitting tensile strength results on test day (21 days from casting)**

<b>Specimen</b>	<b>Splitting Load (lb)</b>	<b>Tensile Strength ft (psi)</b>	<b>Average ft (psi)</b>
1	43,600	386	380
2	41,600	368	
3	43,800	387	

#### A.4 Concrete Fracture Energy FMC2

Initial concrete fracture energy ( $G_f$ ) was determined according to a draft RELIM recommendation TC89-FMT-FMC2. Five notched beams of three different sizes (fifteen beams total) were tested in a simply supported condition as shown in Figure A- 3. Load and deflection of the actuator at midspan was recorded.



Figure A- 3. Concrete Fracture Energy test set-up

Figure A- 4, Table A- 4 and Table A- 5 summarize the chosen specimen geometry.

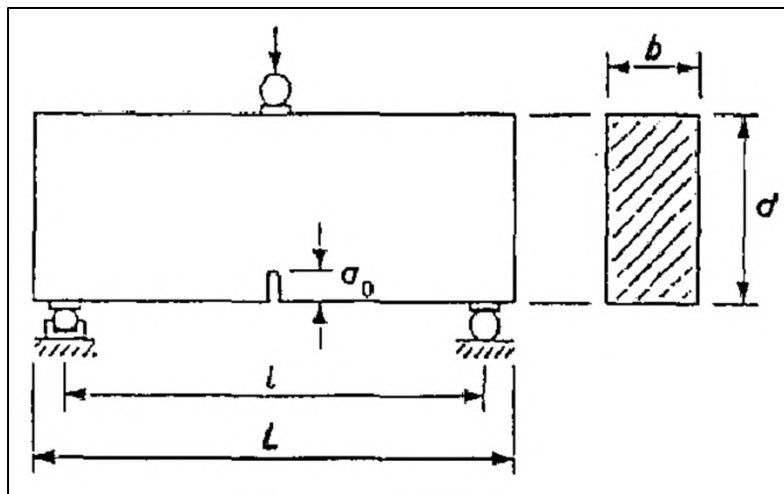


Figure A- 4. Fracture energy specimen geometry

**Table A- 4. Fracture energy specimen geometry and properties**

Specimen Type	d/da	d (in.)	L (in.)	l (in.)	a0 (in.)	Load Rate
Small	4	3	9	7.5	0.53	0.1 in. / 3000 s
Medium	8	6	18	15	1.06	0.1 in. / 2000 s
Large	16	12	36	30	2.13	0.1 in. / 2000 s

**Table A- 5. Geometric considerations and material properties**

<b>b (in.)</b>	3
<b>da (in.)</b>	0.75
<b>l/d</b>	2.5
<b>L/d</b>	3.0
<b>a0/d</b>	0.18
<b>Ec (ksi)</b>	3473
<b>F2.5</b>	0.907
<b>g(α0)</b>	6.44

Figure A- 5, Figure A- 6, and Figure A- 7 show the load history of the small, medium, and large specimens respectively.

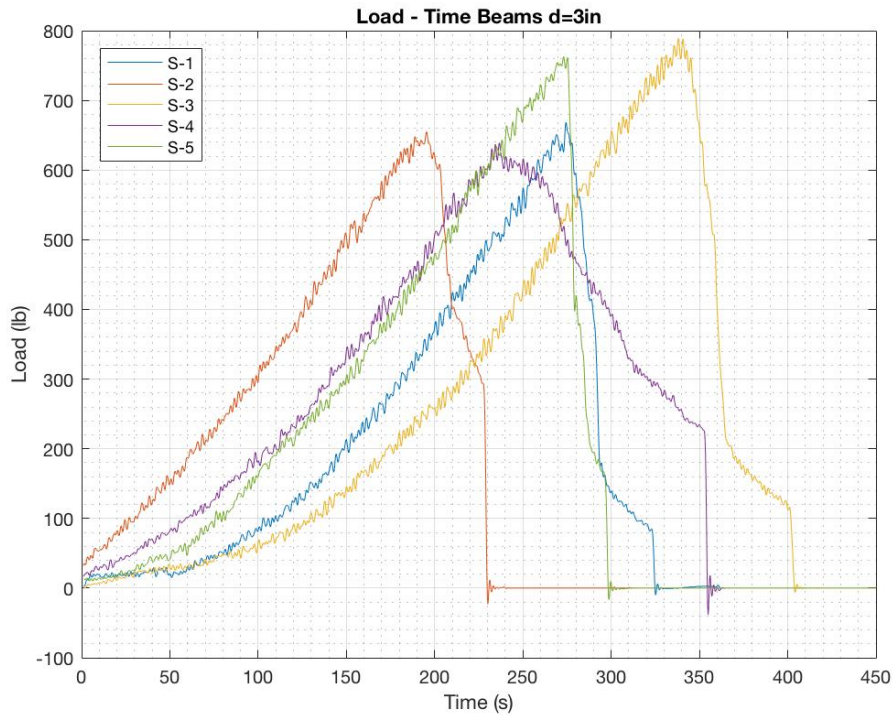


**Figure A- 5. Load – Time graph small fracture energy beams**

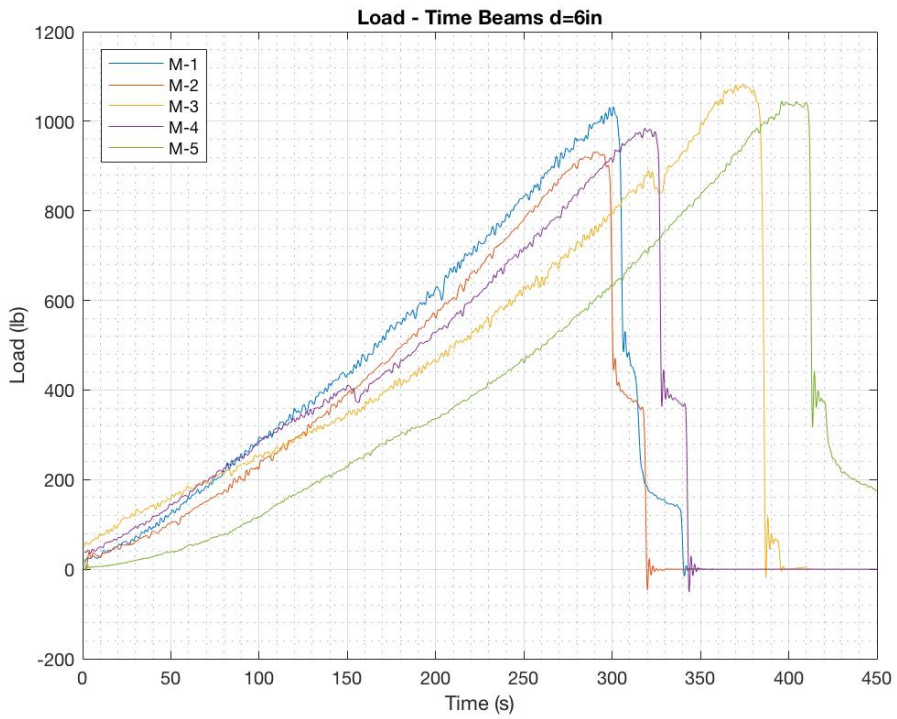


**Figure A- 6. Load – Time graph medium fracture energy beams**

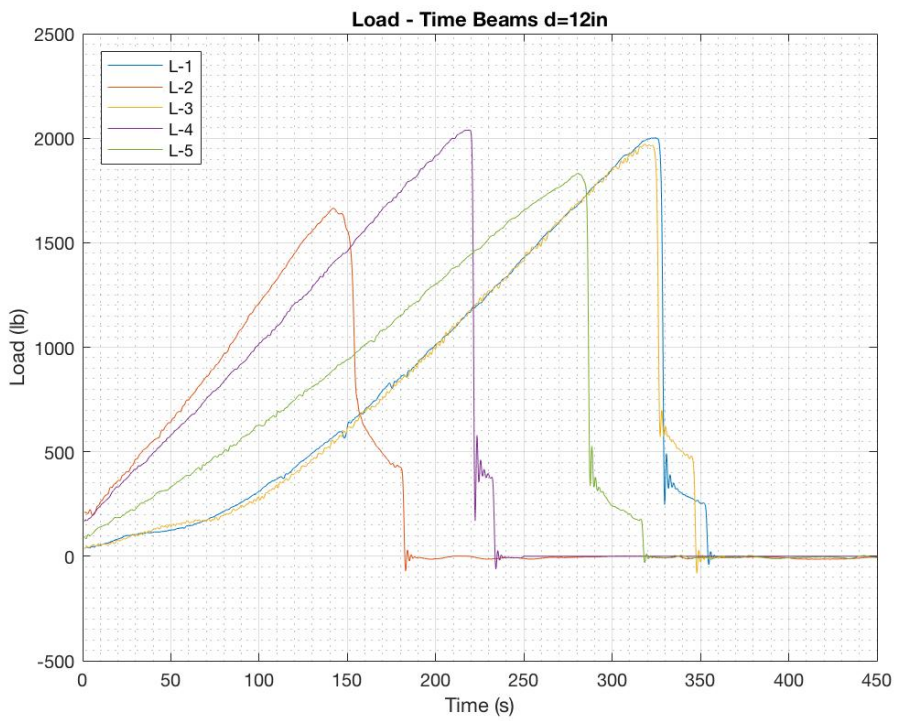


**Figure A- 7. Load – Time graph large fracture energy beams**

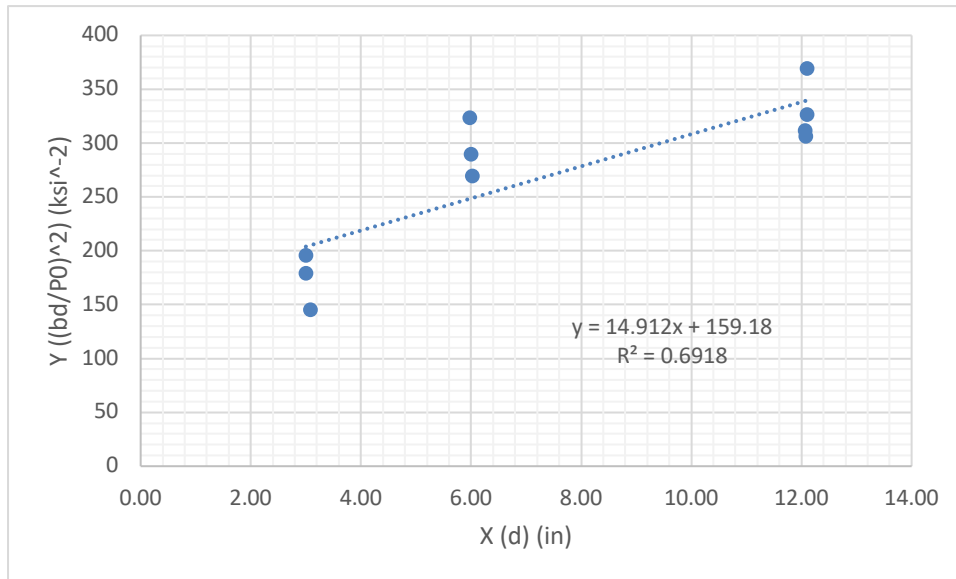


Table A- 6 summarizes the weight and failure load of each specimen.

**Table A- 6. Fracture energy weight and failure load**

Specimen Name	Specimen Weight W (lb)	Failure load Pj (lb)
S-1	7.39	668
S-2	7.67	655
S-3	7.62	789
S-4	7.62	639
S-5	7.54	763
M-1	28.8	1032
M-2	28.4	931
M-3	28.7	1083
M-4	28.6	984
M-5	28.2	1045
L-1	112.0	2001
L-2	112.5	1665
L-3	112.5	1972
L-4	114.0	2039
L-5	110.0	1832

Figure A- 8 shows the normalized load – depth relationship for all 15 beams. Method FMC2 requires only three beams per size so three cases were considered. Table A- 7 shows the resulting fracture energy and statistical values for the three cases: 1) all 15 beams are used in the calculations, 2) only the nine beams that failed closest to 5 min are used and 3) nine beams are chosen to minimize the statistical terms.



**Figure A- 8. Normalized load versus depth relationship**

**Table A- 7. Initial fracture energy and statistical values**

<b>Case</b>	<b>Case 1 (all 15 beams)</b>	<b>Case 2 (nine beams closest to 5 min failure)</b>	<b>Case 3 (nine beams for optimal statistical values)</b>
<b>Gf (psi*in)</b>	0.101	0.106	0.124
<b><math>\omega_a</math></b>	0.219	0.341	0.236
<b><math>\omega_c</math></b>	0.220	0.324	0.190
<b>m</b>	0.383	0.437	0.293

## A.5 Course 3/4" Aggregate



### LA Abrasion (Fine)

Plant Pleasanton-015  
Product 3/4 X #4-A6E



#### Test Information

<b>Test Number</b> 675447363	<b>Sample No</b> 1364095795
<b>Date Started</b> 7/7/2017 7:15:00 AM	<b>Date Sampled</b> 07/07/2017 07:15
<b>Date Completed</b> 07/07/2017 07:15	
<b>Tested By</b> Mike Paulson	
<b>Procedure</b>	
<b>Lab</b>	

#### Test Results

Subsamples	Revolutions	Grading	Mass of Spheres
1	500	A	4584 g
<u>Subsample 1</u>			
<b>Initial Mass</b>	5003.5 g		
<b>Final Mass</b>	3930.7 g		
<b>Loss</b>	21 %		
<u>Results</u>		<u>Targets</u>	<u>Specifications</u>
LA Abrasion (A,500) %	21		<50

StonemontQC

Vulcan Materials Company

Figure A- 9. Course 3/4" aggregate LA abrasion test ASTM-C131

Date : 11/13/2017

Mix Code : 347EG9E1

Description : 3IN LN 470LBS 3/4" 25FA 3-5SL

Sieve Size	Coarse AUGV5A % Passing	Fine AUCBDA % Passing	Combined % Passing	Comb Cumul % Retained % Passing	Comb Indiv % Retained % Passing
2"	100.0	100.0	100.0	0.0	0.0
1-1/2"	100.0	100.0	100.0	0.0	0.0
1"	99.3	100.0	99.6	0.4	0.4
3/4"	88.0	100.0	93.6	6.4	6.0
1/2"	60.7	100.0	79.1	20.9	14.5
3/8"	39.0	100.0	67.6	32.4	11.5
No. 4	6.5	97.0	48.9	51.1	18.7
No. 8		85.0	39.8	60.2	9.1
No. 16		65.0	30.4	69.6	9.4
No. 30		45.0	21.1	78.9	9.4
No. 50		22.0	10.3	89.7	10.8
No. 100		2.0	0.9	99.1	9.4
No. 200		0.4	0.2	99.8	0.8
DRUW lb/ft3					
% Agg	53.2	46.8			
% Coarse Agg	100.0				
% Fine Agg		100.0			
SG	2.68	2.62			
FM	6.55	2.84	4.76		

Figure A- 10 Coarse 3/4" aggregate ASTM-C136 gradation

## A.6 Reinforcing Bar Properties ASTM-A370

Two types of reinforcing bars were used in the project: #4G60 ASTM-A706 for the hoops and #6G100 for the top and bottom mats. The stress – strain curves are shown in Figure A- 11 and Figure A- 12. Summaries of the reinforcing bar properties are shown in Table A- 8and Table A- 9. The #4G60 sample tested was a section of a hoop that was straightened before testing. This may account for the low elastic modulus.

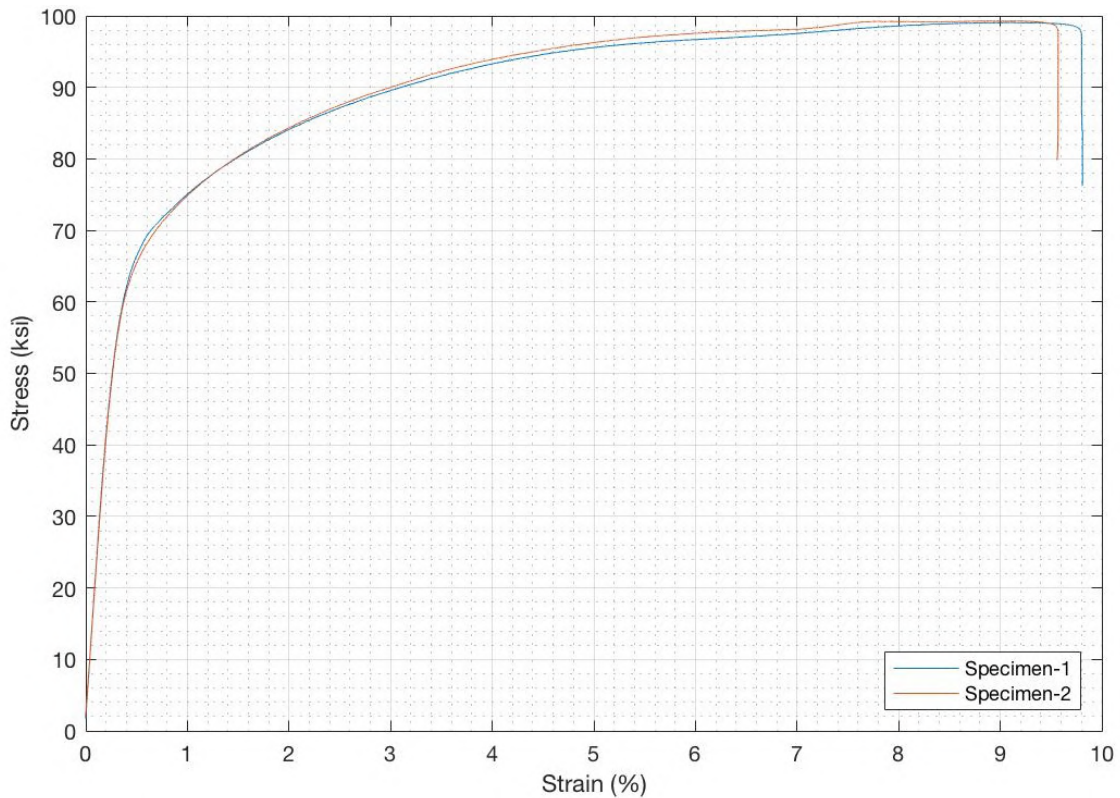
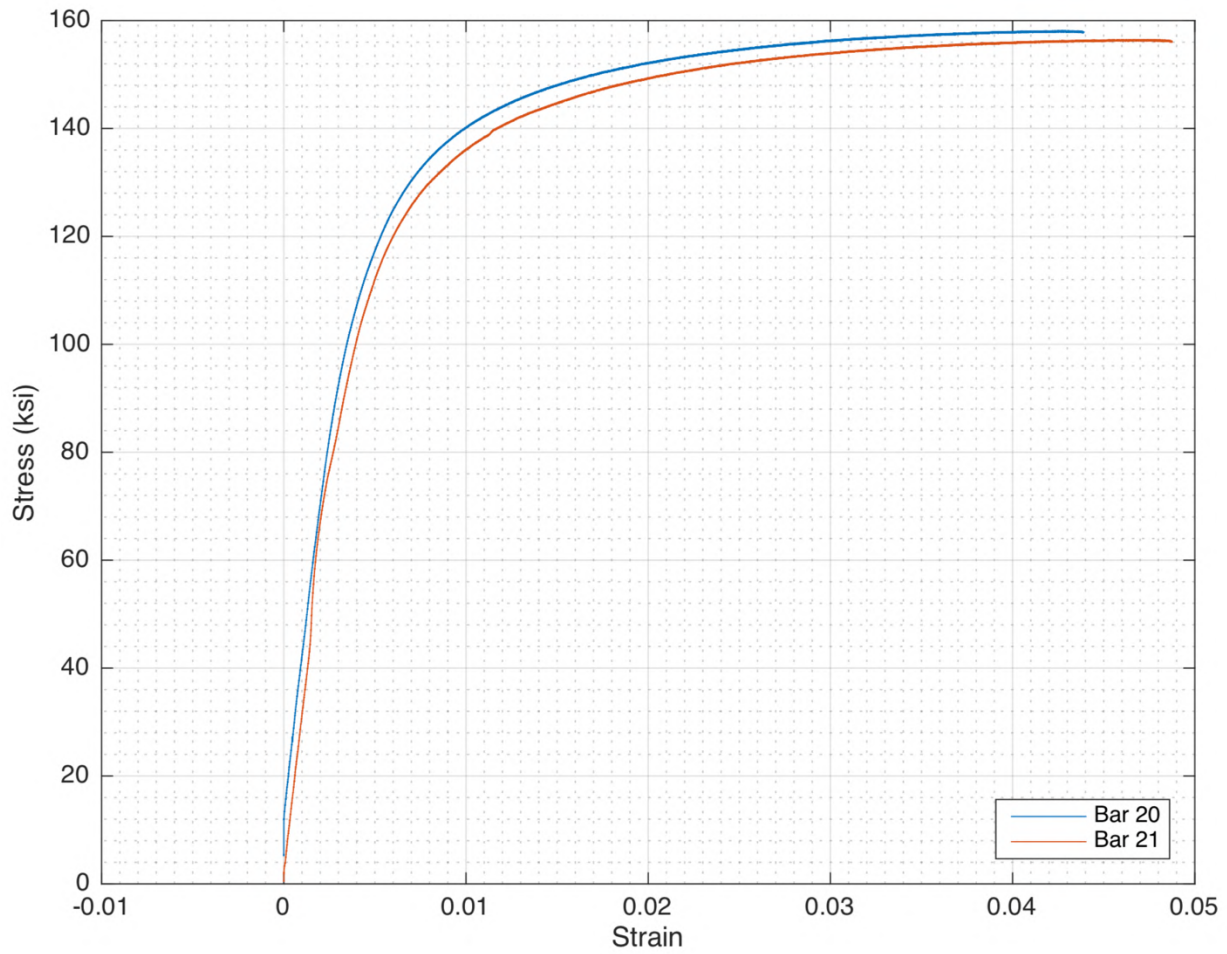


Figure A- 11. Stress - strain graph for hoop reinforcing bar #4G60 ASTM-A706

Table A- 8. Reinforcing bar properties for hoop reinforcing bar #4G60 based on ASTM-A706

Case	Bar 1	Bar 2	Average
E (ksi)	18200	17800	18000
$\sigma_y$ (ksi)	68.6	67.6	68.1
$\epsilon_y$ (%)	0.58%	0.58%	0.58%
$\sigma_{max}$ (ksi)	99.1	99.3	99.2
$\epsilon$ at $\sigma_{max}$ (%)	9.12%	9.08%	9.10%
$\sigma_{rup}$ (ksi)	96.8	98	97.4
$\epsilon_{rup}$ (%)	9.80%	9.57%	9.69%



**Figure A- 12. Stress - strain graph for mat reinforcing bar #6G100**

**Table A- 9. Properties of mat reinforcing bars #6G100 based on ASTM-A706**

Case	Bar 1	Bar 2	Average
E (ksi)	31600	31700	31650
$\sigma_y$ (ksi)	124	118	121
$\epsilon_y$ (%)	0.59%	0.57%	0.58%
$\sigma_{max}$ (ksi)	158	156	157
$\epsilon$ at $\sigma_{max}$ (%)	4.27%	4.62%	4.45%
$\sigma_{rup}$ (ksi)	158	156	157
$\epsilon_{rup}$ (%)	4.39%	4.87%	4.63%

# APPENDIX B. CONCRETE MIXTURE DESIGN

The mixture was designed by Central Concrete as a 4000 psi mixture at 28 days with 3/4" aggregate.

Date :	11/13/2017																																																							
Mix Code :	347EG9E1	Description : 3IN LN 470LBS 3/4" 25FA 3-5SL																																																						
Revision Number :	248	Creation Date : 09 Aug 2016																																																						
Plant :	OAKLAND PLANT (12)	Customer :																																																						
	Created By : Kldiart	Project :																																																						
<b>Specifications</b>																																																								
Consistence Class :	4.00	Max W/C : 1.00																																																						
Strength Class :	3000	Max Agg Size : 1																																																						
Grading Specification :		Min Cement : 471 lb																																																						
		Air Class : 2%																																																						
<table border="1"> <thead> <tr> <th>Material Type</th> <th>Description</th> <th>Supplier Source</th> <th>Design Quantity</th> <th>Specific Gravity</th> <th>Volume ft3</th> </tr> </thead> <tbody> <tr> <td>Cement</td> <td>990100 CEMENT ASTM C150 TYPE II</td> <td>Cemex-Victorville</td> <td>353 lb</td> <td>3.15</td> <td>1.80</td> </tr> <tr> <td>Fly Ash</td> <td>990200 * FLY ASH</td> <td>SRMG-Four Corners</td> <td>118 lb</td> <td>2.00</td> <td>0.95</td> </tr> <tr> <td>Coarse Aggregate</td> <td>990301 3/4 GRAVEL</td> <td>Cemex-Eliot</td> <td>1675 lb</td> <td>2.68</td> <td>10.02</td> </tr> <tr> <td>Fine Aggregate</td> <td>990405 *ASTM C-33 SAND--ANGEL IS</td> <td>Hanson-Oakland</td> <td>1475 lb</td> <td>2.62</td> <td>9.02</td> </tr> <tr> <td>Admixture</td> <td>MASTER POZZOLITH 322N</td> <td>BASF -Cleveland</td> <td>19 lq oz</td> <td>-</td> <td>-</td> </tr> <tr> <td>Water</td> <td>990080 *WATER</td> <td>Central Concrete-Central Concrete</td> <td>33.0 gal</td> <td>1.00</td> <td>4.41</td> </tr> <tr> <td colspan="3"></td> <td><b>Air Content</b></td> <td><b>3.00 %</b></td> <td><b>--</b></td> </tr> <tr> <td colspan="3"></td> <td><b>Yield</b></td> <td><b>3896 lb</b></td> <td><b>--</b></td> </tr> </tbody> </table>			Material Type	Description	Supplier Source	Design Quantity	Specific Gravity	Volume ft3	Cement	990100 CEMENT ASTM C150 TYPE II	Cemex-Victorville	353 lb	3.15	1.80	Fly Ash	990200 * FLY ASH	SRMG-Four Corners	118 lb	2.00	0.95	Coarse Aggregate	990301 3/4 GRAVEL	Cemex-Eliot	1675 lb	2.68	10.02	Fine Aggregate	990405 *ASTM C-33 SAND--ANGEL IS	Hanson-Oakland	1475 lb	2.62	9.02	Admixture	MASTER POZZOLITH 322N	BASF -Cleveland	19 lq oz	-	-	Water	990080 *WATER	Central Concrete-Central Concrete	33.0 gal	1.00	4.41				<b>Air Content</b>	<b>3.00 %</b>	<b>--</b>				<b>Yield</b>	<b>3896 lb</b>	<b>--</b>
Material Type	Description	Supplier Source	Design Quantity	Specific Gravity	Volume ft3																																																			
Cement	990100 CEMENT ASTM C150 TYPE II	Cemex-Victorville	353 lb	3.15	1.80																																																			
Fly Ash	990200 * FLY ASH	SRMG-Four Corners	118 lb	2.00	0.95																																																			
Coarse Aggregate	990301 3/4 GRAVEL	Cemex-Eliot	1675 lb	2.68	10.02																																																			
Fine Aggregate	990405 *ASTM C-33 SAND--ANGEL IS	Hanson-Oakland	1475 lb	2.62	9.02																																																			
Admixture	MASTER POZZOLITH 322N	BASF -Cleveland	19 lq oz	-	-																																																			
Water	990080 *WATER	Central Concrete-Central Concrete	33.0 gal	1.00	4.41																																																			
			<b>Air Content</b>	<b>3.00 %</b>	<b>--</b>																																																			
			<b>Yield</b>	<b>3896 lb</b>	<b>--</b>																																																			

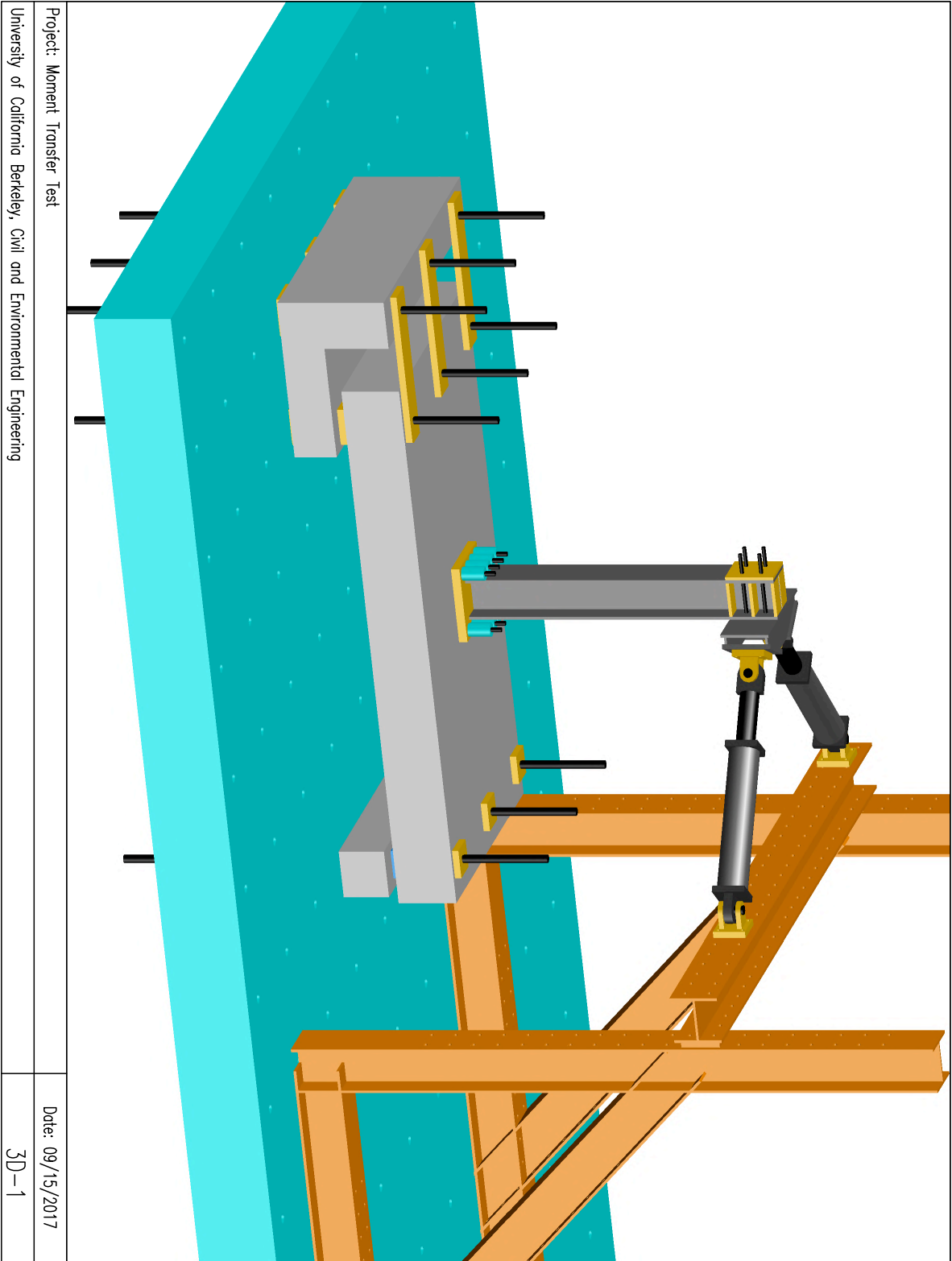
Figure B- 1. Concrete mixture design 347EG9E1 by Central Concrete

DATE	TICKET #	ORDER #	CUSTOMER #	CUST. NAME	PROJECT#	PROJECT NAME			
11/21/17	34087196	3002	1200294	CONCO CEMENT COMPANY					
TIME	LOAD#	QTY	MIX ID	SLUMP	STRENGTH	TOTAL WEIGHT	TRUCK	PLANT #	PLANT NAME
08:04	1	7.00	347EG9E1	4.00	3000.00		487	619	OAKLAND KENNEDY ST PLANT
CONSTITUENT ID	DESCRIPTION			TARGET	ACTUAL	UOM	MOISTURE %		
CUCEM25	990100 CEMENT ASTM			2471.00	2471.00	pounds			
CUFASH	FLY ASH			826.00	826.00	pounds			
AUGV5A	3/4 GRAVEL			11725.00	11725.00	pounds			
AUCSDA	C33 FINE AGG			10717.00	10717.00	pounds			
XUN22	POZZOLITH 322N			133.00	133.00	ounces			
WATER	WATER			231.00	231.00	gallons			

Figure B- 2. Concrete mixture batch ticket with actual weights

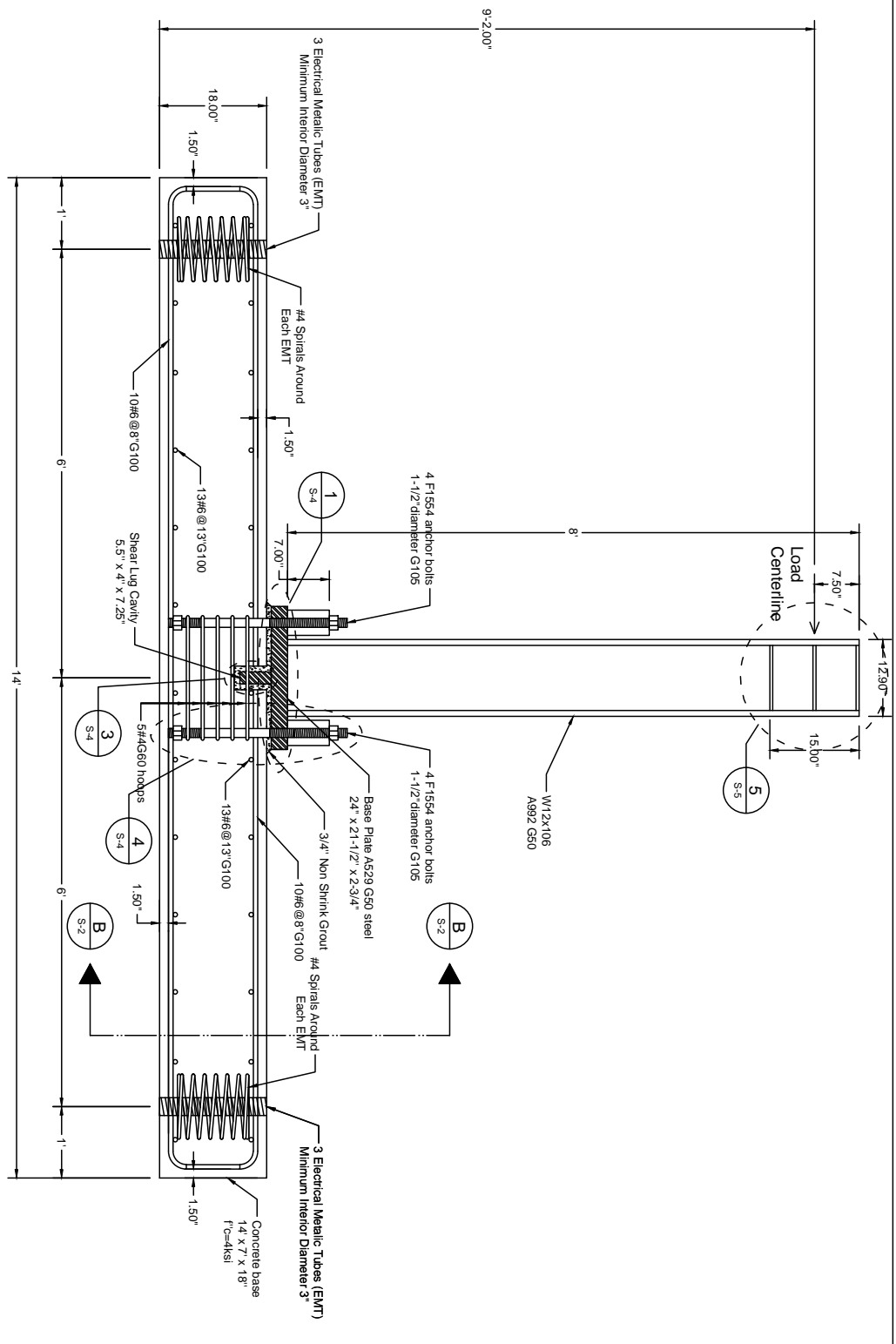
**APPENDIX C. AS-BUILT SPECIMEN DRAWINGS**





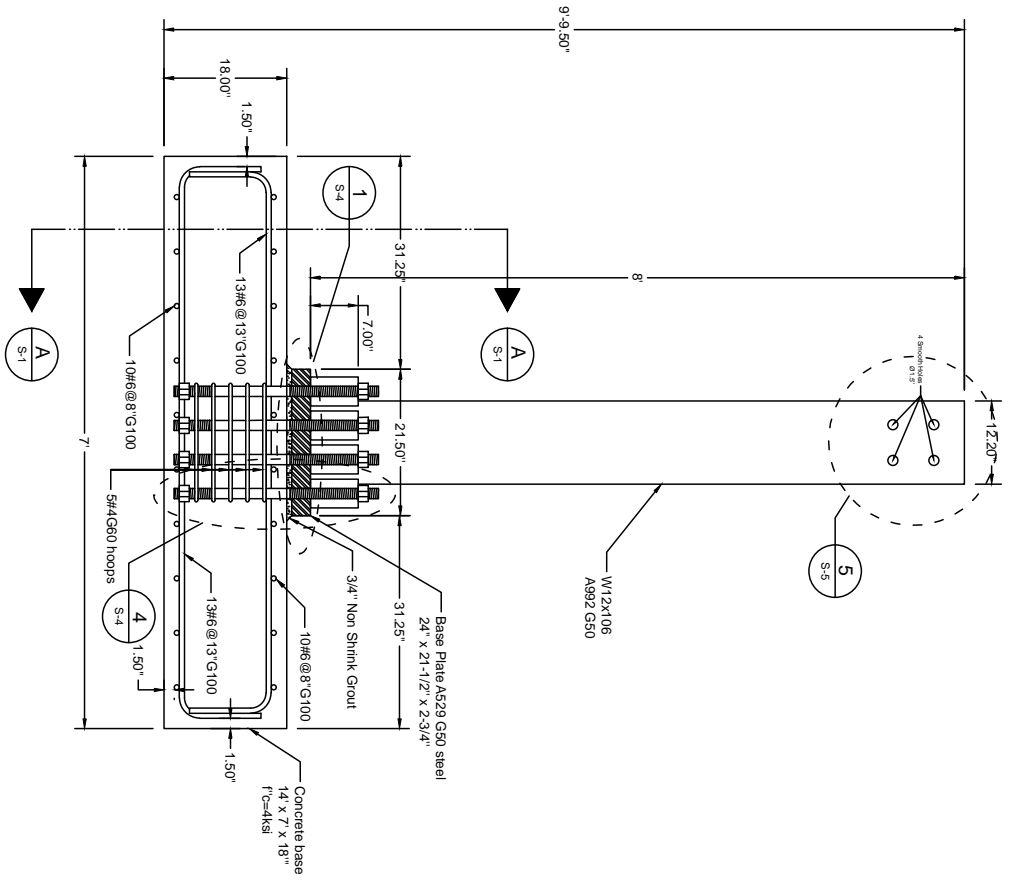
Project: Moment Transfer Test  
University of California Berkeley, Civil and Environmental Engineering

Date: 09/15/2017  
3D-1



## A-A Cross Section

Project: Moment Transfer Test	Date: 07/24/2017
University of California Berkeley, Civil and Environmental Engineering	S-1

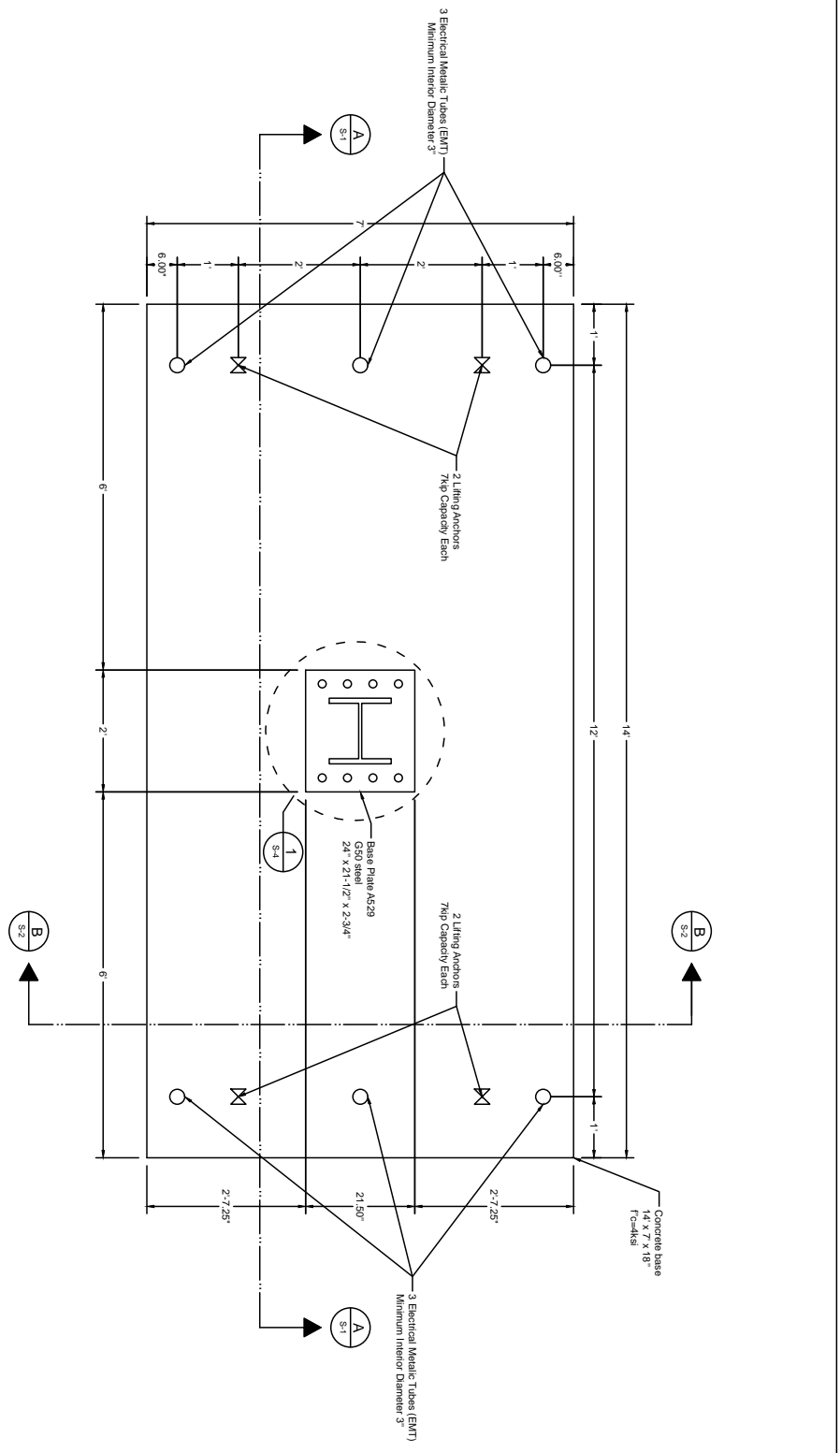


## B-B Cross Section

Project: Moment Transfer Test  
University of California Berkeley, Civil and Environmental Engineering

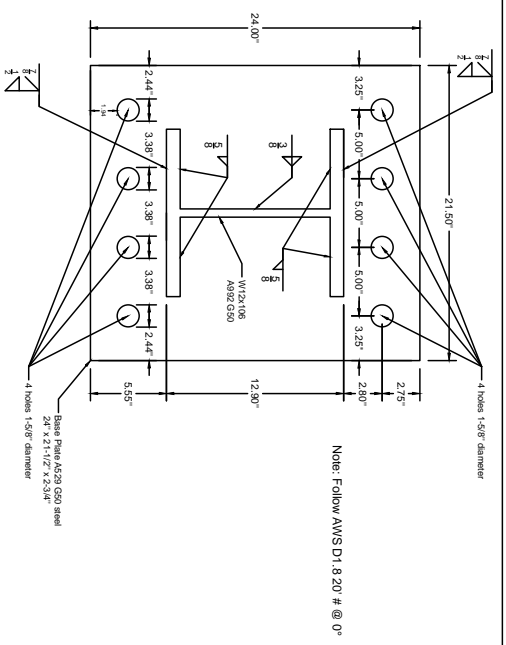
Date: 07/24/2017

S-2

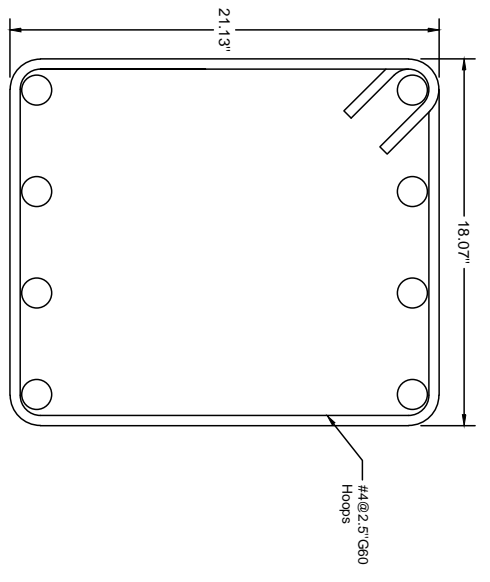


# Plan View

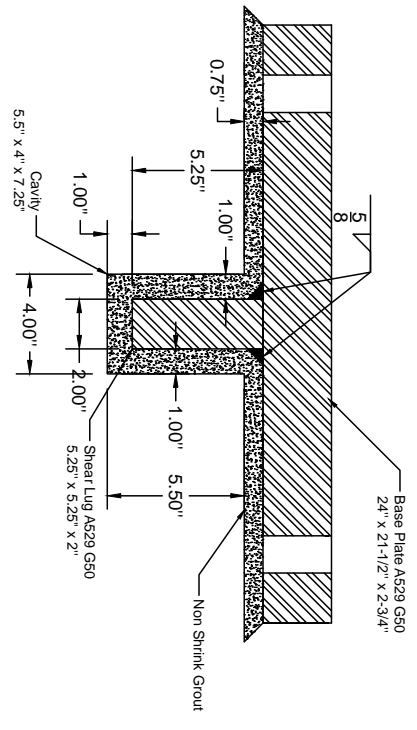
Project: Moment Transfer Test	Date: 07/24/2017
University of California Berkeley, Civil and Environmental Engineering	S-3



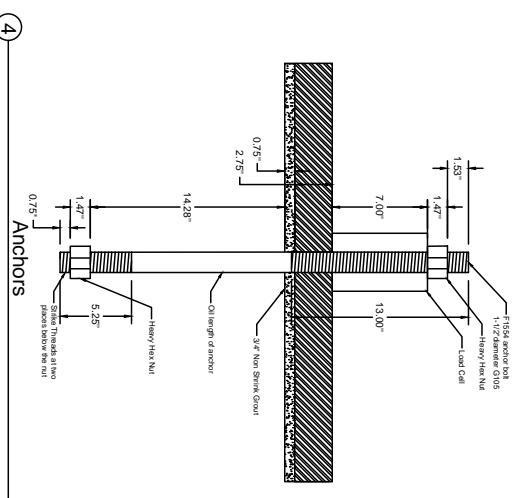
① Base Plate



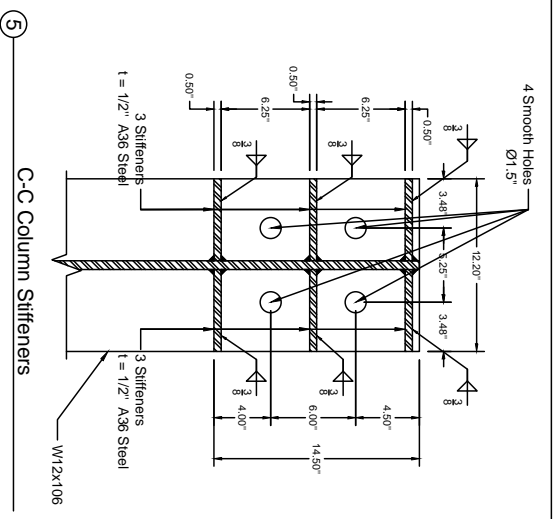
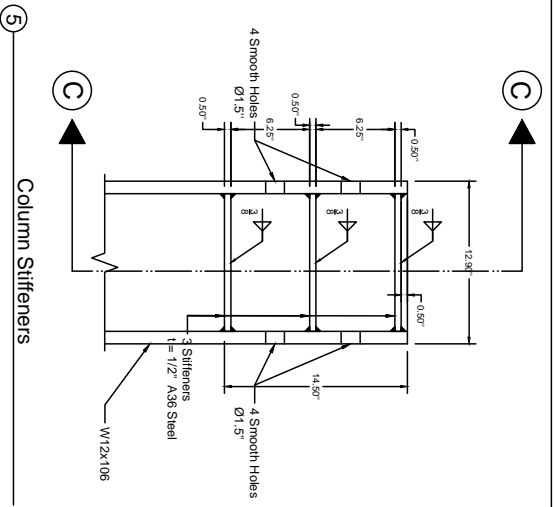
② Hoops



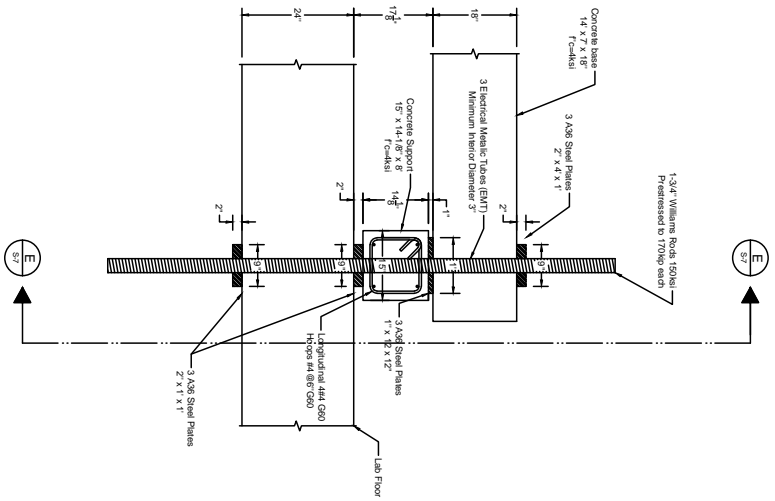
③ Shear Lug



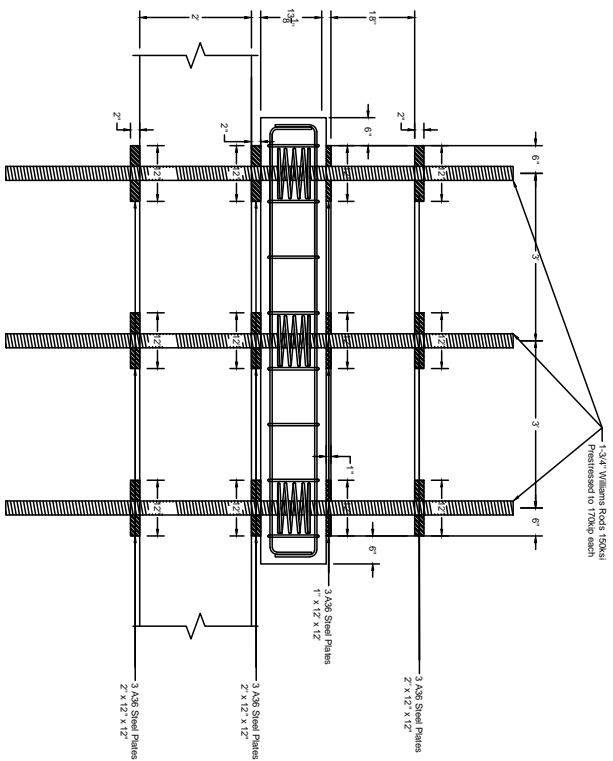
④ Anchors







⑧ Support Type 2



⑨ E-E Support Type 2

Project: Moment Transfer Test University of California Berkeley, Civil and Environmental Engineering	Date: 09/15/2017 S-7
---	-------------------------



# APPENDIX D. ADDITIONAL SPECIMEN DESIGN CALCULATIONS

Detailed calculations of the specimen connection strengths are shown in section 0. All other calculations of considered failure modes are shown below. Table D- 1 shows the factor of safety for all considered failure modes in increasing order.

**Table D- 1. Summary of considered limit states and the factor of safety versus column yielding**

Limit State	FS
Pullout	0.928
Shear Lug	0.943
Tension Flange Welds	1.05
Bearing	1.09
Plate Thickness	1.09
Anchor Rods Tension	1.43
Friction Sliding	1.56
Slab Moment	1.65
Cantilever Tip Rods	1.80
Shear Welds	2.07
Punching Shear	2.17
One Direction Shear	2.34
Column Shear	2.40
Anchor Pryout	2.81
Anchor Rods Shear	3.60
Web Local Yielding (point load)	8.51
Web Buckling	8.51
Tension Plates	8.90
Web Crippling (point load)	12.5
Bolt Hole Bearing	22.8
Plate Shear Block	24.4

Note: Demand based on expected column yield, Capacities based on  $\phi = 1$

Hoops are placed to confine the node according to ACI 352-02 (calculations shown below).

**Confining**

Maximum spacing  
 ACI 352-02 4.2.2.3

$$sh_{max} := \min(0.25 \cdot \min(b_c, h_c), 6 \cdot d_b, 6 \text{ in.}) = 5.13 \text{ in.}$$

$sh := 2.5 \text{ in.}$  Selected spacing

$\frac{sh}{sh_{max}} = 0.488$

 Must be less than 1

+

Minimum Confining Steel Direction 1

$f_y h := 60000 \text{ psi}$  Confining steel yield force

$b''c1 := b_c - 2 \cdot 1.5 \text{ in.} = 17.5 \text{ in.}$  Core dimension of tied column, outside to outside edge of trans-verse reinforcement bars, perpendicular to the transverse reinforcement area  $A_{sh}$  being designed

$A_g := b_c \cdot h_c = 492 \text{ in.}^2$

$A_c := (b_c - 2 \cdot 1.5 \text{ in.}) (h_c - 2 \cdot 1.5 \text{ in.}) = 368 \text{ in.}^2$

$$A_{sh_{min1}} := \max\left(0.3 \cdot sh \cdot b''c1 \cdot \frac{f'_c}{f_y h} \left(\frac{A_g}{A_c} - 1\right), 0.09 \cdot sh \cdot b''c1 \cdot \frac{f'_c}{f_y h}\right) = 0.274 \text{ in.}^2$$

$A_{sh1} := 2 \cdot 0.2 \text{ in.}^2 = 0.4 \text{ in.}^2$  Legs 2 # 4 G60 @ 2.5 in.

$\frac{A_{sh_{min1}}}{A_{sh1}} = 0.685$

 Must be less than 1

Minimum Confining Steel Direction 2

$f_y h := 60 \text{ ksi}$  Confining steel yield force

$b''c2 := h_c - 2 \cdot 1.5 \text{ in.} = 21 \text{ in.}$  Core dimension of tied column, outside to outside edge of trans-verse reinforcement bars, perpendicular to the transverse reinforcement area  $A_{sh}$  being designed

$$A_{sh_{min2}} := \max\left(0.3 \cdot sh \cdot b''c2 \cdot \frac{f'_c}{f_y h} \left(\frac{A_g}{A_c} - 1\right), 0.09 \cdot sh \cdot b''c2 \cdot \frac{f'_c}{f_y h}\right) = 0.329 \text{ in.}^2$$

$A_{sh2} := 2 \cdot 0.2 \text{ in.}^2 = 0.4 \text{ in.}^2$  Legs 2 # 4 G60 @ 2.5 in.

$\frac{A_{sh_{min2}}}{A_{sh2}} = 0.823$

 Equal to 1 if condition is met

## Pullout

ACI 318-14 17.4.3 Crushing of concrete due to bearing on anchor head.

$N_p := 8 \cdot A_b \cdot f'_c = 77.5$  kips      Single anchor load that causes concrete crushing

$\psi_c P := 1.4$       Uncracked concrete

$nN_{pn} := nb \cdot \psi_c P \cdot N_p = 434$  kips      Group load that causes concrete crushing

$FS := \frac{nN_{pn}}{468 \text{ kips}} = 0.927$       Factor of safety against column yielding

$\sigma_{bearing} := \frac{N_{cbg}}{nb \cdot A_b \cdot f'_c} = 3.47$       Bearing stress on head when breakout occurs as a multiple of  $f'_c$  (No modification factors used)

+

## Side-Face Blowout

ACI 318-14 17.4.4 For a single headed anchors with deep embedments close to an edge ( $h_{ef} > 2.5c_1$ ), side face blowout is not applicable.

## Anchors in Shear

### Concrete Breakout in Shear

ACI 318-14 17.5.2 **NOT APPLICABLE** because shear is transmitted as compression through the slab to the supports.

### Anchor Pryout

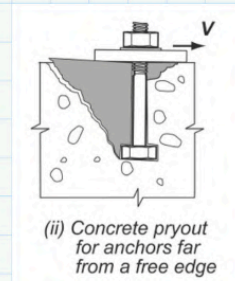
ACI 318-14 17.5.3

$k_{cp} := 2$

$k_{cp} = 2.0$  for  $h_{ef} \geq 2.5$  in.

$N_{cpg} := N_{cbg} = 134$  kips

$V_{cpg} := k_{cp} \cdot N_{cpg} = 269$  kips      Compare to anchor rods as a group



$FS := \frac{V_{cpg}}{98.3 \text{ kips}} = 2.73$       Factor of safety against column yielding

## Punching Shear

### Notation

Input

Output

Condition Check

$$f'c := 3700 \text{ psi}$$

$$B := 21.5 \text{ in.} \quad \text{Base plate dimensions}$$

$$N := 24 \text{ in.}$$

### Punching Shear Capacity

The critical section is taken a rectangular area offset from the outer edge of the base plate a distance of  $d/2$ .

$$d_{avg} := 18 \text{ in.} - 1.5 \text{ in.} - 0.75 \text{ in.} = 15.8 \text{ in.} \quad \text{Average } d \text{ for both perpendicular direction of the slab.}$$

$$b_o := 2 (B + N + 2 \cdot d_{avg}) = 154 \text{ in.} \quad \text{Perimeter of the critical section.}$$

$$\beta := \frac{N}{B} = 1.12$$

$$\alpha_s := 40 \quad \text{For interior columns}$$

$$vc1 := 4 \sqrt{\frac{f'c}{\text{psi}}} \text{ psi} = 243 \text{ psi}$$

$$vc2 := \left( 2 + \frac{4}{\beta} \right) \sqrt{\frac{f'c}{\text{psi}}} \text{ psi} = 340 \text{ psi}$$

$$vc3 := \left( 2 + \frac{\alpha_s \cdot d_{avg}}{b_o} \right) \sqrt{\frac{f'c}{\text{psi}}} \text{ psi} = 370 \text{ psi}$$

$$vc := \min(vc1, vc2, vc3) = 243 \text{ psi}$$

$$vc = 243 \text{ psi}$$

### Punching Shear Demand

Loads based on column yield.

$$P_u := 0.8 \text{ kips}$$

$$M_u := 9050 \text{ kips} \cdot \text{in.}$$

$$c_1 := N = 24 \text{ in.} \quad \text{Plate dimensions}$$

$$c_2 := B = 21.5 \text{ in.}$$

$$b_1 := c_1 + d_{avg} = 39.8 \text{ in.}$$

$$b_2 := c_2 + d_{avg} = 37.3 \text{ in.}$$

$$\gamma_f := \frac{1}{1 + \left(\frac{2}{3}\right) \sqrt{\frac{b_1}{b_2}}} = 0.592$$

ACI 318-14 8.4.2.3.2 Fraction of moment demand that will be resisted by moment in the slab.

$$\gamma_v := 1 - \gamma_f = 0.408$$

Fraction of moment demand that will be resisted by shear stress in the slab.

$$c := \frac{b_1}{2} = 19.9 \text{ in.}$$

$$J_c := d_{avg} \cdot \frac{(c_1 + d_{avg})^3}{6} + \frac{(c_1 + d_{avg}) \cdot d_{avg}^3}{6} + d_{avg} \cdot \frac{(c_2 + d_{avg}) \cdot (c_1 + d_{avg})^2}{2} = (6.54 \cdot 10^5) \text{ in}^4$$

$$v_u := \frac{P_u}{b_o \cdot d_{avg}} + \gamma_v \cdot M_u \cdot \frac{c}{J_c} = 112 \text{ psi}$$

$$\frac{v_c}{v_u} = 2.16$$

Must be greater than 1.

### One Direction Shear

Using effective width from previous moment calculation.

$$b_{shear} := 84 \text{ in.}$$

Full slab width is considered effective

$$V_c := 2 \cdot \sqrt{\frac{f'_c}{\text{psi}}} \left( \frac{b_{shear}}{\text{in.}} \cdot \frac{d_{avg}}{\text{in.}} \right) \frac{\text{kips}}{1000} = 161 \text{ kip}$$

$$V_u := 68.8 \text{ kips}$$

From column moment capacity

$$\frac{V_c}{V_u} = 2.34$$

Must be greater than 1

## Ultimate Moment Capacity

The ultimate capacity of the slab is checked against the expected yield capacity of the column.

$$f_y := 100000 \text{ psi} \quad \text{Expected yield stress of reingorcing bars}$$

$$b_{moment} := 84 \text{ in.}$$

$$a := \frac{A_s \cdot f_y}{b_{moment} \cdot 0.85 \cdot f'_c} = 1.67 \text{ in}$$

$$d := 18 \text{ in.} - 1.5 \text{ in.} - .75 \frac{\text{in.}}{2} = 16.1 \text{ in.}$$

$$M_n := A_s \cdot f_y \cdot \left( d - \frac{a}{2} \right) = (6.73 \cdot 10^3) \text{ kips} \cdot \text{in.}$$

$$Mu_{slabyield} := 339 \text{ kips} \cdot \text{in.} \quad \text{From expected moment yield of column}$$

$$\frac{M_n}{Mu_{slabyield}} = 19.8 \quad \text{Must be greater than 1}$$

## Transverse Steel

Minimum steel is used.

$$A_{smin} := \max \left( 0.0018 \cdot \frac{60}{100}, 0.0014 \right) \cdot 18 \text{ in.} \cdot 168 \text{ in.} = 4.23 \text{ in.}^2 \quad \text{ACI318-14 7.6.1.1}$$

13#6G100 are selected.

$$A_{strans} := 13 \cdot 0.44 \text{ in.}^2 = 5.72 \text{ in.}^2$$

## Moment Anchorage Test Specimen: Loads, Column, Base Plate and Anchor Rods

### Assumptions

Base plate, anchor rods, punching shear and one direction shear are designed for the expected moment capacity of the column using  $\phi$  of 1.

Shear lug and anchor rods are designed to resist all the shear individually.

Moment is calculated at the face of the joint

### Notation

Input

Output

Condition Check

### Data

$E := 29000$  ksi

$f'c := 3700$  psi

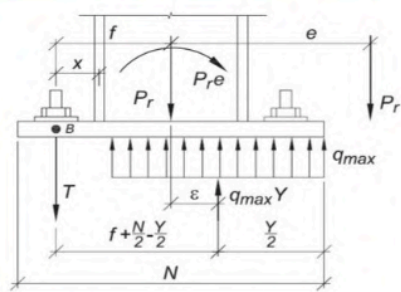
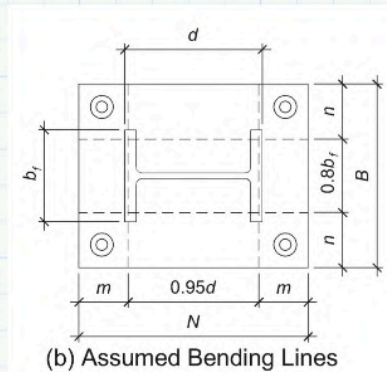


Fig. 3.4.1. Base plate with large moment.



$B := 21.5$  in.

$N := 24$  in.

Column: W12x106 A529 G50

$bf := 12.2$  in.

$d := 12.9$  in.

$tf := 0.99$  in.

$tw := 0.61$  in.

$f := 9.25$  in.

$$x := f - \frac{d}{2} + \frac{tf}{2} = 3.3 \text{ in}$$

$h := 15.9 \cdot tw = 9.7$  in

$$\frac{h}{tw} = 15.9$$

$$F_{ycol} := 50000 \text{ psi}$$

$$F_{ucol} := 65000 \text{ psi} \quad \text{Fucol is from 65-100ksi}$$

$$Z_x := 164 \text{ in.}^3$$

$$S_x := 145 \text{ in.}^3$$

$$r_y := 3.11 \text{ in.}$$

$$R_y := 1.2$$

AISC-341-16 Table A3.1 Expected yield and rupture overstrength factors

$$R_t := 1.2$$

$$\varphi_M := 1$$

### Expected Ultimate Moment

$$\varphi_M M_n := \varphi_M \cdot F_{ycol} \cdot R_t \cdot Z_x = (9.8 \cdot 10^3) \text{ kips} \cdot \text{in.}$$

$$L_p := 1.76 \cdot r_y \cdot \sqrt{\frac{E}{F_{ycol} \cdot R_y}} = 120 \text{ in.}$$

Maximum length so lateral torsional buckling will not govern

### Expected Yield Moment

$$\varphi_M M_y := \varphi_M \cdot F_{ycol} \cdot R_y \cdot S_x = (8.7 \cdot 10^3) \text{ kips} \cdot \text{in.}$$

### Shear

$$\frac{\frac{h}{tw}}{2.24 \cdot \sqrt{\frac{E}{F_{ycol}}}} = 0.295$$

Must be less than 1 for local buckling

$$C_v := 1$$

$$V_n := 0.6 F_{ycol} \cdot (d \cdot tw) C_v = 236 \text{ kips}$$

### Loads

$$P_u := 1 \text{ kips} +$$

Self weight of column and actuator. Some axial load is necessary or equations do not work

$$M_u := \varphi_M M_y = (8.7 \cdot 10^3) \text{ kips} \cdot \text{in.}$$

$$L := 88.5 \text{ in}$$

Distance from force application to bottom of W section

$$V_u := \frac{M_u}{L} = 98.3 \text{ kips}$$

Lateral load that will yield the column



$$\frac{V_n}{V_u} = 2.4$$

Must be greater than 1

$$e := \frac{Mu}{Pu} = (8.7 \cdot 10^3) \text{ in.}$$

Almost no axial load so excentricity is very large

### Bearing on concrete

ACI 318-14 22.8

A1 << A2 The base plate area is small compared to the concrete pedestal area.

Factor of 2 included.

$$\varphi_{Bear} := 0.65$$

$$f_{pMax} := \varphi_{Bear} \cdot 0.85 \cdot f'_c \cdot 2 = (4.09 \cdot 10^3) \text{ psi}$$

$$q_{max} := \varphi_{Bear} \cdot 0.85 \cdot f'_c \cdot 2 \cdot B = 87.9 \frac{\text{kips}}{\text{in.}}$$

### Minimum excentricity

Minimum excentricity so AISC Design Guide for plate, bearing and bolts applies.

$$e_{min} := \frac{N}{2} - \frac{Pu}{(2 \cdot q_{max})} = 12 \text{ in.}$$

$$\frac{e_{min}}{e} = 0.001$$

Must be less than 1

### Base plate

Calculations based on ASCE Design Guide 1

$$\left(f + \frac{N}{2}\right)^2 = 452 \text{ in.}^2$$

$$2 \cdot Pu \cdot \frac{(e+f)}{q_{max}} = 198 \text{ in.}^2$$

$$\frac{\left(2 \cdot Pu \cdot \frac{(e+f)}{q_{max}}\right)}{\left(f + \frac{N}{2}\right)^2} = 0.439$$

Must be less than 1

$$Y1 := \left(f + \frac{N}{2}\right) - \sqrt{\left(f + \frac{N}{2}\right)^2 - 2 \cdot \frac{Pu \cdot (e+f)}{q_{max}}} = 5.33 \text{ in.}$$

$$Y2 := \left(f + \frac{N}{2}\right) + \sqrt{\left(f + \frac{N}{2}\right)^2 - 2 \cdot \frac{Pu \cdot (e+f)}{q_{max}}} = 37.2 \text{ in.}$$

$$Y := Y1 = 5.33 \text{ in.}$$

Choose realistic Y from Y1 and Y2

$$T_{total} := q_{max} \cdot Y - Pu = 468 \text{ kips}$$

Tension force of all anchor rods on one side at column yield.

$$z := f + \frac{N}{2} - \frac{Y}{2} = 18.6 \text{ in.}$$

Internal lever arm

### Base Plate Thickness

$$Fy_{plate} := 50000 \text{ psi} \quad \text{Steel plate A529 G50}$$

$$Fu_{plate} := 70000 \text{ psi}$$

$$n := \frac{(B - 0.8 \cdot bf)}{2} = 5.87 \text{ in.}$$

$$m := \frac{(N - 0.95 \cdot d)}{2} = 5.87 \text{ in.}$$

$$Maxmn := \max(m, n) = 5.87 \text{ in.}$$

$$x1 := 1.49 \cdot Maxmn \cdot \sqrt{\frac{f_{pMax}}{Fy_{plate}}} = 2.5 \text{ in.}$$

$$x2 := 2.11 \cdot \sqrt{\frac{f_{pMax} \cdot Y \cdot \left( Maxmn - \frac{Y}{2} \right)}{Fy_{plate}}} = 2.49 \text{ in.}$$

$$t_{pMin1} := \text{if}(Y \geq Maxmn, x1, x2) = 2.49 \text{ in.}$$

$$t_{pMin2} := 2.11 \cdot \sqrt{\frac{T_{total} \cdot x}{B \cdot Fy_{plate}}} = 2.53 \text{ in.}$$

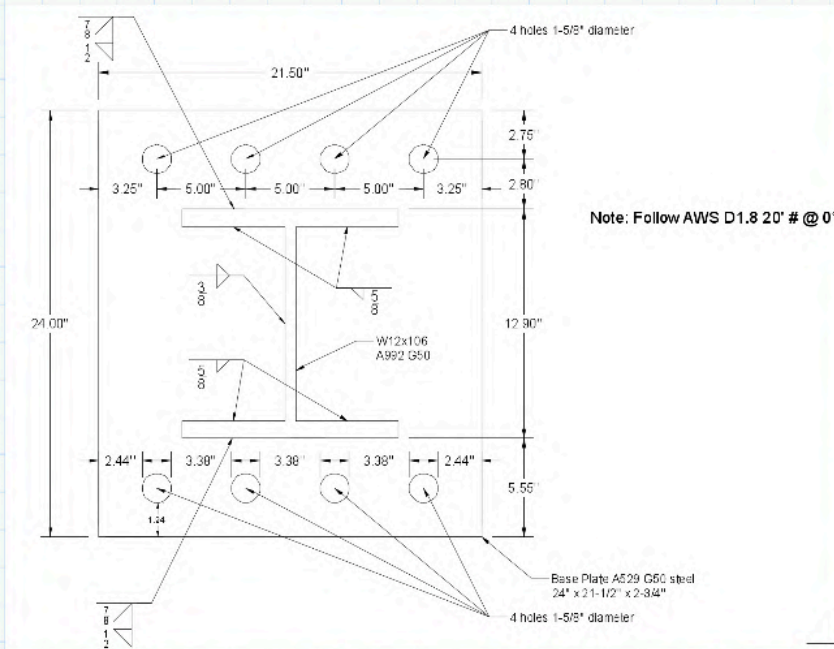
$$t_{pMin} := \max(t_{pMin1}, t_{pMin2}) = 2.53 \text{ in.}$$

$$tp := \left( 2 + \frac{3}{4} \right) \text{ in.}$$

$$\frac{tp}{t_{pMin}} = 1.09$$

Must be greater than 1

## Welds



### 1. Tension Fillet Welds (tfw) on Flange

$$F_{EXX} := 70000 \text{ psi}$$

All welds 70,000 psi electrode

$$w_{tfw} := \frac{9}{8} \text{ in.}$$

1/2in weld on one side and 5/8in on other side

$$k1 := \left(1 + \frac{1}{8}\right) \text{ in.} = 1.13 \text{ in.}$$

$$Lw_{tfw} := d - 2 \cdot k1 = 10.7 \text{ in.}$$

$$R_{n1} := 0.707 \cdot w_{tfw} \cdot Lw_{tfw} \cdot (0.6 \cdot F_{EXX} \cdot 1.5) = 534 \text{ kips}$$

### 2. Tension Fillet Welds (tfw) on Flange, Base Metal

$$Fy_{BM} := 50000 \text{ psi}$$

Column steel properties

$$Fu_{BM} := 65000 \text{ psi}$$

$$R_{n2A} := 0.6 \cdot Fy_{BM} \cdot Lw_{tfw} \cdot w_{tfw} = 359 \text{ kips}$$

$$R_{n2B} := 0.6 \cdot F_{u_{BM}} \cdot Lw_{tfw} \cdot w_{tfw} = 467 \text{ kip}$$

$$R_{n2} := \min(R_{n2A}, R_{n2B}) = 359 \text{ kips}$$

### 3. Partial Joint Penetration weld (PJP) on Flange

$$w_{PJP} := \frac{7}{8} \text{ in.}$$

$$Lw_{PJP} := d = 12.9 \text{ in.}$$

$$R_{n3} := 0.6 \cdot F_{EXX} \cdot Lw_{PJP} \cdot \left( w_{PJP} - \frac{1}{8} \text{ in.} \right) = 406 \text{ kip}$$

### 4. Partial Joint Penetration weld (PJP) on Flange, Base Metal

$$R_{n4} := F_{y_{BM}} \cdot \left( w_{PJP} - \frac{1}{8} \text{ in.} \right) \cdot Lw_{PJP} = 484 \text{ kip}$$

$$R_{n5} := F_{u_{BM}} \cdot \left( w_{PJP} - \frac{1}{8} \text{ in.} \right) \cdot Lw_{PJP} = 629 \text{ kip}$$

### Flange Weld Summary

$$R_n := \min(R_{n1}, R_{n2}) + \min(R_{n3}, R_{n4}, R_{n5}) = 766 \text{ kip}$$

$$P_{fw} := \frac{R_n \cdot (d - tf)}{L} = 103 \text{ kips}$$

$$\frac{P_{fw}}{Vu} = 1.05$$

Must be greater than or equal to 1

### 1. Shear Weld

$$w_s := \frac{3}{8} \text{ in.}$$

$$Lw_s := 2 \cdot \left(9 + \frac{1}{8}\right) \text{ in.} = 18.3 \text{ in}$$

$$R_{ns1} := 0.6 \cdot F_{EXX} \cdot 0.707 \cdot w_s \cdot Lw_s = 203 \text{ kips}$$

### 2. Shear Weld - Base Metal

$$R_{ns2} := 0.6 \cdot F_{yBM} \cdot w_s \cdot Lw_s = 205 \text{ kips}$$

### Web Weld Summary

$$R_{ns} := \min(R_{ns1}, R_{ns2}) = 203 \text{ kips}$$

+

$$\frac{R_{ns}}{Vu} = 2.07$$

Must be greater than 1

## Anchor rods

$$nb := 4$$

Number of bolts resisting tension (bolts on one side)

$$Tu := \frac{T_{total}}{nb} = 117 \text{ kips}$$

Tension per anchor rod

$$Rn := 166.7 \text{ kips}$$

Chose 4 anchor rods 1-1/2in F1554 G105

$$\frac{Rn}{Tu} = 1.43$$

Must be greater than 1

**Table 3.1. ASTM F1554 Anchor Rod (rod only) Available Tensile Strength, kips**

Rod Diameter, in.	Rod Area, $A_b$ , in. <sup>2</sup>	LRFD			ASD		
		$\phi R_n$ $\phi = 0.75$			$R_n/\Omega$ $\Omega = 2.00$		
		Grade 36 kips	Grade 55 kips	Grade 105 kips	Grade 36 kips	Grade 55 kips	Grade 105 kips
5/8	0.307	10.0	12.9	21.6	6.68	8.63	14.4
3/4	0.442	14.4	18.6	31.1	9.60	12.4	20.7
7/8	0.601	19.6	25.4	42.3	13.1	16.9	28.2
1	0.785	25.6	33.1	55.2	17.1	22.1	36.8
1 1/8	0.994	32.4	41.9	69.9	21.6	28.0	46.6
1 1/4	1.23	40.0	51.8	86.3	26.7	34.5	57.5
1 1/2	1.77	57.7	74.6	124	38.4	49.7	82.8
1 3/4	2.41	78.5	102	169	52.3	67.6	113
2	3.14	103	133	221	68.3	88.4	147
2 1/4	3.98	130	168	280	86.5	112	186
2 1/2	4.91	160	207	345	107	138	230
2 3/4	5.94	194	251	418	129	167	278
3	7.07	231	298	497	154	199	331
3 1/4	8.30	271	350	583	180	233	389
3 1/2	9.62	314	406	677	209	271	451
3 3/4	11.0	360	466	777	240	311	518
4	12.6	410	530	884	273	353	589

Table from AISC Design Guide 1

## Anchor Rods in Shear

As recommended by the Design Guide 1 AISC only half of the rods are assumed to resist shear.

$$Vu = 98.3 \text{ kips} \quad +$$

$$Fu_{rod} := 125000 \text{ psi}$$

$$Ab := 4 \cdot 1.77 \text{ in.}^2 = 7.08 \text{ in.}^2 \quad \text{Area of 4 bolts}$$

$$Vn := 0.4 \cdot Fu_{rod} \cdot Ab = 354 \text{ kips}$$

$$\frac{Vn}{Vu} = 3.6$$

Must be greater than 1

### Minimum plate edge distance

$$c_{min} := 1.25 \cdot 1.5 \text{ in.} = 1.88 \text{ in.} \quad 1\text{-}1/4 \text{ of the bolt diameter}$$

$$c_{actual} := 2.75 \text{ in.} \quad \text{From center to closest edge}$$

$$\frac{c_{actual}}{c_{min}} = 1.47 \quad \text{Must be greater than 1}$$

### Minimum Anchor Rod Spacing

AISC J3.3

$$db_{rod} := 1.5 \text{ in.}$$

$$spacing_{min} := \left(2 + \frac{2}{3}\right) \cdot db_{rod} = 4 \text{ in.}$$

$$spacing_{actual} := 5 \text{ in.} \quad \text{Center to center spacing of bolts}$$

$$\frac{spacing_{actual}}{spacing_{min}} = 1.25 \quad \text{Must be greater than 1}$$

### Bolt Hole Bearing Strength

AISC J3.10

$$lc := 1.94 \text{ in.} \quad \text{Dist from edge of hole to edge of plate} \quad +$$

$$Rn := \min(1.5 \cdot lc \cdot tp \cdot Fu_{plate}, 3 \cdot db_{rod} \cdot tp \cdot Fu_{plate}) = 560 \text{ kips}$$

$$Rn \cdot nb = (2.24 \cdot 10^3) \text{ kips}$$

$$\frac{Rn \cdot nb}{Vu} = 22.8 \quad \text{Must be greater than 1}$$

### Plate Shear Block

AISC J4.3

$$A_{gv} := 2.75 \text{ in.} \cdot t_p \cdot 2 = 15.1 \text{ in}^2$$

$$A_{nv} := 1.94 \text{ in.} \cdot t_p \cdot 2 = 10.7 \text{ in}^2$$

$$A_{nt} := 3 \cdot 3.38 \text{ in.} \cdot t_p = 27.9 \text{ in}^2$$

$$R_{n_{SBlock1}} := 0.6 \cdot F_{u_{plate}} \cdot A_{nv} + 1 \cdot F_{u_{plate}} \cdot A_{nt} = 2400 \text{ kips}$$

$$R_{n_{SBlock2}} := 0.6 \cdot F_{y_{plate}} \cdot A_{gv} + 1 \cdot F_{u_{plate}} \cdot A_{nt} = 2406 \text{ kips}$$

$$R_{n_{SBlock}} := \min(R_{n_{SBlock1}}, R_{n_{SBlock2}}) = 2400 \text{ kips}$$

$$R_{n_{SBlock}} = (2.4 \cdot 10^3) \text{ kips}$$

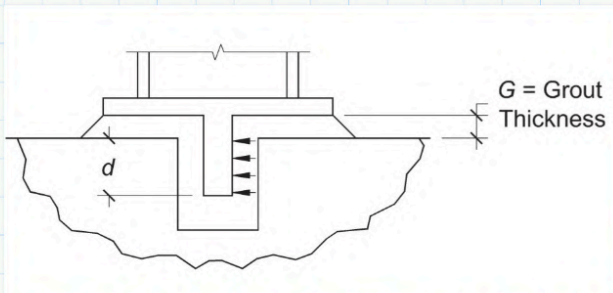
$$\frac{R_{n_{SBlock}}}{V_u} = 24.4$$

Must be greater than 1



## Shear Lug

AISC Design Guide 1 is used for shear lug design.



### Lug Properties

$$l := 5.25 \text{ in.}$$

$$G := 0.75 \text{ in.}$$

$$d := 4.5 \text{ in.}$$

$$h := G + d = 5.25 \text{ in.}$$

$$t := 2 \text{ in.}$$

$$F_{y\text{lug}} := 50000 \text{ psi}$$

### Weld

$$t_w := \frac{5}{8} \text{ in.}$$

$$F_{EXX} := 70000 \text{ psi}$$

### 1. Bearing

$$A_{req} := \frac{Vu}{1.3 \cdot f'_c} = 20.4 \text{ in.}^2$$

$$d_{req} := \frac{A_{req}}{l} = 3.89 \text{ in.}$$

$$\frac{d}{d_{req}} = 1.16$$

Must be greater than 1

## 2. Concrete Breakout

$$A_v := 18 \text{ in.} \cdot 84 \text{ in.} - 12 \text{ in.} \cdot 2.5 \text{ in.} = (1.48 \cdot 10^3) \text{ in}^2 \quad \text{Projected area by 45 degree planes (AISC Design Guide 1 Fig 4.9.3)}$$

$$V_{conc} := 4 \cdot \sqrt{\frac{f'_c}{\text{psi}}} \cdot \frac{A_v}{\text{in.}^2} \cdot \frac{\text{kips}}{1000} = 361 \text{ kips}$$

$$\frac{V_{conc}}{Vu} = 3.67 \quad \text{Must be greater than 1}$$

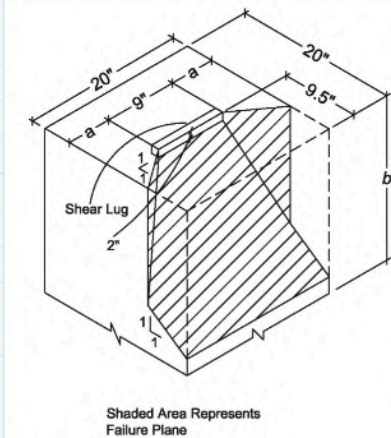


Fig. 4.9.3. Lug failure plane.

## 3. Lug Thickness

$$Mu_{lug} := Vu \cdot \left( G + \frac{d}{2} \right) = 295 \text{ kip} \cdot \text{in} \quad \text{Cantilever model}$$

$$t_{req} := \sqrt{\frac{Mu_{lug} \cdot 4}{F_{ylug} \cdot l}} = 2.12 \text{ in.}$$

$$\frac{t}{t_{req}} = 0.943 \quad \text{Must be less than 1}$$

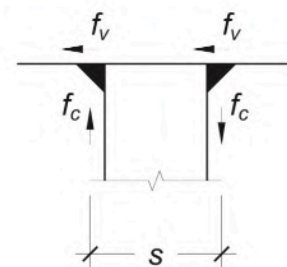


Fig. 4.9.4. Forces on shear lug welds.

## 4. Welds

$$s := t + 2 \cdot \frac{1}{3} \cdot t_w = 2.417 \text{ in.}$$

$$f_c := \frac{Mu_{lug}}{s \cdot l} = 23.2 \frac{\text{kip}}{\text{in}}$$

$$f_v := \frac{Vu}{2 \cdot l} = 9.36 \frac{\text{kips}}{\text{in.}}$$

$$f_r := \sqrt{f_c^2 + f_v^2} = 25.1 \frac{\text{kips}}{\text{in.}}$$

$$R_n := 0.6 \cdot F_{EXX} \cdot 1.5 \cdot t_w \cdot 0.707 = 27.8 \frac{\text{kips}}{\text{in.}}$$

$$\frac{R_n}{f_r} = 1.11$$

Must be greater than 1

Minimum safety factor for shear lug

$$a := \min\left(\frac{d}{d_{req}}, \frac{V_{conc}}{Vu}, \frac{t}{t_{req}}, \frac{R_n}{f_r}\right) = 0.943$$

## Moment Anchorage Test Specimen: Prestressed Anchors, Rebar Hooks, Deflections, Point Load, Actuators

### Assumptions

Designed for Expected moment of the column.

### Notation

Input

Output

Condition Check

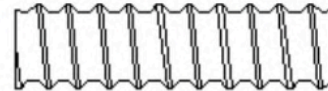
### Data

$f'_c := 3700$  psi

150ksi Williams rod 1-3/4in diameter ASTM A722-07



Structural Properties	
Yield Stress	Ultimate Stress
120 KSI (827 MPa)	150 KSI (1034 MPa)
Elongation in 20 bar diameters	Reduction of Area
4%	20% min.



Unique Thread Form

R71 150 KSI All-Thread-Bar - ASTM A722\*

Nominal Bar Diameter & Pitch	Minimum Net Area Thru Threads	Minimum Ultimate Strength	Prestressing Force			Nominal Weight	Approx. Thread Major Dia.	Part Number
			0.80f pu A	0.70f pu A	0.60f pu A			
1" - 4 (26 mm)	0.85 in <sup>2</sup> (549 mm <sup>2</sup> )	128 kips (567 kN)	102 kips (454 kN)	89.3 kips (397 kN)	76.5 kips (340 kN)	3.09 lbs./ft. (4.6 Kg/M)	1-1/8" (28.6 mm)	R71-08
1-1/4" - 4 (32 mm)	1.25 in <sup>2</sup> (807 mm <sup>2</sup> )	188 kips (834 kN)	150 kips (667 kN)	131 kips (584 kN)	113 kips (500 kN)	4.51 lbs./ft. (6.71 Kg/M)	1-7/16" (36.5 mm)	R71-10
1-3/8" - 4 (36 mm)	1.58 in <sup>2</sup> (1019 mm <sup>2</sup> )	237 kips (1054 kN)	190 kips (843 kN)	166 kips (738 kN)	142 kips (633 kN)	5.71 lbs./ft. (8.50 Kg/M)	1-9/16" (39.7 mm)	R71-11
1-3/4" - 3-1/2 (46 mm)	2.60 in <sup>2</sup> (1664 mm <sup>2</sup> )	390 kips (1734 kN)	312 kips (1388 kN)	273 kips (1214 kN)	234 kips (1041 kN)	9.06 lbs./ft. (13.5 Kg/M)	2" (50.8 mm)	R71-14
2-1/4" - 3-1/2 (57 mm)**	4.08 in <sup>2</sup> (2632 mm <sup>2</sup> )	613 kips (2727 kN)	490 kips (2181 kN)	429 kips (1909 kN)	368 kips (1636 kN)	14.1 lbs./ft. (20.8 Kg/M)	2-1/2" (63.5 mm)	R71-18
2-1/2" - 3 (65 mm)	5.19 in <sup>2</sup> (3350 mm <sup>2</sup> )	778 kips (3457 kN)	622 kips (2766 kN)	545 kips (2422 kN)	467 kips (2074 kN)	18.2 lbs./ft. (27.1 Kg/M)	2-3/4" (69.9 mm)	R71-20
3" - 3 (75 mm)	6.85 in <sup>2</sup> (4419 mm <sup>2</sup> )	1027 kips (4568 kN)	822 kips (3656 kN)	719 kips (3198 kN)	616 kips (2740 kN)	24.1 lbs./ft. (35.8 Kg/M)	3-1/8" (79.4 mm)	R71-24

\*\* The 2-1/4" diameter bar is not covered under ASTM A722.

- ACI 355.1R section 3.2.5.1 indicates an ultimate strength in shear has a range of .6 to .7 of the ultimate tensile strength. Designers should provide adequate safety factors for safe shear strengths based on the condition of use.
- Per PTI recommendations for anchoring, anchors should be designed so that:
  - The design load is not more than 60% of the specified minimum tensile strength of the prestressing steel.
  - The lock-off load should not exceed 70% of the specified minimum tensile strength of the prestressing steel.
  - The maximum test load should not exceed 80% of the specified minimum tensile strength of the prestressing steel.

## Lateral Friction Resistance

Lateral load will be resisted by between the slab and the laboratory strong floor that are prestressed together with nine Williams rods.

$PT := 170$  kips      Pretensioning force per bar

$L := 9$  in.      Length of square metal plate

$\mu := 0.1$       Friction coefficient steel plate - concrete lab floor

$P := 9 (PT) + 5.5$  kips =  $(1.54 \cdot 10^3)$  kips      Total prestressing force of nine bars plus self weight

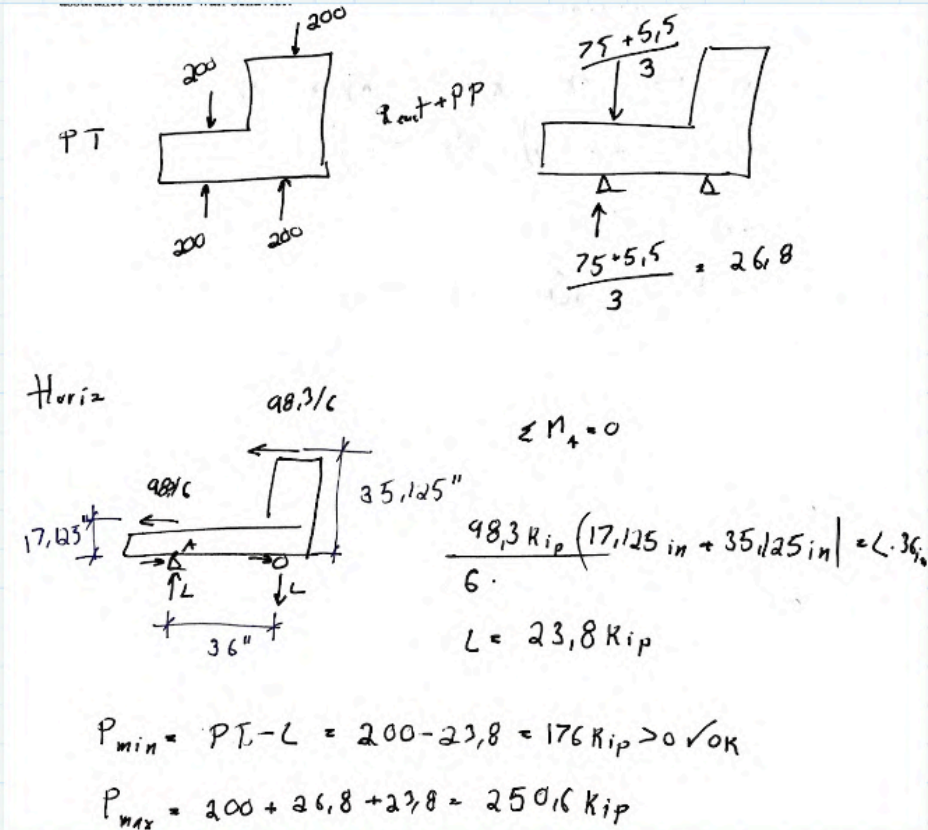
$Fr := \mu \cdot P = 154$  kips

$Vu := 98.3$  kips      Lateral load that must be resisted at limit state of column yielding.

$$FS := \frac{Fr}{Vu} = 1.56$$

## Bearing Pressure

Based on ACI 318-14 22.8 Bearing pressure.  
See image below for load combinations



$$P_u := (250.6 \text{ kips} - 30 \text{ kips})$$

Prestressing force and reaction at column yield limit state (minus 30 because I prestressed to 170 kips)

$$A_1 := L^2 - (\pi \cdot 1.5 \text{ in.}^2) = 76 \text{ in.}^2$$

Load area

$$C := 1$$

C taken as 1 because the load cannot spread at 45 degrees through the element to a larger bearing surface on the other side.

$$\phi B_n := C \cdot 0.85 \cdot f'_c \cdot A_1 = 240 \text{ kips}$$

$$\frac{\phi B_n}{P_u} = 1.09$$

Must be greater than 1

+

Also, minimum pressure is larger than zero meaning contact is not lost.

## Tension Plates

$$T_u := \frac{V_u}{6} = 16.4 \text{ kips}$$

$$t := 0.5 \text{ in.} \quad \text{Plate thickness}$$

$$b := 9 \text{ in.} \quad \text{Plate width}$$

$$f_{y_{pl}} := 36000 \text{ psi} \quad \text{A36 steel}$$

$$f_{u_{pl}} := 58000 \text{ psi}$$

### Yield

$$A_{npl} := t \cdot b = 4.5 \text{ in.}^2$$

$$T_{n1} := 0.9 \cdot A_{npl} \cdot f_{y_{pl}} = 146 \text{ kip}$$

### Fracture

$$A_{epl} := A_{npl} - t \cdot 2 \text{ in.} = 3.5 \text{ in.}^2$$

$$T_{n2} := f_{u_{pl}} \cdot A_{epl} = 203 \text{ kips}$$

$$T_n := \min(T_{n1}, T_{n2}) = 146 \text{ kip}$$

$$\frac{T_n}{T_u} = 8.9$$

Must be greater than 1

nine Williams rods prestressing the

### Point Load Web Failure

Beam Dimentions

W12x106

$F_{yw} := 50000 \text{ psi}$  Beam minimum yield stress

$d := 12.9 \text{ in.}$  Beam height

$tw := 0.61 \text{ in.}$  Web thickness

$bf := 12.2 \text{ in.}$  Flange width

$k1 := \left(1 + \frac{1}{8}\right) \text{ in.}$  Dist from centerline to end  
of curved part of web

$tf := 0.99 \text{ in.}$  Flange thickness

$h := 15.9 \cdot tw = 9.7 \text{ in.}$

Web Local Yielding

AISC J10.2

$k := \frac{(bf - 2 k1)}{2} = 4.98 \text{ in.}$

$lb := 15 \text{ in.}$  Bearing length

$Rn := F_{yw} \cdot tw \cdot (2.5 \cdot k + lb) = 837 \text{ kip}$

$$\frac{Rn}{Vu} = 8.51$$

Must be greater than 1



### Web Crippling

AISC J10.3

Point of load application is more than  $d/2$  from end of beam.

$$R_n := 0.8 \cdot t_w^2 \cdot \left( 1 + 3 \cdot \frac{l_b}{d} \cdot \left( \frac{t_w}{t_f} \right)^{1.5} \right) \cdot \sqrt{\frac{(E \cdot F_{yw} \cdot t_f)}{t_w}} = (1.23 \cdot 10^3) \text{ kips}$$

$$\frac{R_n}{V_u} = 12.5$$

Must be greater than 1

### Web Sideways Buckling

AISC J10.4

Compression flange is not restrained

$L_b := 88.2 \text{ in.}$  Length of laterally unrestrained column

$$\frac{\left( \frac{h}{t_w} \right)}{\left( \frac{L_b}{b_f} \right)} = 2.2$$

$$\frac{\left( \left( \frac{h}{t_w} \right) \right)}{1.7} = 1.29$$

+

Must be greater than 1

Web sideways buckling does not govern.

### Cantilever Tip Rods

$$F_{yrod} := 36000 \text{ psi}$$

$$d_{rod} := 1.25 \text{ in.}$$

$$Ty := \pi \cdot \left( \frac{d_{rod}}{2} \right)^2 \cdot F_{yrod} = 44.2 \text{ kips}$$

$$4 \cdot Ty = 177 \text{ kip}$$

$$\frac{4 \cdot Ty}{Vu} = 1.8$$

Must be greater than 1

# APPENDIX E. CHANNEL LIST

Table E- 1. Channel list for moment transfer test December 12, 2017

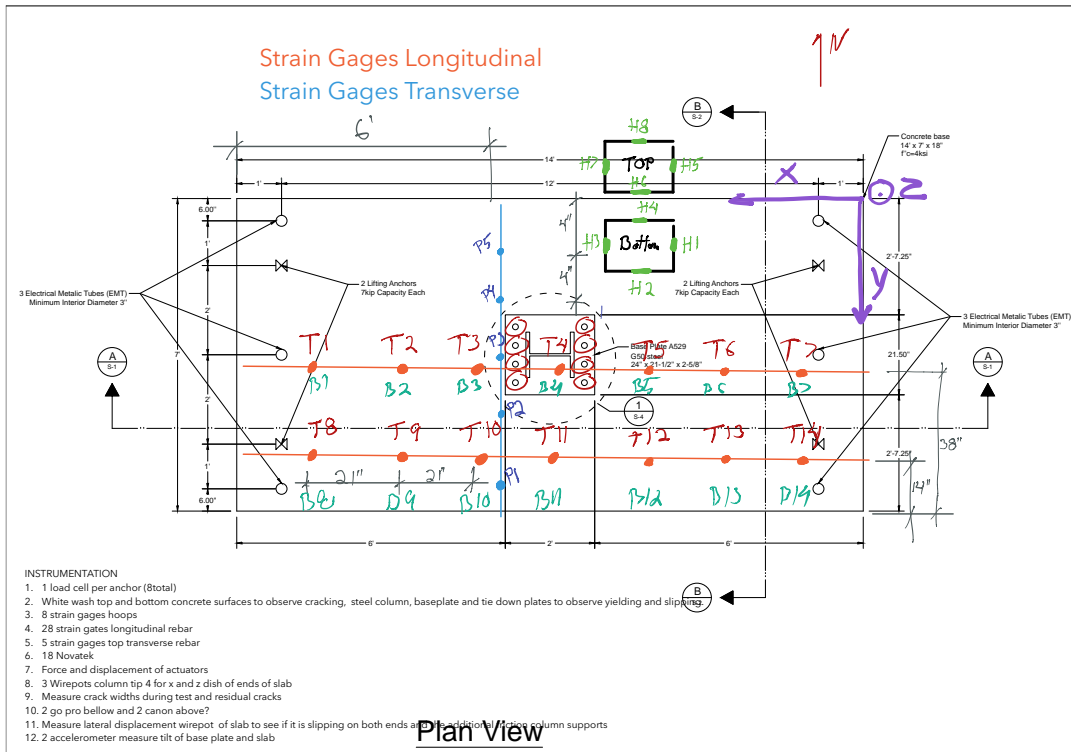
Number	Name	Type	Unit	Description	Address
1	LC-N	Load Cell	Force	South Actuator	0-2-0
2	Disp-N	Disp. Transducer	Disp		0-2-1
3	LC-S	Load Cell	Force	North Actuator	0-2-2
4	Disp-S	Disp. Transducer	Disp		0-2-3
5	-	-	-	-	0-2-4
6	-	-	-	-	0-2-5
7	-	-	-	-	0-2-6
8	-	-	-	-	0-2-7
9	T1	Strain Gauge	Strain	Top longitudinal strain gages from West to East and North to South	0-3-0
10	T2	Strain Gauge	Strain		0-3-1
11	T3	Strain Gauge	Strain		0-3-2
12	T4	Strain Gauge	Strain		0-3-3
13	T5	Strain Gauge	Strain		0-3-4
14	T6	Strain Gauge	Strain		0-3-5
15	T7	Strain Gauge	Strain		0-3-6
16	T8	Strain Gauge	Strain		0-3-7
17	T9	Strain Gauge	Strain		0-4-0
18	T10	Strain Gauge	Strain		0-4-1
19	T11	Strain Gauge	Strain		0-4-2
20	T12	Strain Gauge	Strain		0-4-3
21	T13	Strain Gauge	Strain		0-4-4
22	T14	Strain Gauge	Strain		0-4-5
23	B1	Strain Gauge	Strain	Bottom longitudinal strain gages West to East and North to South	0-4-6
24	B2	Strain Gauge	Strain		0-4-7
25	B3	Strain Gauge	Strain		0-5-0
26	B4	Strain Gauge	Strain		0-5-1
27	B5	Strain Gauge	Strain		0-5-2
28	B6	Strain Gauge	Strain		0-5-3
29	B7	Strain Gauge	Strain		0-5-4
30	B8	Strain Gauge	Strain		0-5-5
31	B9	Strain Gauge	Strain		0-5-6
32	B10	Strain Gauge	Strain		0-5-7
33	B11	Strain Gauge	Strain		0-6-0

Number	Name	Type	Unit	Description	Address	
34	B12	Strain Gauge	Strain		0-6-1	
35	B13	Strain Gauge	Strain		0-6-2	
36	B14	Strain Gauge	Strain		0-6-3	
37	H1	Strain Gauge	Strain	Hoop Strain Gages	0-6-4	
38	H2	Strain Gauge	Strain		0-6-5	
39	H3	Strain Gauge	Strain		0-6-6	
40	H4	Strain Gauge	Strain		0-6-7	
41	H5	Strain Gauge	Strain		0-7-0	
42	H6	Strain Gauge	Strain		Hoop Strain Gages	0-7-1
43	H7	Strain Gauge	Strain		0-7-2	
44	H8	Strain Gauge	Strain		0-7-3	
45	P1	Strain Gauge	Strain	Transverse Strain Gages	0-7-4	
46	P2	Strain Gauge	Strain		0-7-5	
47	P3	Strain Gauge	Strain		0-7-6	
48	P4	Strain Gauge	Strain		0-7-7	
49	P5	Strain Gauge	Strain		0-8-0	
50	N1	Linear Potentiometer	Disp	Top surface W-E and N-S	0-8-1	
51	N2	Linear Potentiometer	Disp	Top surface W-E and N-S	0-8-2	
52	N3	Linear Potentiometer	Disp	Top surface W-E and N-S	0-8-3	
53	N10	Linear Potentiometer	Disp	Top surface W-E and N-S	0-8-4	
54	N11	Linear Potentiometer	Disp	Top surface W-E and N-S	0-8-5	
55	N12	Linear Potentiometer	Disp	Top surface W-E and N-S	0-8-6	
56	N25	Linear Potentiometer	Disp	Specimen uplift west	0-8-7	
57	N4	Linear Potentiometer	Disp	Top surface W-E and N-S	0-9-0	
58	N5	Linear Potentiometer	Disp	Top surface W-E and N-S	0-9-1	
59	N6	Linear Potentiometer	Disp	Top surface W-E and N-S	0-9-2	
60	N7	Linear Potentiometer	Disp	Top surface W-E and N-S	0-9-3	
61	N16	Linear Potentiometer	Disp	Top surface W-E and N-S	0-9-4	
62	N15	Linear Potentiometer	Disp	Top surface W-E and N-S	0-9-5	
63	N14	Linear Potentiometer	Disp	Top surface W-E and N-S	0-9-6	
64	N13	Linear Potentiometer	Disp	Top surface W-E and N-S	0-9-7	
65	N8	Linear Potentiometer	Disp	Top surface W-E and N-S	0-10-0	
66	N23	Linear Potentiometer	Disp	Relative specimen - support slide east	0-10-1	
67	N9	Linear Potentiometer	Disp	Top surface W-E and N-S	0-10-2	
68	N17	Linear Potentiometer	Disp	Top surface W-E and N-S	0-10-3	
69	N24	Linear Potentiometer	Disp	Absolute support slide east end	0-10-4	
70	N18	Linear Potentiometer	Disp	Top surface W-E and N-S	0-10-5	

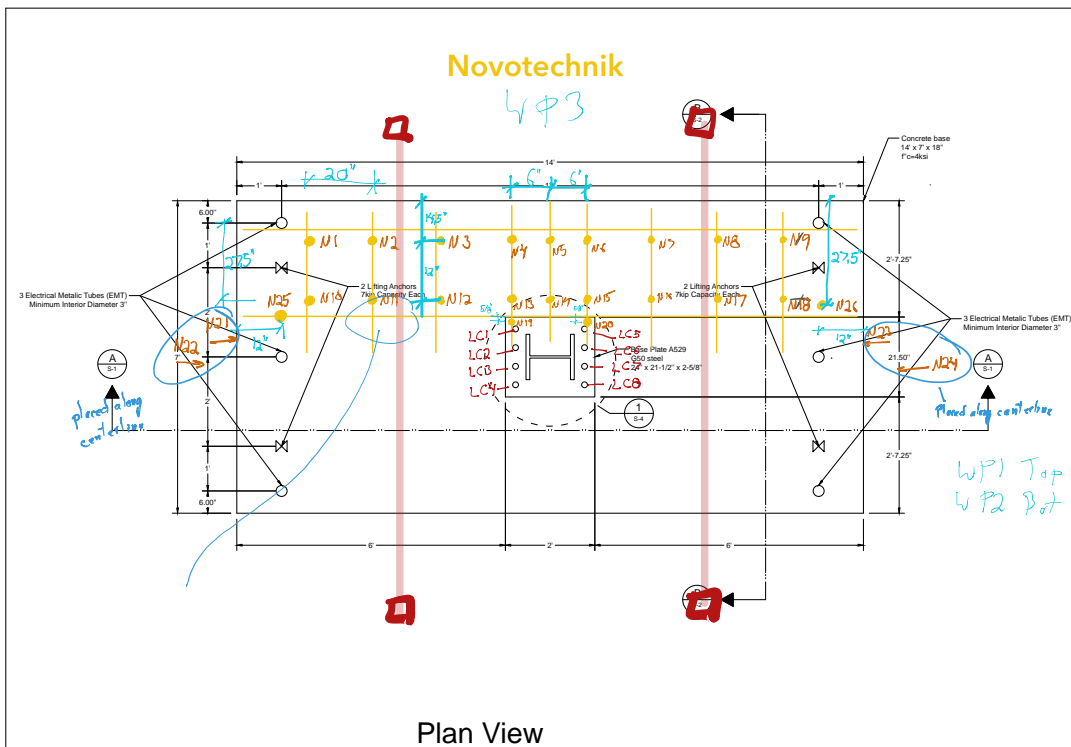
<b>Number</b>	<b>Name</b>	<b>Type</b>	<b>Unit</b>	<b>Description</b>	<b>Address</b>
71	N26	Linear Potentiometer	Disp	Support lift west	0-10-6
72	-	-	-	-	0-10-7
73	N21	Linear Potentiometer	Disp	Absolute specimen slide west end	0-11-0
74	N22	Linear Potentiometer	Disp	Absolute Support slide west	0-11-1
75	N19	Linear Potentiometer	Disp	Base plate lift up west	0-11-2
76	N20	Linear Potentiometer	Disp	Base plate lift up east	0-11-3
77	-	-	-	-	0-11-4
78	-	-	-	-	0-11-5
79	-	-	-	-	0-11-6
80	-	-	-	-	0-11-7
81	WP1	String Potentiometer	Disp	Long Column Disp (E-W)	0-12-0
82	WP2	String Potentiometer	Disp	Transverse Column Disp (N-S)	0-12-1
83	WP3	String Potentiometer	Disp	Angled column Disp	0-12-2
84	-	-	-	-	0-12-3
85	-	-	-	-	0-12-4
86	-	-	-	-	0-12-5
87	-	-	-	-	0-12-6
88	-	-	-	-	0-12-7
89	-	-	-	-	0-13-0
90	-	-	-	-	0-13-1
91	-	-	-	-	0-13-2
92	-	-	-	-	0-13-3
93	-	-	-	-	0-13-4
94	-	-	-	-	0-13-5
95	-	-	-	-	0-13-6
96	-	-	-	-	0-13-7
97	LC1	Load Cell	Force	Load cell on individual anchors	0-14-0
98	LC2	Load Cell	Force		0-14-1
99	LC3	Load Cell	Force		0-14-2
100	LC4	Load Cell	Force		0-14-3
101	LC5	Load Cell	Force		0-14-4
102	LC6	Load Cell	Force		0-14-5
103	LC7	Load Cell	Force		0-14-6
104	LC8	Load Cell	Force		0-14-7

## **APPENDIX F. INSTRUMENTATION LOCATION**

Below are sketches that indicate the location of each instrument.



Project: Moment Transfer Test	Date: 07/24/2017
University of California Berkeley, Civil and Environmental Engineering	S-3



Project: Moment Transfer Test	Date: 07/24/2017
University of California Berkeley, Civil and Environmental Engineering	S-3

# APPENDIX G.PHOTOGRAPHS



Figure G- 1. Support type 1 form



Figure G- 2. Support type 2 form with through holes



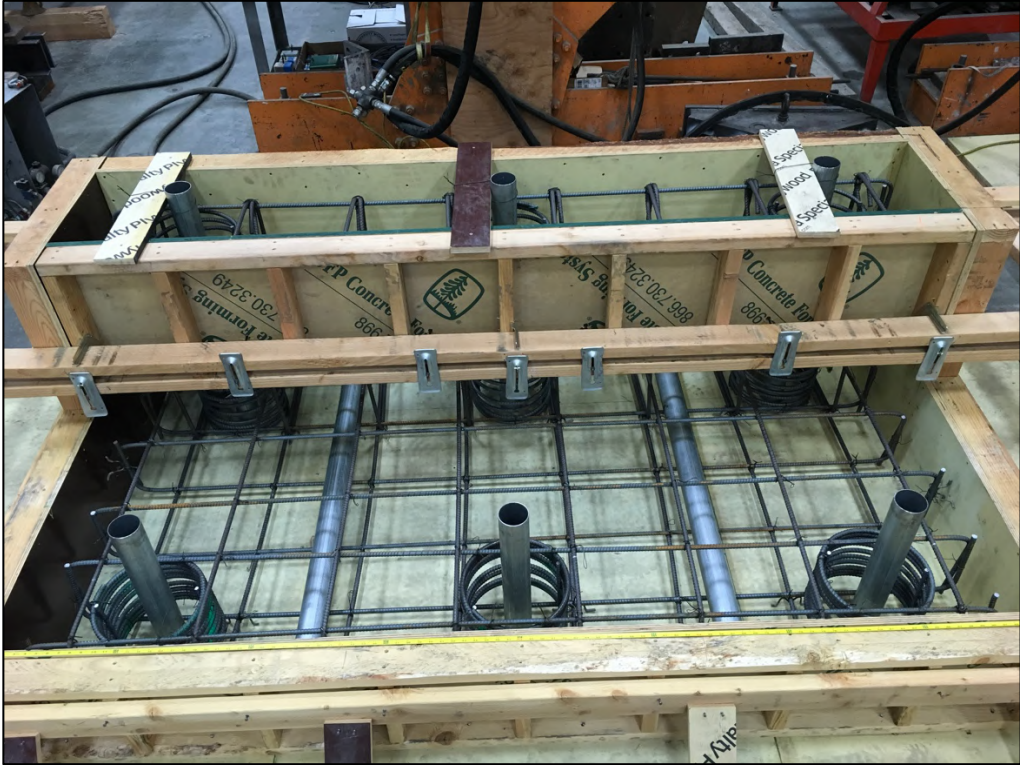


Figure G- 3. Support type 1 form with reinforcement ready to cast #1



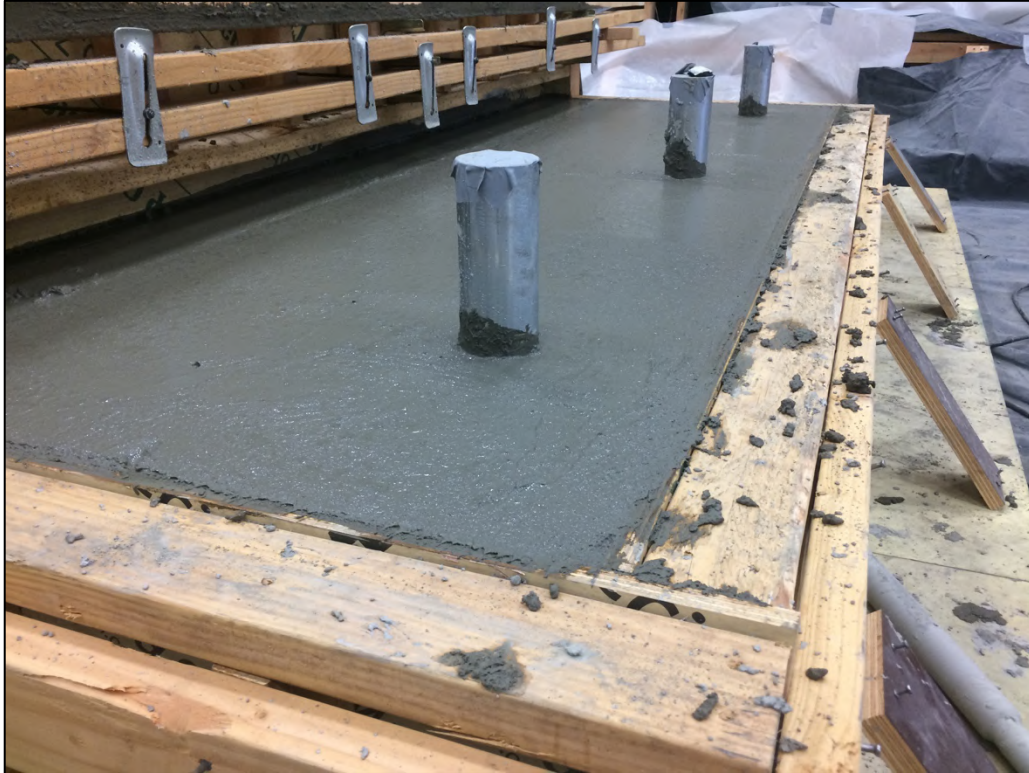
Figure G- 4. Support type 1 form with reinforcement ready to cast #2



Figure G- 5. Casting support type 1 October 25, 2017 #1



Figure G- 6. Casting support type 1 October 25, 2017 #2



**Figure G- 7. Support type 1 hours after casting bottom section**



**Figure G- 8. Support type 1 casting top section October 25, 2017 #1**



**Figure G- 9. Support type 1 casting top section October 25, 2017 #2**



**Figure G- 10. Support type 2 casting October 25, 2017**



**Figure G- 11. Specimen form and support type 2 form in the background**



**Figure G- 12. Anchors delivery**



**Figure G- 13. Installation of strain gages #1**



**Figure G- 14. Installation of strain gages #2**

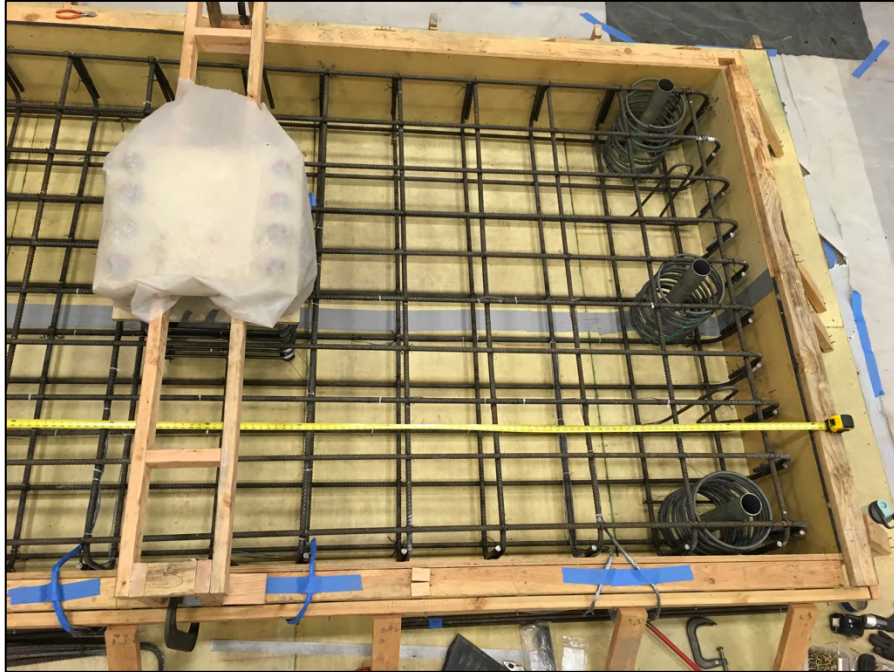


**Figure G- 15. Specimen form with reinforcement ready to cast #1**

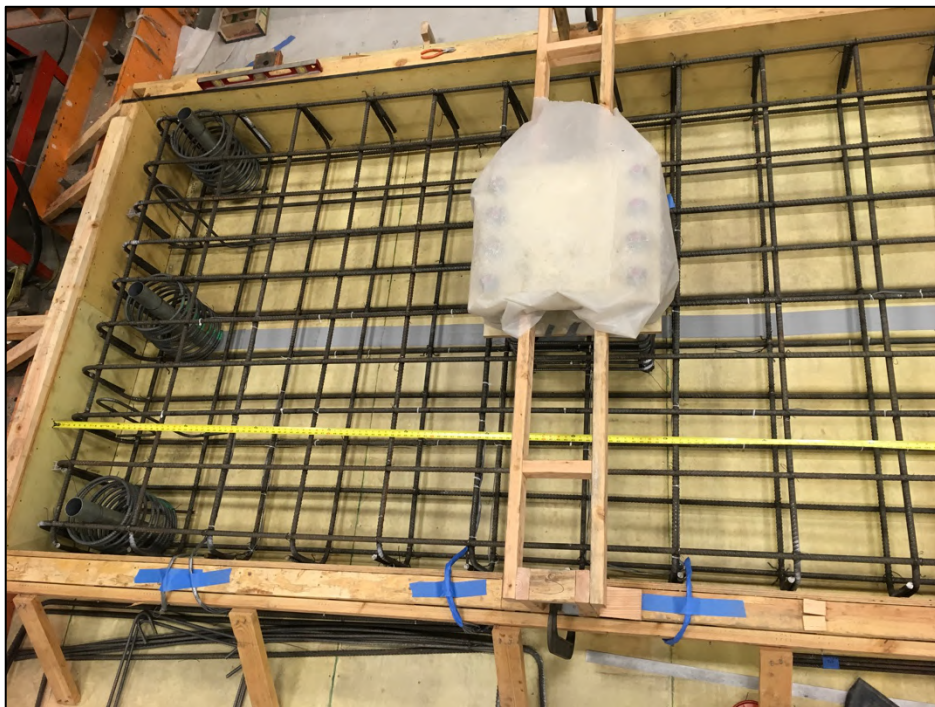


**Figure G- 16. Specimen form with reinforcement ready to cast #2**

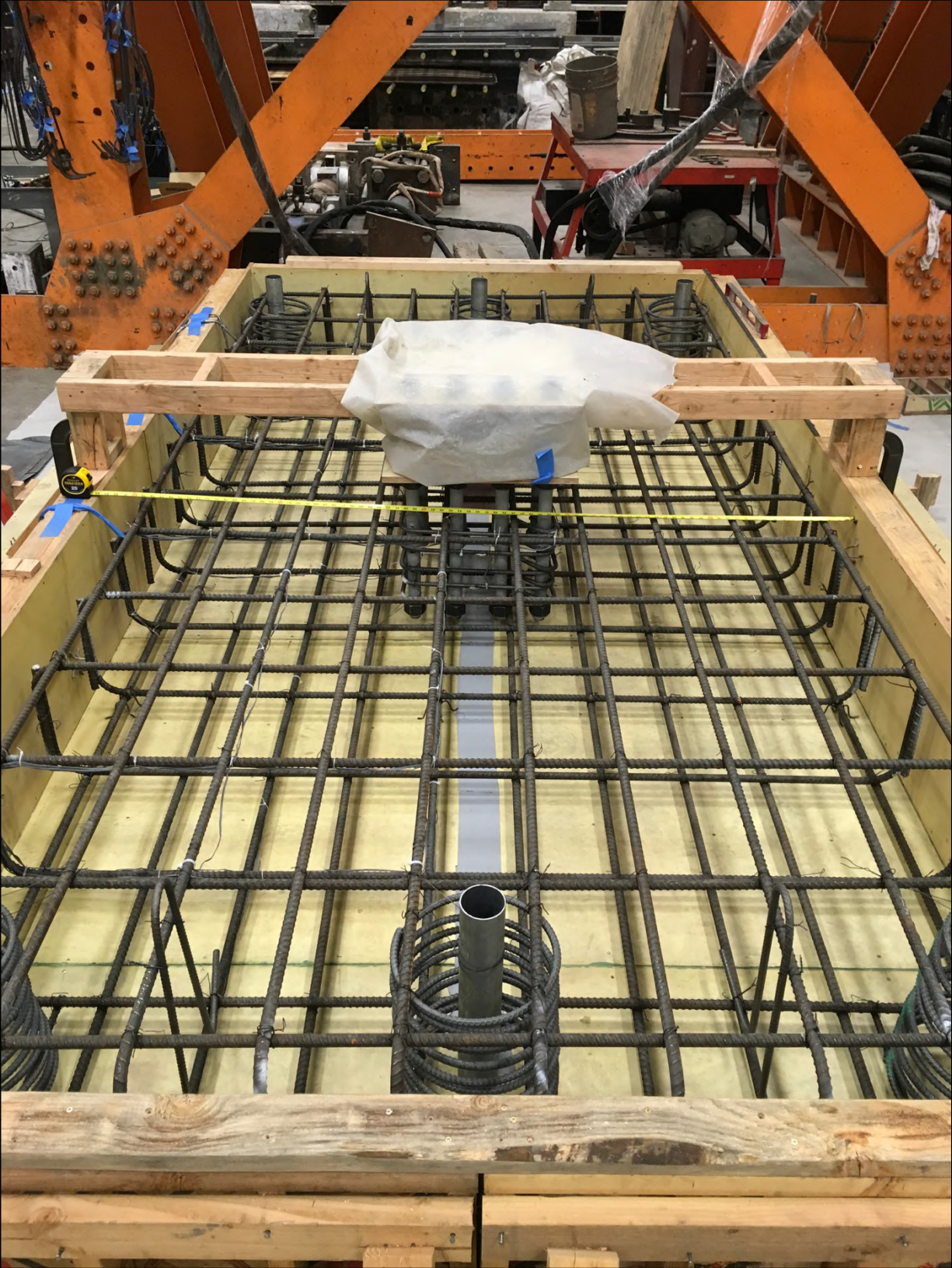
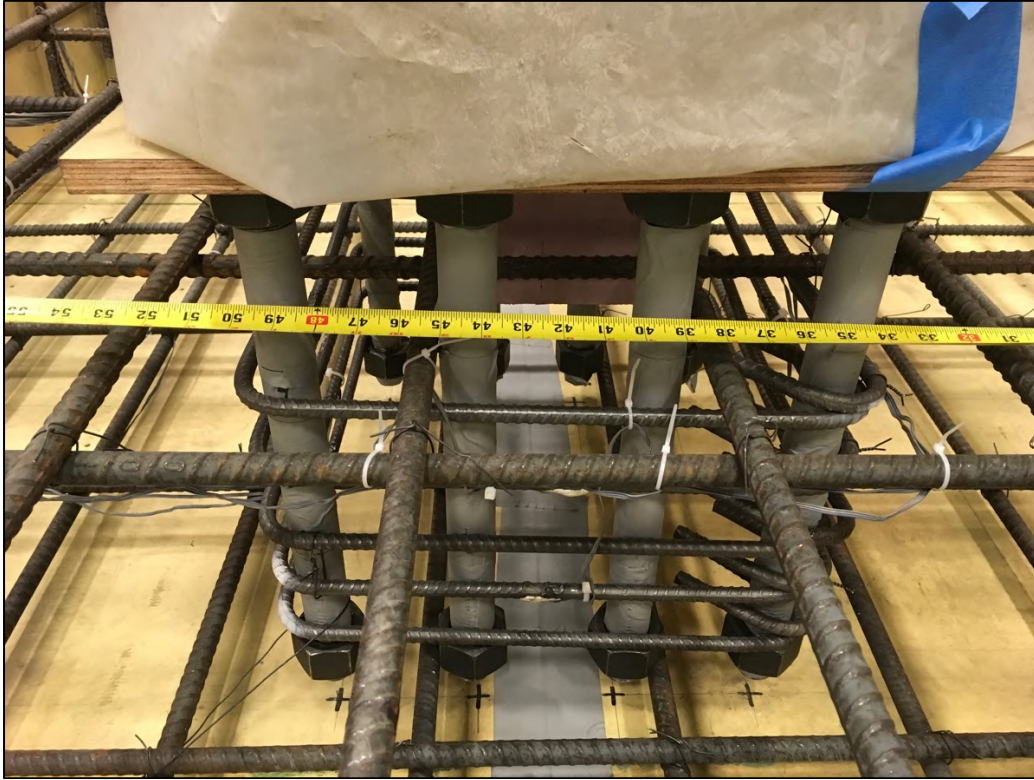


Figure G- 17. Specimen form with reinforcement ready to cast #3





**Figure G- 18. Specimen anchors ready to cast**



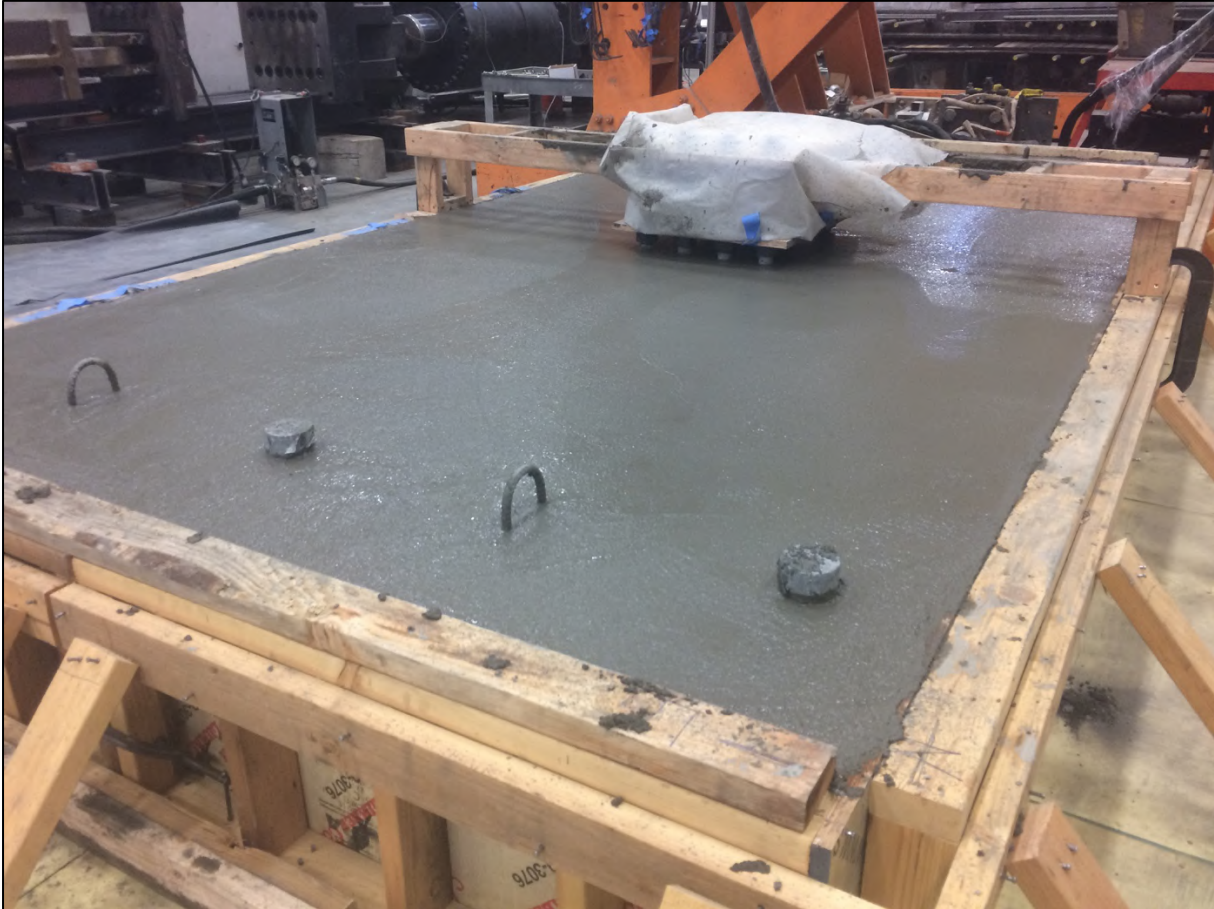
**Figure G- 19. Specimen form with reinforcement ready to cast #3**



Figure G- 20. Specimen casting November 21, 2017



Figure G- 21. Specimen hours after casting November 21, 2017 #1



**Figure G- 22. Specimen hours after casting November 21, 2017 #2**



**Figure G- 23. Removal of foam from specimen to reveal hole for shear lug #1**



**Figure G- 24. Removal of foam from specimen to reveal hole for shear lug #2**



**Figure G- 25. Column delivery**



Figure G- 26. Support type 1 demolding



**Figure G- 27. Demolding specimen**



**Figure G- 28. Specimen on temporary supports**



**Figure G- 29. Moving supports into final position**

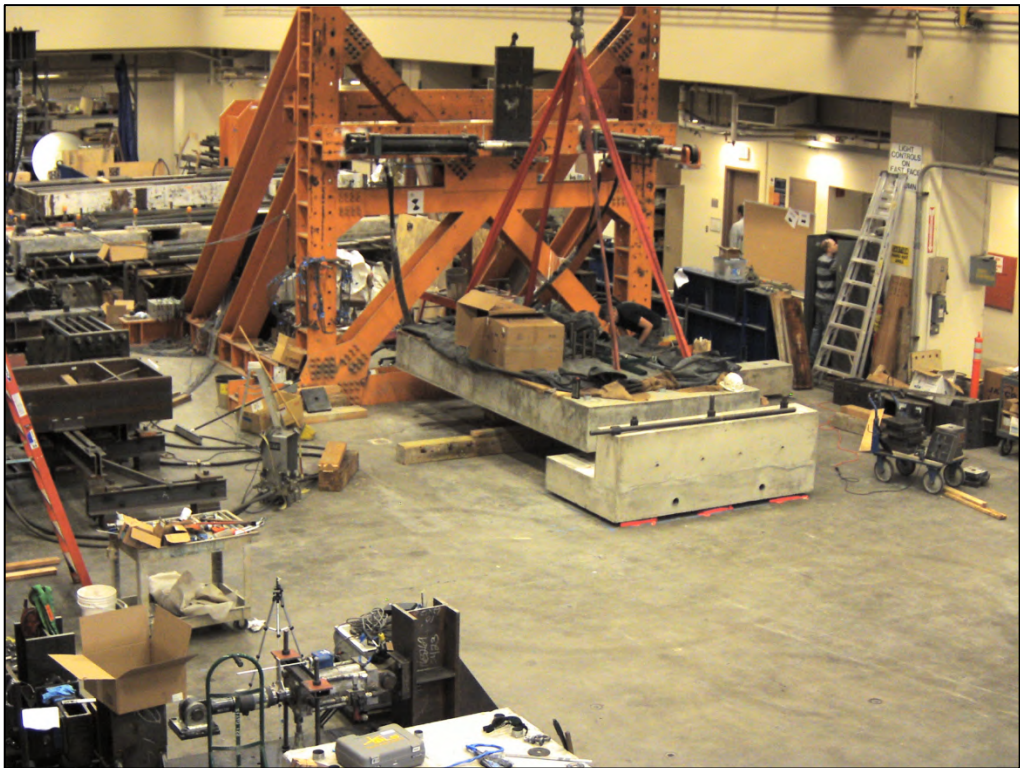


**Figure G- 30. Specimen moved onto supports with overhead crane**



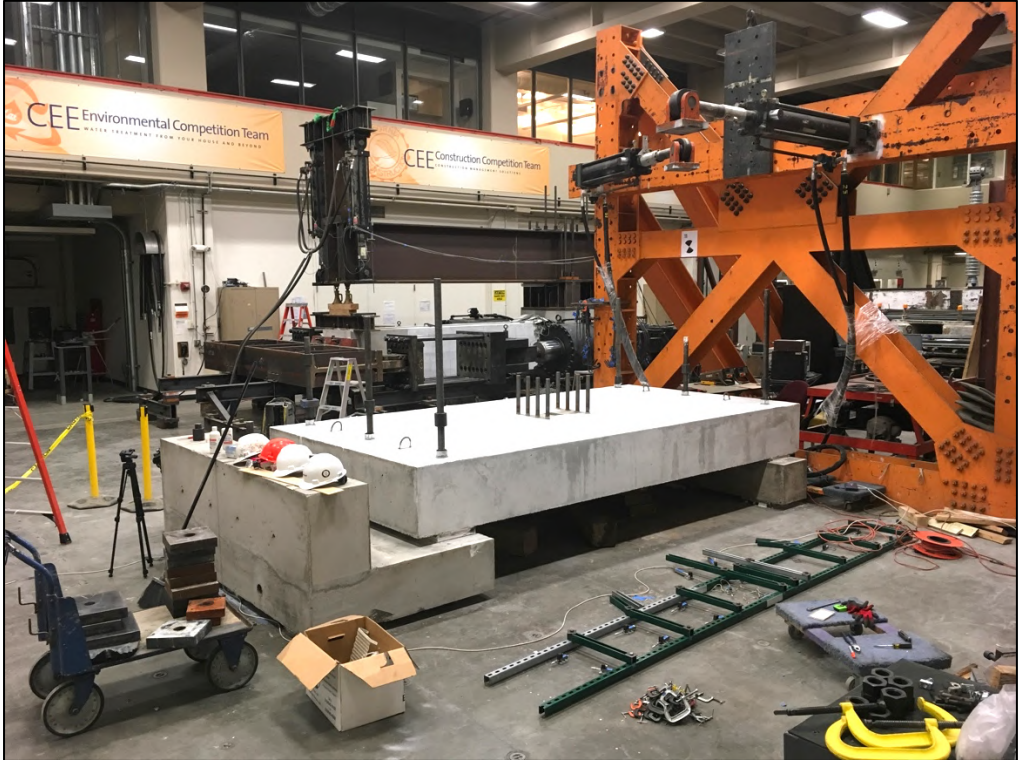


**Figure G- 31. Specimen in final position on supports #1**



**Figure G- 32. Specimen in final position on supports #2**



Figure G- 33. Specimen in final position with column #1



Figure G- 34. Specimen in final position with column #2



**Figure G- 35. Instrumentation cable management**



**Figure G- 36. Crack marking during a pause while testing December 12, 2017**

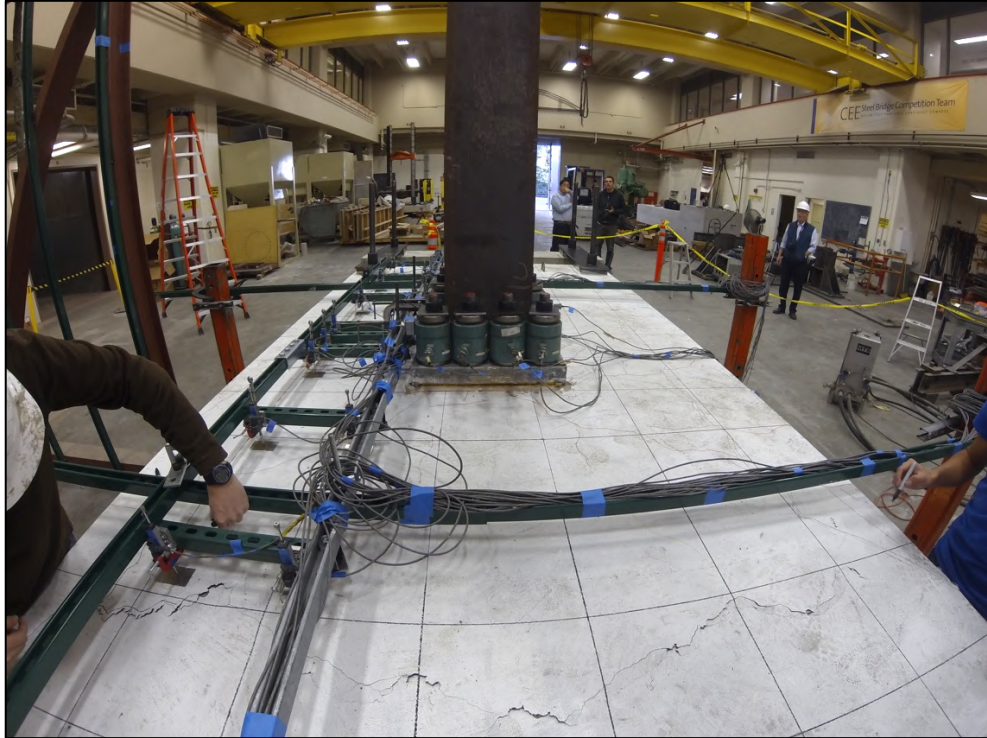


**Figure G- 37. Specimen top surface after test as seen from the west December 12, 2017**

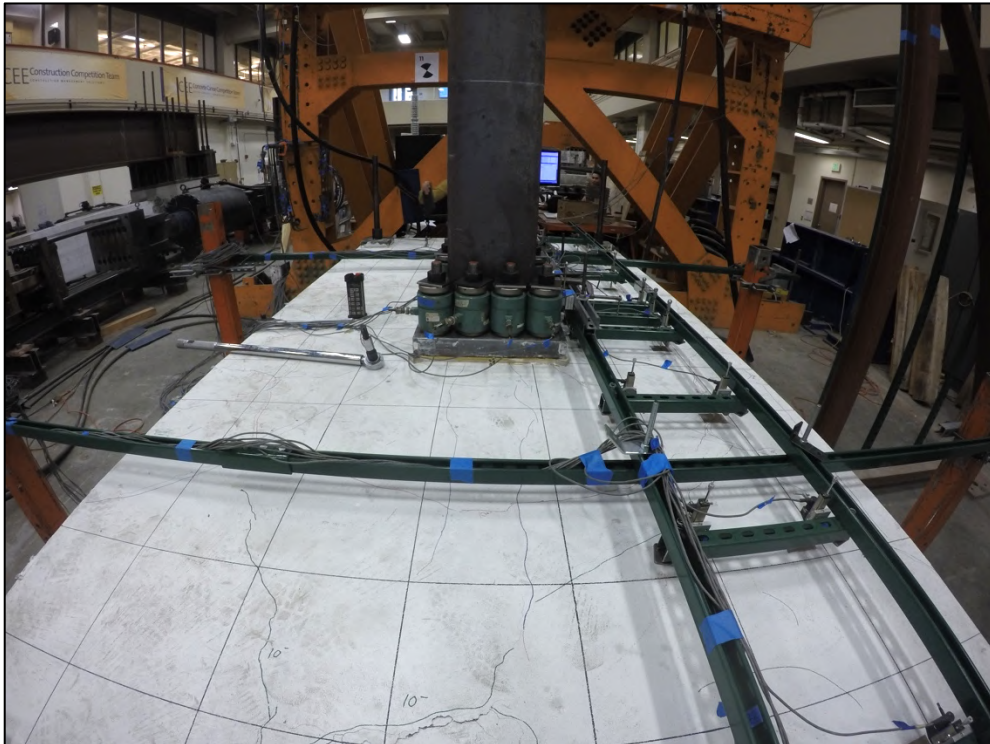


**Figure G- 38. Specimen top surface after test as seen from the east December 12, 2017**



Figure G- 39. Specimen bottom surface after test as seen from the west December 12, 2017



Figure G- 40. Specimen bottom surface after test as seen from the east December 12, 2017



**Figure G- 41. Construction of fracture energy molds for large beams**



**Figure G- 42. Medium fracture energy beams hours after casting November 21, 2017**



**Figure G- 43. Large fracture energy beams hours after casting November 21, 2017**





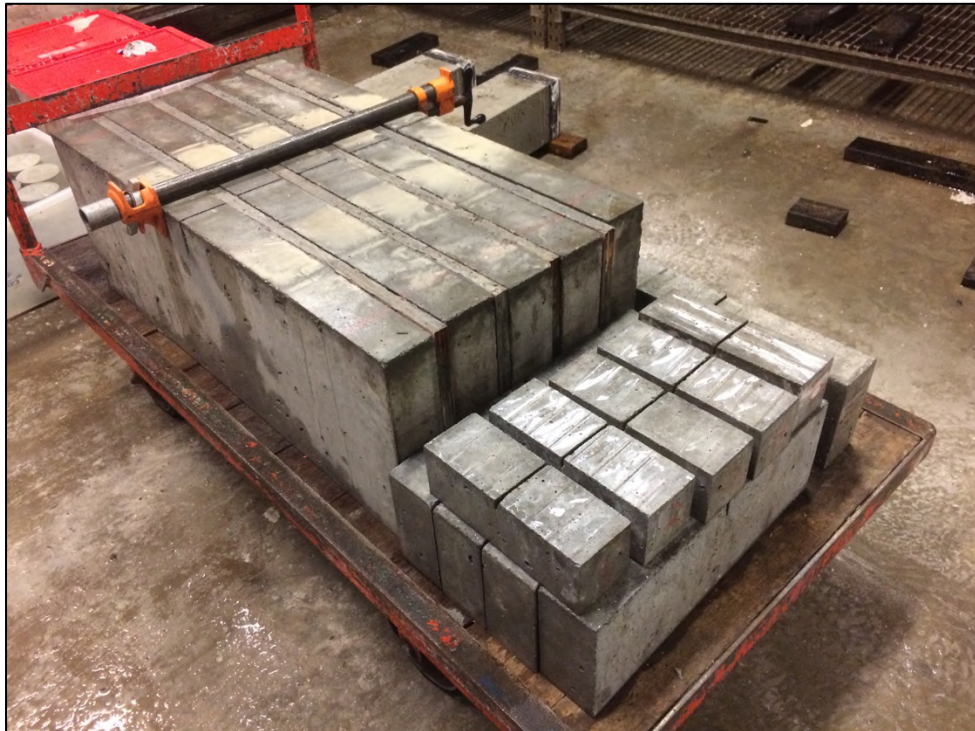
Figure G- 44. Fracture energy beams with top plate attached with hydrostone



Figure G- 45. Fracture energy beams after removing from lime bath



**Figure G- 46. Madium fracture energy beams held together and saw cut**



**Figure G- 47. All fracture energy beams removed from lime bath and saw cut**



**Figure G- 48. Cylinders hours after casting November 21, 2017**



**Figure G- 49. Cylinder compression testing**



**Figure G- 50. Reinforcing bar testing**